

Spatial Resolution Enhancement using Deep Learning and Data Augmentation for Cloud-based Infrastructure

PHD THESIS

submitted by
Moataz Ahmed

supervised by
Dr. Tuong Thuy Vu

Co-Supervised by
Dr. Tomas Henrique Maul

School of Environmental and Geographical Sciences
The University of Nottingham
Malaysia Campus

January 2019

Abstract

Satellite data have fundamentally changed how we perceive and understand the world we live in. The amount of data produced is rapidly increasing and classical computing resources and processing tools are no longer sufficient. These massive amounts of data require huge storage in addition to advanced computing capacity in order to allow users to benefit from the derived datasets. Cloud computing has provided the required storage and computing capacity on a scalable level to add or remove resources according to requirements. Simultaneously, recent advances in data processing techniques such as Deep Learning (DL) have paved the way to integrated solutions for Earth Observation (EO) big data understanding.

By bringing together a unique combination of computing capacity, ultra fast data storage and advanced data processing techniques, our ability to derive useful insights will be revolutionised. This thesis focuses on harnessing cloud computing and deep learning capabilities to enhance spatial resolution of satellite imagery data. Particularly, the thesis highlights cloud computing architectures to accommodate satellite image processing services. A conceptual data model was developed to enable utilising cloud computing resources with EO big data in near real-time. Moreover, a state-of-the-art super resolution algorithm (SRCNN) was adapted and tested in detail to be exploited with the satellite image domain. In addition, a novel fusion-based data augmentation approach was developed to boost super resolution accuracy. To evaluate the super resolution accuracy with a real-life application, landcover classification was adopted to assess the accuracy between super resolved Landsat-8 data and crowd-source data collected using the Google Earth interface. The accuracy achieved opens a wide field of research with deep learning and data augmentation in the satellite image super resolution domain.

Acknowledgements

I would like to express my sincere gratitude and thanks to my supervisors, Dr. Tuong Thuy Vu and Dr. Tomas Maul. I was lucky enough to have both of them supporting, guiding and helping me throughout the period of this study. Thanks also to Dr. Alexander Lechner for his valuable advice, extremely supportive and constructive comments during my last year of this study. I would like to extend my gratitude and thanks to the Ministry of Higher Education in Malaysia, The University of Nottingham Malaysia campus and Amazon Web Services for sponsoring my research. I would like to convey my thanks to all my colleagues, especially Darshana, Karmen, Jolene, Amer, Tuong, Ijaz, Ibrahim, Haixia and Mei Shin. Special recognition is due to my dad and sisters for their patience and prayers. I would like to dedicate this thesis to the soul of my mother.

List of publications and awards

- Multi-Modal Remote Sensing Data Fusion Framework. **Moataz Ahmed**, Tuong Thuy Vu, Tomas Maul. The International Archives of Photogrammetry, Remote Sensing and Spatial Information Sciences, Copernicus GmbH, 42-85, 2017.
- An Integrated Cloud-Based Framework for Remote Sensing Data Processing. **Moataz Ahmed**, Tuong Thuy Vu, Tomas Maul, International Journal of Geoinformatics 12-02, 2016.
- Towards Landcover Classification Service on Cloud Computing Platform. **Moataz Ahmed**, DC Wickramasinghe and Tuong Thuy Vu, IEEE IWGRS, 2015.
- Cloud computing providers for satellite image processing service: A comparative study. **Moataz Ahmed** and Tuong Thuy Vu. International Conference of Space Science and Communication (IconSpace), 2015.
- CROWD-2-CLOUD - Remote Sensing Landcover Verification with Crowd-Sourcing Data, **Moataz Ahmed**, Dai Huynh, Darshana Wickramasinghe, Tuong Thuy Vu. FOSS4G 2015.
- AWS Research Education Grant of $10,000 from Amazon Web Services to be used as cloud credit to run my algorithms.
- Travel Grant to attend and present my paper at the 9th International Free Open Source Software for Geospatial Conference (FOSS4G), Seoul 2015.

List of abbreviations and acronyms

VHR Very High Resolution

SR Super Resolution

HR High Resolution

SAAS Software As A Service

PAAS Platform As A Service

IAAS Infrastructure As A Service

EO Earth Observation

EOD Earth Observation Big Data

MODIS Moderate Resolution Imaging Spectroradiometer

TOA Top Of Atmosphere

ANN Artificial Neural Network

CNN Convolutional Neural Network

SVM Support Vector Machines

EOS Earth Observation Systems

HPC High Performance Computing

GEE Google Earth Engine

AWS Amazon Web Services

WMS Web Map Service

WCS Web Coverage Service

WPS Web Processing Service

OGC Open-Geospatial Consortium

GPU Graphical Processing Unit

TPU Tensor Processing Unit

SDI Spatial Data Infrastructure

VM Virtual Machine

ESA European Space Agency

TIRS Thermal Infrared Sensor

S3 Simple Storage Service

SWIR Short-wave Infrared

NIR Near Infrared

PSNR Peak Signal to Noise Ratio

Relu Rectified Linear Unit

SRCNN Super Resolution Covolutional Neural Network

AOI Area Of Interest

Contents

1 Introduction **1**

1.1 Motivation 1
1.2 Research questions 4
1.3 Research Objectives 5
1.4 Thesis Contributions 5
1.5 Background 6
1.5.1 Remote sensing big data 6
1.5.2 Cloud computing 10
1.5.3 Machine learning 11
1.6 Thesis Structure 14
1.6.1 Chapter 2: Literature review and state-of-the-art 14
1.6.2 Chapter 3: Integrated cloud-based framework for remote sensing big data processing 14
1.6.3 Chapter 4: Satellite image spatial resolution enhancement as a service 15
1.6.4 Chapter 5: Boosting accuracy using data augmentation techniques 15
1.6.5 Chapter 6: Evaluating Super Resolution Accuracy via Landcover Classification Tasks 16
1.6.6 Chapter 7: Conclusion and future work 16

2 Cloud Computing Providers for Satellite Image Understanding Services 17
2.1 Background . . . 17
2.2 Literature Review . . . 20
2.3 Conclusion . . . 41

3 Integrated cloud-based framework for remote sensing big data processing 47
3.1 Introduction . . . 48
3.2 Remote Sensing and Cloud Computing Survey . . . 49
3.2.1 Methods . . . 50
3.2.2 Conclusion . . . 61
3.3 Conceptual Data Model Design . . . 62
3.3.1 Receiving and Indexing Data . . . 63
3.3.2 Data Processing . . . 64
3.3.3 Information Retrieval . . . 65
3.4 Landsat 8 Imagery Classification As A Service . . . 65
3.4.1 Data acquisition and indexing . . . 66
3.4.2 Data processing . . . 73
3.4.3 Information retrieval . . . 73
3.5 Conclusion . . . 74

4 Satellite Image Resolution Enhancement using Deep Learning 76
4.1 Resolution Enhancement Introduction . . . 77
4.1.1 Interpolation based . . . 78
4.1.2 Fusion based . . . 78
4.1.3 Super Resolution . . . 79
4.2 Satellite Image Super Resolution . . . 81
4.3 Creating training dataset for single-image super resolution . . . 86
4.4 SRCNN . . . 92
4.4.1 SRCNN Adjustments . . . 94

4.5 Results . . . 95
4.5.1 Experiment 1 . . . 95
4.5.2 Experiment 2 . . . 97
4.5.3 Experiment 3 . . . 98
4.6 Conclusion . . . 102

5 Boosting accuracy using data augmentation techniques 103
5.1 Introduction . . . 104
5.2 Background . . . 105
5.3 Methodology . . . 108
5.4 Results . . . 116
5.5 Conclusions . . . 119

6 Evaluating Super Resolution Accuracy via Landcover Classification Tasks 122
6.1 Introduction . . . 123
6.2 Methodology . . . 125
6.2.1 Study area . . . 125
6.3 Evaluation Methodology . . . 127
6.4 Experiments and Results . . . 128
6.4.1 Experiment 1: Landsat-8 . . . 128
6.4.2 Experiment 2: Sentinel-2 . . . 131
6.4.3 Experiment 3: Landsat-8 super-resolved using scale factor of 3 against Sentinel-2 as ground-truth . . . 133
6.5 Conclusion . . . 134

7 Conclusion 135
7.1 Deep learning and Remote Sensing . . . 136
7.2 Summary . . . 137
7.3 Contributions . . . 138
7.4 Future work . . . 138

List of Figures

1.1 A: Landsat-8 (6x6) patch covering area of 8.1km with mixed pixels of .5km, B: Landsat-8 (3x3) patch covering area of 8.1km with mixed pixels of 2.7km 2
1.2 Searching hits from Scopus database for ”sub-pixel” OR ”super resolution” AND ”satellite data” in title, abstract and keywords from 2015 to 2018 3
1.3 Gartner hype cycle for emerging technologies, 2014. 7

2.1 APPS4GMES Architecture [Niggemann et al., 2014] 22
2.2 Comparison of geospatial data processing performance by [Zhong et al., 2012]. 28
2.3 Scalability evaluation. 28
2.4 Angel et al [Ferrn et al., 2013] system architecture. 29
2.5 Execution time for 15 forecasting tasks on Amazon EC2 Vs. HPC cluster in [Huang et al., 2013]. 32

3.1 Aspects to consider before using a satellite image processing service 51
3.2 The level of understanding cloud computing models among survey groups (users, analysts and developers). 52
3.3 Platform preference for future EOD processing tasks 53
3.4 Reasons to choose between cloud computing and personal desktops for satellite image processing tasks. 54

3.5 Participants perspective regarding the usefulness of cloud computing models in EOD processing 55
3.6 Level of earth observation data usage among survey participants . 56
3.7 Types of remote sensing data used by participants 58
3.8 Spatial resolution accuracy 59
3.9 The most applied image classification methodology 60
3.10 Open-source vs proprietary geospatial processing tools among users, analysts and developers groups 60
3.11 Conceptual Data Model. 63
3.12 Cloud computing architecture 67
3.13 Landsat-8 landcover classification model 67
3.14 Available criteria for the searching mechanism 70
3.15 Search interface. 71
3.16 Results interface. 72

4.1 The overlapping areas between scenes. 82
4.2 Task 1 takes a mosaic of AOIs and generates footprints for training instances. 87
4.3 Example of task 1 after creating (64x64 pixels) training footprints for AOI over Kuala Lumpur. 88
4.4 Task 2 receives shapefiles as input and assigns projection per polygon. 88
4.5 Task 3 matches the projected footprint with the mosaic (AOI) and subsets the training samples. 88
4.6 Example of task 3 after warping a projected footprints. 89
4.7 Task 4 and 5 synthesis the low resolution training samples through down and up scale of instances. 89
4.8 Example of synthesised low-resolution training sample after down/up-scaling process in task 4 and 5. 90
4.9 Task 6 splits dataset into training, validation and test sets. 90
4.10 Training area from peninsular Malaysia. 91

4.11 Training area from east side of Malaysia (Sarawak) 91
4.12 Set5 dataset examples. 92
4.13 SRCNN architecture by [Dong et al., 2016]. 93

5.1 SRCNN architecture including the proposed data augmentation methods at the input layer where E refers to edge detection layer, C contrast enhanced layer and U unsharp mask layer. 109
5.2 Difference between convolution output of manually added gradient edge feature (C) and convolution output for same training sample without adding gradient edge feature (B) while original training sample is (A). 111
5.3 Difference between convolution output of manually added contrast enhanced feature (C) and convolution output for same training sample without adding contrast enhanced feature (A) while original training sample is (B). 112
5.4 Difference between convolution output of manually added unsharp mask feature (C) and convolution output for same training sample without adding unsharp mask feature (A) while original training sample is (B). 113
5.5 Examples from test set results of the proposed fusion-based augmentation compared with ground truth samples. 117
5.6 Comparison between RGB channels with and without instance augmentation learning convergence. 118
5.7 Comparison between the learning convergence of different channel augmentations added to RGB channels. 119
5.8 Example of denoise process where A represents the original sample, B represents the added salt-and-pepper noise and C is the result. 120
5.9 Example of dehaze process where A represents the original sample, B represents the synthesised haze and C is the result. . . . 120

6.1 Difference in contrast affects the PSNR accuracy. 124
6.2 Study area showing intersection between Sentinel-2 zone T47NQE and Landsat-8 127/057 path/row footprints. 127
6.3 Landsat-8 test sample (A) with classification map of original high-resolution version (B) and classification map of super-resolved sample (C) and land-cover ground-truth sample (D) while colors (red = built-up, green = vegetation, blue = water and yellow = bare-land). 129

List of Tables

2.1 Processing times for 40 Landsat-8 scenes 23
2.2 Public and Private Cloud Environment 25
2.3 EC2 and HPC computing environments [Huang et al., 2013] . . . 31
2.4 Review summary 35

3.1 Landsat-8 Processing Levels 68
3.2 Landsat-8 OLI and TIRS bands 69

4.1 Spatial resolution improvements from 1999 to 2017 77
4.2 Comparison between PSNR values of 64x64 input dimensions against msiSRCNN and bicubic interpolation 33x33 in logarithmic decibel dB. 97
4.3 Comparison between RGB against RGB+IR/NIR bands and msiSRCNN 98
4.4 Experiment 3A using kernels of size 9x9 Level1, 1x1 Level2, 5x5 Output, n_1 = 128 and n_2 = 64. 99
4.5 Experiment 3B using kernels of size 9x9 Level1, 1x1 Level2, 5x5 Output, n_1 = 64 and n_2 = 32. 100
4.6 Experiment 3C using kernels of size 7x7 Level1, 1x1 Level2, 5x5 Output, n_1 = 128 and n_2 = 64. 100
4.7 Experiment 3D using kernels of size 7x7 Level1, 1x1 Level2, 5x5 Output, n_1 = 64 and n_2 = 32. 100

4.8 Experiment 3E using kernels of size 9x9 Level1, 1x1 Level2, 1x1 Level3, 5x5 Output, $n_1 = 64$, $n_2 = 32$ and $n_3 = 16$. 101
4.9 A comparison between different architectures and their effects on accuracy. 101

5.1 A comparison between different augmentation approaches testing results 117

6.1 Error matrix for experiment 1-A 130
6.2 Error matrix for experiment 1-B 131
6.3 Experiment 2-A error metrics 132
6.4 Experiment 2-B error metrics 132
6.5 Experiment 3 error metrics 133

Chapter 1

Introduction

1.1 Motivation

Massive advances have been witnessed in remote sensing technologies recently. Whether improving sensors or processing techniques, these advances are reflected in terms of the 5 Vs of big data [Yang et al., 2016a], i.e.: volume, velocity, variety, veracity and value. The spatial, spectral and temporal resolutions of Remote Sensing data are core contributors to the volume factor. Moreover, very high spatial resolution (VHR) datasets are increasingly emerging as superior solution components that cover the needs of various geospatial and remote sensing applications [Romero et al., 2016]. For example, sub-metre spatial resolution has been reached by recently launched satellites such as WorldView-4 [Digital Globe, 2017]. As a result, next generation processing techniques are needed to deal with these next generation datasets.

In line with progress in sensor accuracy, data processing techniques are continually being developed and refined. Machine learning has emerged as a powerful paradigm to extract useful information from data [Tuia et al., 2015]. The algorithms developed have obtained the highest accuracy in computer vision applications especially as the focus has gradually turned to deep learning. Due to its ability to form useful hierarchical representations of complex data, deep

learning has made significant contributions to the field of image understanding [Huang et al., 2015]. It is a perfect match for big data problems [Schmitt and Zhu, 2016] and it has shown high performance levels in classical computer vision problems. However, deep learning algorithms have been used in few remote sensing applications such as classification [Liu et al., 2017] [Kussul et al., 2017], feature selection and extraction [Zhang and Wang, 2015]. The accuracy of the obtained results from the aforementioned applications has encouraged remote sensing communities and scientists to employ deep learning techniques in new domains such as satellite image spatial resolution enhancement and that is reflected on the number of published papers utilising from learning-based methodologies compared with classical interpolation methods [Ball et al., 2017, Mei et al., 2017, Haut et al., 2018, Huang et al., 2017a].

In the context of remote sensing data interpretation, spatial resolution is of vital importance due to the fact that it limits the amount of information to be extracted from a scene. For instance, the accuracy of landcover classification tasks is largely affected by the mixed pixels (refer to Fig. 1.1).

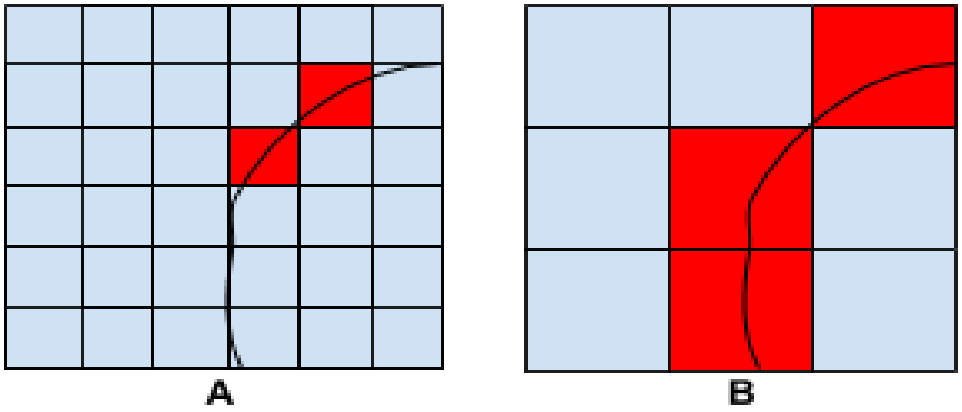


Figure 1.1: A: Landsat-8 (6x6) patch covering area of 8.1km with mixed pixels of .5km, B: Landsat-8 (3x3) patch covering area of 8.1km with mixed pixels of 2.7km

More than 3 decades ago, the term Super Resolution was developed, referring to the construction of higher resolution image from a low resolution input image [Yue et al., 2016]. Super resolution algorithms were exclusively applied to the conventional photos domain until 2001 when [Tatem et al., 2001] used super resolution to map the urban areas using IKONOS [Corp, 2016] scenes at sub-pixel level.

Now, simultaneously with the hype of deep learning since 2015 [Gartner, 2018], the number of papers published utilising learning-based super resolution with remote sensing data is expected to be doubled or tripled. To measure the effect of the deep learning hype on satellite image super resolution applications, an investigation of the Scopus abstract database searching for papers published from 2012-2018 with the phrase ”sub-pixel” OR ”super resolution” AND ”satellite data” in title, abstract and keywords received 111 hits from 40 journals and international conferences. As we can see from figure 1.2, the number of articles doubled from 9 in 2016 to 18 in 2017 while in 2018 the number of articles reached 20. It is clearly noticed that satellite image SR is gaining more attention by remote sensing and computer scientists.

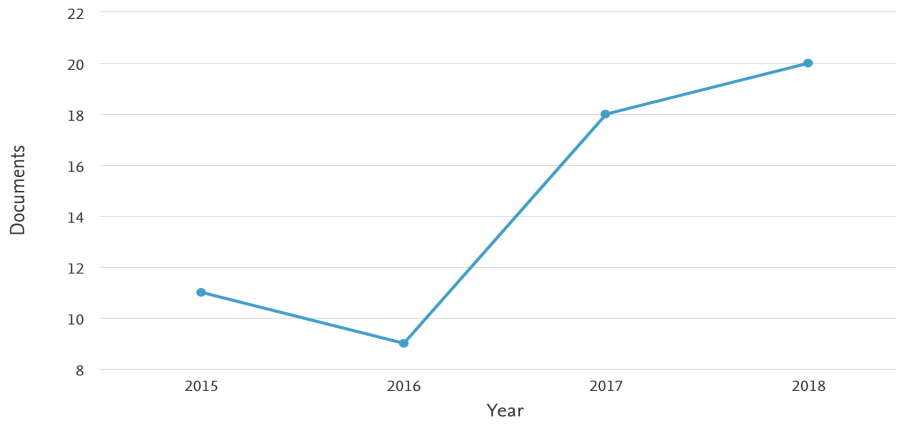


Figure 1.2: Searching hits from Scopus database for ”sub-pixel” OR ”super resolution” AND ”satellite data” in title, abstract and keywords from 2015 to 2018

As a consequence of those advancements in both earth observation data volume and processing techniques, the need for infrastructure that can accommodate both is developed. To fix the broken thread, cloud computing arose as a solution that can host compute-intensive tasks such as deep learning applications and big data storage. As a reaction, space agencies such as National Aeronautics and Space Administration (NASA) [NASA, 2018a] and European Space Agency (ESA) [ESA, 2018a] cooperated with cloud computing providers such as Amazon Web Service (AWS) [AWS, 2018] and Google Cloud [Google, 2018] to host their acquired earth observation data. This step opened the field to harnessing the advancements in processing techniques alongside earth observation data availability.

In line with the aforementioned growth, this thesis focuses on utilising deep learning techniques to super resolve satellite image in addition to addressing the effects of data augmentation techniques in deep learning super resolution tasks. Also, an end-to-end cloud-based framework was developed to enable harnessing of cloud-hosted, low resolution data for super resolution and classification tasks. Moreover, a novel, fusion-based augmentation methodology is developed to improve super resolution accuracy.

1.2 Research questions

This thesis aims to answer the following main question:

"To what extent can remote sensing scientists benefit from deep learning accompanied by cloud computing to support earth observation data processing?"

To answer this core research question, further questions were addressed:
1- How are cloud computing architectures used to enable near real-time EOD processing and algorithms? (chapter 2)

2- How does cloud computing help in automating EOD processing and interpretation? (chapter 3)
3- Utilising deep learning, what is the possibility of enhancing satellite image spatial resolution? (chapter 4)
4- What are some potential ways to boost satellite image super resolution algorithms? (chapter 5)
5- How to validate that satellite image textures and spectral characteristics are not affected after SR? (chapter 6)

1.3 Research Objectives

Having said that deep learning is used to recognise patterns in data in a way similar to the human brain, the assumption is that a machine can predict the missing values in a low resolution scene to produce the high resolution version. This study aims to explore the possibility of enhancing low-to-medium spatial resolution satellite images using deep learning. A complete learning system is developed starting from building a cloud based system to generate the training dataset, until having the final higher resolution output.

1.4 Thesis Contributions

The contributions of this thesis are as follows:

- Highlighting the most recent developments in cloud-based geo-processing services.
- Identifying the most important factors to be considered in cloud computing platforms for the purpose of satellite image processing services.
- Development of a dynamic conceptual data model for geo-processing services based on a cloud computing architecture.

- Development of a near real-time cloud-based land-cover classification service.
- Extending a state-of-the-art Super-Resolution Convolutional Neural Network (SRCNN) algorithm to enhance satellite image spatial resolution.
- A novel fusion-based data augmentation technique was introduced to increase satellite image super resolution accuracy.
- Increasing the frequency of land-cover change monitoring by super-resolving Landsat-8 (30 meter) to be used with Sentinel-2 (10 meter).

1.5 Background

This section reviews the required background to gain understanding for this thesis. Subjects reviewed include the evolution of remote sensing big data, cloud computing services which can harness remote sensing big data processing tasks, machine learning methodologies which can be utilized in remote sensing data inferences, super resolution as an applied concept to enhance spatial resolution of satellite data as well as crowd-sourced data as an aiding factor in deep learning tasks.

1.5.1 Remote sensing big data

The terminology Big Data refers to any source of extremely massive data volumes which exceeds the capacity of our conventional database systems. In its special report for 2014, Gartner's hype cycle categorised Big Data as the peak of Inflated Expectations and going through the Trough Disillusionment stage (See Figure 1.3).

This tells us that not only Big Data is a hype but also the market is already mature enough to realize how Big Data could be useful for organizations. This

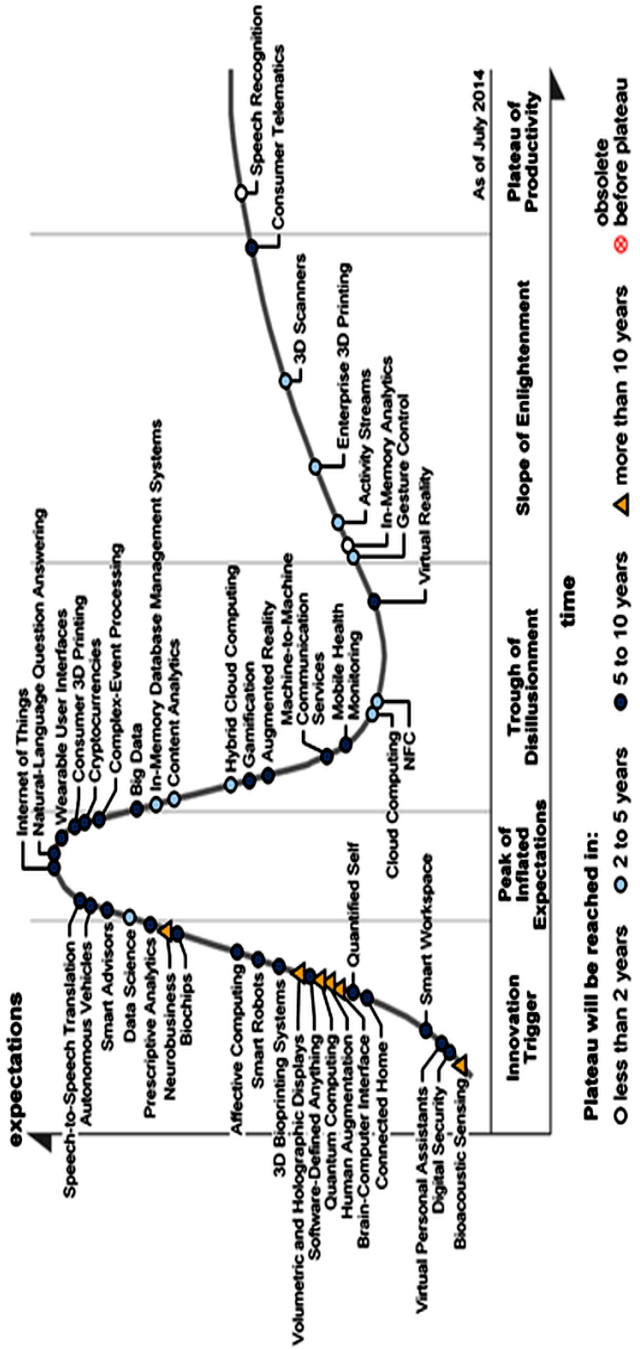


Figure 1.3: Gartner hype cycle for emerging technologies, 2014.

applies to any kind of sensor which is producing any data format whether images, videos, text or even voice. Currently we are witnessing a tremendous wave of data coming from the space. Hundreds of Tera-bytes of remotely sensed signals are being received at ground stations. The operating satellites immerse us with all kinds of needed datasets about land-cover, land surface temperature, wave height, ocean color and many more. Varying low to Very High Resolution (VHR) datasets are being acquired by different sensors observing different regions of the earth. The variation here is reflected on the 5 V's model of Big Data which can be described as follows:

Volume

The growing number of orbiting satellites accumulate to the amount of daily collected Earth Observation Data (EOD). For instance, Landsat-8 scene is around 2 GB of data and this represents only one scene which covers area around 170km x 185km. Taking into consideration that Landsat-8 is just one of hundreds of operating satellites sending back EOD, this resulted in having a massive amount of data that could be used to derive useful information and provide better understanding about the Earth.

Variety

From the perspective of spatial scale, variety is concerning the various resolution accuracy offered by different types of operating sensors. Spatial resolution refers to the smallest object that could be distinguished from the space. Some high resolution satellites such as WorldView-2 [Satellite Imaging Corp, 2018] offers .46m while others with low resolution such as Moderate Resolution Imaging Spectroradiometer (MODIS) has 250m spatial resolution and every level serves specific types of applications. While from a spectral perspective, a satellite can carry different types of sensors such as Landsat-8 which carries Operational Land Imager (OLI) sensor for spectral bands and Thermal Infrared Sensor (TIRS) for thermal bands which measure the surface temperature.

Velocity

The velocity of remote sensing data can be reflected by temporal resolution. Which means how long does it take from the satellite to capture the same scene. For instance, Landsat-8 takes 16 days to revisit the same spot, while MODIS takes 1 day. Another viewpoint that may reflect the velocity characteristic is the consumed time since taking the scene to make it ready for users to download and utilize it. Landsat-8 and Sentinel-2 are available for usage after few hours from capturing the scene [AWS, 2017a, AWS, 2017b].

Veracity

One of the most important aspects of Big Data in general and Remote Sensing Big Data specifically is the veracity. Sensor readings from the space are usually associated with distortions, uncertainty and accuracy measurements that needs to be validated. For instance, cloud coverage in Landsat-8 scenes.

Value

Accumulating that amount of multi-dimensional data paved the way to yield useful information. However, to make a good use of remote sensing big data and increase its value, we need to have enough capacity to extract information and meanings from such massive data. The capacity here referring to the computing power that is capable of dealing with such big data in addition to processing algorithms that can extract meaningful information.

Conclusion

Taking into consideration the above characteristics, the need to have platforms that can accommodate the aforementioned data is developed. On the same line, Computing and storage capacities are getting well improved due to the rise of Cloud Computing era recently. In the next section, we will explain how cloud computing paradigm aided in exhibiting the value of earth observation big data

and the different types of cloud computing layers which facilitated the development, hosting and deployment of EOD processing services.

1.5.2 Cloud computing

The cloud computing paradigm appeared as an approach that allows storing, processing and networking on multiple nodes instead of single machines which fostered big data advancements [Bastian et al., 2010, Yang et al., 2016a]. It provides end-to-end solutions for big data applications including collecting, storing, managing, processing, analyzing, understanding and visualizing data. Moreover, cloud computing is affordable at pay-as-you-go pricing model which saves a lot of cost in addition to offering scalability options. SAAS, PAAS and IAAS are considered the backbone of such elastic model. We can describe them as follows:

Software As A Service (SAAS)

This is the highest level of abstraction in cloud computing architectures and the most used tier. It provides the functionality of any sophisticated application through the web browser utilizing from the scalability and elasticity options. For example, converting landsat data from raw values to top of atmosphere (TOA) on Google Earth Engine [Google, 2018].

Platform As A Service (PAAS)

PAAS model affords every tool needed to develop and deploy any piece of software used through the browser. Google Earth Engine also provides the capability to write your own software and run the application using only web browser. The platform is meant to support the developer with all needed tools starting from writing the code until launching the software.

Infrastructure As A Service (IAAS)

This is the lowest layer in cloud computing architecture. It delivers all the needed processing cores, storage disks and networking virtually to the users and its their responsibility to develop and deploy all required software to use the allocated resources.

Conclusion

Cloud computing offered a variety of solutions to serve the big data eruption. Alongside with the big data, the way is paved to implement extensive algorithms to extract useful information from EO data. In the next section, data processing growth is explained in terms of depth and capabilities to extract meaningful insights from data.

1.5.3 Machine learning

Machine learning is a member in the artificial intelligence family of approaches in which the developed algorithms are meant to learn from data. The learning here is an automated process without writing explicit instructions to determine the behavior of the application. e.g. autonomously drive cars. Remote sensing applications also adopted machine learning algorithms nevertheless classification is the dominating utilization. In this section, we will explore different types of algorithms categorized by the learning method.

Supervised machine learning

Supervised learning is the most used approach in machine learning especially practical projects. It depends on learning the mapping functions between input data X and output target Y. The model/algorithm should be able to learn $f(X)$ in order to get Y. The main idea is to have the best mapping function after the training phase so that the model can predict with high accuracy when it gets a

new input data. In a classification problem, the input X data might be 20X20 pixels cropped samples form a satellite image, while the labeled data Y might be class number e.g.1 = Vegetation, 2 = Water etc. The model should be able to classify any new sample that is cropped from different satellite scene with high accuracy. The supervised learning method is problematic due to the need for labeling data step. The unsupervised learning method on the other hand draws inferences from input data without the need to have labeled/target data as we explain in the next few lines.

Unsupervised machine learning

Unlike supervised learning method, the unsupervised learning doesn't need labeled data to learn the mapping between input data and output prediction. It aims to learn the structure and distribution of the data without looking at the target. Clustering is one of the most noted problems to be solved by unsupervised learning technique like K-means.

Semi-supervised machine learning

In between supervised and unsupervised learning methods, the semi-supervised learning methodology is useful when there is a large amount of training data but only some of it are labeled. In such case, the unsupervised technique is used to learn structure of the input data, then the supervised learning could be used to make predictions of unlabeled data so that it can be added as a labeled training data. Following that way, the labeled data are increased and can be fed to the supervised algorithm to boost the accuracy of predictions for new unseen input data. This process can be achieved using several ways such as label propagation or spreading models [Chapelle et al., 2006].

Deep learning

Inspired by the explosive computational growth, deep learning emerged as an advanced subset of machine learning which aims at analysing data using a logic similar to how the human brain represents and processes information. In order to achieve this, the design of the training models is structured as layers. Every layer is extracting features that helps in predicting the target data. The architecture of Deep Learning models corresponds to a subset of Artificial Neural Networks (ANN) with a sufficiently large numbder of layers which mimic the biological neural networks of the human brain.

Conclusion

Deep learning is the lifeline which assimilated all the recent advancements in both data and computation capabilities. The current achieved accuracy in different problem domains encouraged remote sensing community to utilise ANN and other DL techniques. In the literature review chapter, the applied methodologies are explored.

Super Resolution

Due to the aforementioned appealing signal processing techniques, a set of resolution enhancement methodologies arose which are able to increase the resolution to a greater extent than traditional image processing functions. The traditional processing includes interpolation methods such as bilinear and bicubic interpolation. In order to obtain high-resolution version, those interpolation techniques compute the missing intermediate pixel values by averaging the original low-resolution image with fixed values. The SR techniques are more ambitious as it aims at estimating the missing high-resolution details which are not present in the original high resolution image. In this thesis we are targeting the learning-based SR methodology in which the algorithm attempts to learn the mapping function between pair of low and high resolution images.

Crowd-sourced Data

Volunteered geographic information can play an important role in both processing and validation of EOD. It has been allowing citizens to participate in urban planning and mapping activities. For instance, in [Fritz et al., 2012] crowd-sourced data are used to generate a global scale landcover maps while in [Schepaschenko et al., 2015] a forest cover map is created using satellite images and validated using crowd-sourced data. In this thesis crowd-sourced data are used to train and validate landcover classification task to measure the effect of super-resolving satellite images.

1.6 Thesis Structure

The rest of the thesis is organised as follows:

1.6.1 Chapter 2: Literature review and state-of-the-art

In this chapter we explain into details cloud computing models. Moreover, The utilisation of cloud computing platforms in remote sensing big data processing is reviewed to assess the integrity and usability perspectives. This chapter is based on a published paper in the proceedings of International Conference on Space Science and Communication (IconSpace) 2015. However, the manuscript here is updated to match with the most recent updates in the field especially the appearance of Google Earth Engine as a platform for remote sensing data processing on the cloud.

1.6.2 Chapter 3: Integrated cloud-based framework for remote sensing big data processing

This chapter presents the achieved work to build an automated cloud-based framework to download, store and process satellite images once received at

ground stations. The processing framework is used to classify Landsat-8 imagery using SVM supervised classification algorithm in addition to generating training datasets which is a problematic step in any machine learning application. The classification task will be used later in chapter 6 for validation of a deep learning algorithm while the training dataset creation task will be used in chapter 5 to train the deep learning model. This work is based on a published paper in the International Journal of Geoinformatics 2016. However, the manuscript here is updated to fit with the most recent developments in the field.

1.6.3 Chapter 4: Satellite image spatial resolution enhancement as a service

In this chapter, we explain how deep learning techniques accompanied with EO big data and cloud computing can be used to enhance spatial resolution of satellite images. Various resolution enhancement approaches were explored in detail with particular focus on super resolution using deep learning techniques. We demonstrate how to re-train and fine-tune a convolutional neural network which was tested originally to super-resolve conventional photos to fit with satellite image super resolution purposes.

1.6.4 Chapter 5: Boosting accuracy using data augmentation techniques

This chapter presents a novel data augmentation approach to increase the accuracy of satellite image resolution enhancement algorithms. We propose a fusion-based augmentation approach which can support super resolution model with useful data representations at early stage of training. Moreover, we compare several augmentation techniques including the traditional augmentation approaches. This work will be presented in Living Planet Symposium 2019.

1.6.5 Chapter 6: Evaluating Super Resolution Accuracy via Landcover Classification Tasks

Chapter 6 proposes integrated evaluation approach which can harness super-resolved Landsat-8 and Sentinel-2 products alongside crowd-sourced data to derive continuous monitoring of the Earth at refined spatial and temporal resolutions. The evaluation of Landsat-8 super resolution accuracy involved producing landcover classification maps and accumulating it to Sentinel-2 classification maps to increase the frequency of landcover production for the same AOI. This chapter is partially based on a published paper in FOSS4G 2015.

1.6.6 Chapter 7: Conclusion and future work

We summarise the thesis work and draw a conclusion and road-map for future work to deal with remote sensing big data and deep learning techniques.

Chapter 2

Cloud Computing Providers for Satellite Image Understanding Services

2.1 Background

Remote Sensing technologies have a wide scope of applications. Whether urban planning, agriculture, environmental management, or climate change, remote sensing products are the indispensable sources of information in our daily life activities [Robila, 2006]. In the past, lesser remote sensing data were available and limited in spatial, spectral and temporal resolutions. This limitation made it difficult to analyse data and derive the proper information about the Earth surface [EIJ, 2018]. Recently, the picture was changed. Earth Observation Systems (EOS) became more advanced and complicated. According to the Index of Objects Launched into Outer Space which is maintained by the United Nations Office for Outer Space Affairs (UNOOSA) [UNOOSA, 2018] the number of currently operating satellites is 4921 and expected to be increased very soon since there will be launching soon for Landsat-9 [NASA, 2018b].
According to the mission and objectives, satellites are equipped with instruments

and sensors for collecting data and communicating it back to the Earth. These advanced sensors generate higher spectral and spatial resolution images than before, which can contribute effectively in better understanding of the Earth as an integrated system. Subsequently, different Earth Observation datasets (EOD) became more complicated with respect to structure and much bigger in terms of size. In terms of size, for example Landsat 5 uncompressed scene size is 366MB approximately whereas Landsat 8 scene size is 5 times more (greater with 2 GB). From dimensionality perspective, Landsat 8 scenes have 16-bit pixel value with 11 bands while Landsat TM and ETM+ have 8-bit pixel value with 6 and 7 bands, respectively.

As reported by NASA, Landsat 8 is acquiring 400 scenes per day [NASA, 2018a] which means the ground stations are expected to receive approximately 1 TB from only one satellite per day. This can easily give rise to the broad term Big Data which is the key basis for productivity growth, innovation and better understanding. Considering the main characteristics of Big Data, Volume, Variety and Velocity "3Vs" act as a challenge for remote sensing scientists and experts nowadays [Ye et al., 2013, Cavallaro et al., 2015]. Volume describes the data size and Variety means different types of satellite images while Velocity means how fast data are being created.

In the matter of Volume, bear in mind that the above approximate estimation is per 1 satellite per day while as reported by [Tatem et al., 2008], there are approximately 160 operating EO satellites now in Earth orbit. With reference to Variety, the current operating satellites are carrying sensors with different spatial, spectral and temporal resolution which can capture various images types. Temporal resolution is considered as the main factor which determines the velocity characteristic of EOD. Satellites have different temporal resolution starting from low $>$16 days to revisit same place, to high temporal resolution $<$24 hours [Corp, 2018]. Accumulating these advancements can help in better understanding of image objects and interrelation among them.

In order to process and analyse this vast amount of data, it is not possible to use

traditional storage servers and computing power. Previously, traditional servers were being used to process EOD. Nevertheless, these servers were very limited in terms of hardware capabilities and it was very expensive to upgrade servers hardware.

Fortunately, starting from 1990s, High Performance Computing (HPC) technologies played an important role in utilizing remote sensing data in general [Zhang, 2010] [Plaza et al., 2011].

However, HPC main focus is to take advantage of every ounce of resource without considering the big picture which includes also scalability and storage space [Scaling, 2018]. Most of HPC systems are relying on network attached file systems to store data and don't have major attached storage capacity.

Moreover, scalability options here can't exceed the HPC/supercomputer limitation [Chavarr et al., 2012]. For these aforementioned reasons, HPC still lacking elasticity and scalability options which motivated remote sensing scientists to search for more suitable solution.

Between 2000 to 2006, the term cloud computing has come into existence and NIST [NIST, 2018] defined it as a model which enables convenient and on-demand network access to a shared pool of computing, storage and other resources with configurable settings. Hence, cloud computing considered as a convenient solution since it provides resilient storage capacity and elastic computing services in form of Software As A Service (SAAS) Platform As A Service (PAAS) and Infrastructure As A Service (IAAS) models. Also, Cloud Computing can reduce the costs, since it's possible to pay as use and on demand [Xiaoqiang and Yuejin, 2010] instead of purchasing advanced hardware and software licenses to process EO Big Data. Many research studies conducted to find out how can cloud computing models fit with remote sensing applications and what are the gained benefits from utilizing IAAS, PAAS and SAAS models [Kiemle et al., 2016, Gançarski, 2014]. However, still the current research has only scratched the surface of using Cloud Computing for EO big data processing.

Most of complete and on-going researches so far were targeting either feasibility of using Cloud Computing for processing geo-data (mainly vector format) in general or just a few specific satellite image processing tasks like NDVI calculation, satellite image sharpening, filtering, classification and DEMs. [Almeer, 2012, Yang, 2011, Huang et al., 2013, Wang, 2011, Padarian et al., 2015, Huang et al., 2010, Golpayegani and Halem, 2009, Niggemann et al., 2014, Pan and Zhang, 2013, Chen et al., 2012a, Wang et al., 2013]. It infers that this research topic is still in its early stage. In the next section, cloud computing providers who supported earth observation data processing activities are reviewed. After careful consideration, Amazon Web Services (AWS) [AWS, 2018] and Google Earth Engine (GEE) [Gorelick et al., 2017a] appeared to be the most dominating platforms in cloud computing in general and EO data processing particularly. As we published in [Ghaffar and Vu, 2015] indicating that Amazon AWS, Microsoft Azure and CloudSigma platforms were the most dominating in 2014, in this manuscript we updated the cloud computing providers to include Google Earth Engine since it emerged to replace many providers nowadays.

2.2 Literature Review

To cope with the advent of advanced earth observation systems, recent developments in geo-processing have adopted both HPC and cloud computing platforms. Mascolo et al [Mascolo et al., 2014] implemented a tool for data analysis and content-based retrieval of polarimetric SAR data on top of public cloud computing services. Given the difficulty that might be faced when rely on single machine to analyse these large scale datasets, Mascolo et al used Apache Spark on top of Amazon EC2 elastic infrastructure. Moreover, machine learning algorithms were involved to create indexes and store products in a database. The system works efficiently with scale of 0.6 Petabyte of images and archived data. However, the comparison of the performance between different approaches or

architectures wasn't reported.

Ferrer and Symonds [Marc Ferrer1, 2014] presented an overview of PaaS Platform as a Service specialized in earth observation through a project addressing Oil and Gas market. Using Helix Nebula [CERN, 2018], Ferrer and Symonds utilized cloud computing infrastructure assets like scalability, failure management and data sharing. From software perspective, they preferred using distributed processing and computing clusters, and for monitoring resources they proposed Ganglia to keep tracking hardware real time utilization and performance. Likewise, Goor [Goor, 2014] presented a web-based application Vito-EOData, which is built using a stack of technologies to improve the performance of the infrastructure of Earth Observation data exploration systems and provides on-demand data processing. This stack included Hadoop as a distributed processing framework, cloud computing paradigm which enables scalable and dynamic resources provisioning, tools and frameworks like NoSQL, MapReduce, OLAP and Rasdaman array based raster data management system. Erwin indicated that this novel approach was required to cope with current evolution and continuous growing of earth observation data.

In [Yu et al., 2016], Wenyang et al utilized cloud computing to host multi-modal environmental monitoring platform. NDVI, NDWI and MODIS Terra MOD09A1 [USGS, 2018b] datasets are scheduled for downloading, preprocessing, and information extraction via automated engine. Moreover, Wenyang et al studied the integrity between cloud computing infrastructure and multi-source remote sensing big data to build on-demand processing services. Wenyang et al reported how cloud computing helped in overcoming the data-intensive processing applications in the field of remote sensing.

Niggemann et al [Niggemann et al., 2014] presented APPS4GMES system which is built on top of cloud computing IaaS "Infrastructure As A Service" model to overcome the big data processing challenge and provide dynamic and automated processing of EO data through a new design of architecture utilizing computing power and storage capacity of cloud computing.

As shown in Figure2.1, APPS4GMES architecture allows using cloud computing infrastructure to host all services related to water quality and quantity analysis, agriculture, environment and fire monitoring REDD. The entrance point for the user/client comes through APPS4GMES portal and initiating requests over OGC WMS, WCS, WFS then the services chain manager starts calling the intended service and retrieving metadata and cached raster data if found. The proposed architecture performance was compared with standard desktop machine configured with Windows 8 operating system, 4 CPUs 3.7GHz and 8GB Ram. While the cloud infrastructure equipped with 5 Ubuntu 12.10 64bit virtual machines with 40 X 2.9GHz CPUs, 30GB Ram and 300GB HDD storage. Niggemann et al experimented the atmospheric correction using MODTRAN followed by supervised land use classification for 40 Landsat 8 scenes covering the whole Germany soil, snow, water, cloud, cloud-shadow, coniferous forest and vegetation.

Table 2.1 shows the downloading and processing time spent on desktop and cloud virtual machine environments. It is obvious that cloud solution is much

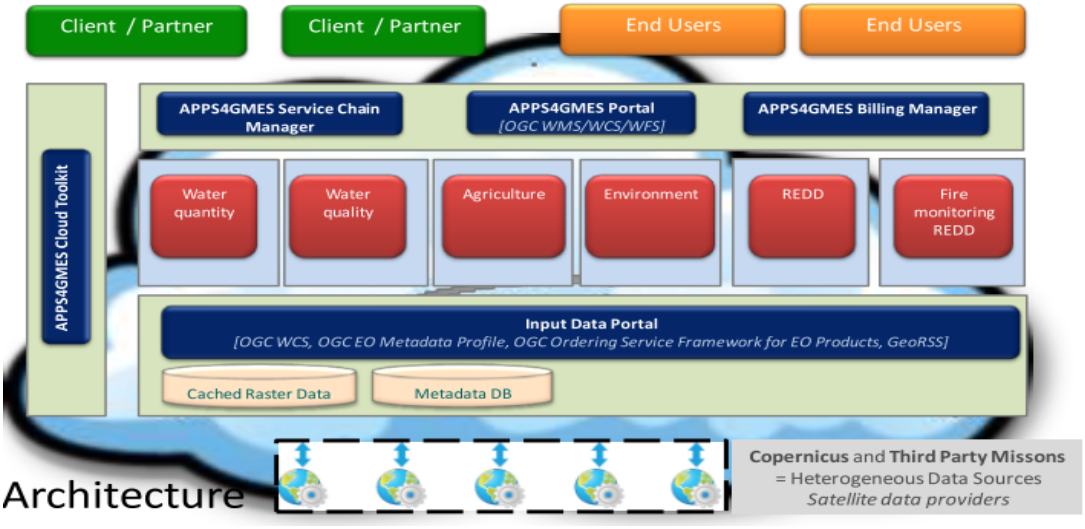


Figure 2.1: APPS4GMES Architecture [Niggemann et al., 2014]

better than standalone desktop in terms of processing and downloading time. However, the study did not employ more complicated algorithms on Landsat-8 datasets.

In [Kristof et al., 2014] Kristof et al worked on same direction to migrate

Table 2.1: Processing times for 40 Landsat-8 scenes

Item	Desktop	Cloud VM
Download [min]	65	25
Processing [min]	325	33
Total [min]	390	58

Geo-big data processing from traditional servers to cloud computing infrastructure. As a case study, they discussed how to enhance the performance of IQmulus project [Project, 2018] by shifting to cloud infrastructure. Based on specific development and enhancement directions, they figured out remote sensing big data processing challenges by adopting distributed processing and data partitioning techniques. Kristf et al relied on Apache Hadoop [Foundation, 2018] which includes 2 major components, Hadoop Distributed File System (HDFS) and MapReduce framework. They indicated that the developed workflow enabled faster processing in comparison to the original solution, however they did not report any quantitative measurements about those enhancements. In a study of Almeida et al [Almeida et al., 2014], they asserted the benefits from using cloud computing as infrastructure through a real world project SenSyF which is a cloud based framework to process Sentinel and Copernicus data. SynSyF framework offers the developers a platform to implement and test applications before turning them to distributed pool of cloud computing resources. Software Development Kit (SDK) is built on top of the processing infrastructure and integrated with the SenSyF Sandbox [SenSyF Project, 2018] environment including GDAL, NEST, BEAM, GRASS and ORFEO tools. Results showed superiority of cloud computing approach in

comparison with traditional sequential processing. However, the selected processing tasks were still considered simple without applying more complicated algorithms. Febrier et al [Febrier and Montmory, 2014] believed that the recent Earth Observation data flood can be mastered using big data technologies and cloud computing paradigm. Recommendations based on previous experiences and learned lessons from using cloud computing services are shared through Thales Open Space GEO-Cloud project.

In [Xing et al., 2014] cloud computing services are used to build Geospatial Cyber Infrastructure (GCI) capable of hosting 312 GB of high resolution aerial photos in addition to processing services to segment, detect and recognize any artefact. Xing et al preferred the use of cloud computing as a platform as it is considered the standard platform for analysing big data. In order to evaluate the performance, two different environments were experimented, public cloud Amazon Web Services and private cloud Eucalyptus platform. Public cloud refers to that type of service which doesn't include any responsibility from the user towards the management of resources as everything is at the vendor's side while private cloud infrastructure and management resides on company's data center.

In [Xing et al., 2014] both clouds were configured with the same capabilities except that physical CPU, storage, memory and network are infinite in public cloud but limited to 4 Intel six-core XEON E52620 2.0 GH, 64 GB, 1 Gbps and 4 TB in the private Eucalyptus platform as mentioned in Table 2.2.

In terms of scalability and cost, private cloud was considered as a better option with less cost and computation time, however it could be argued because private cloud is limited in terms of scalability options which are available easily in public cloud services. Moreover, the upfront cost of building private cloud is very high and authors did not mention the actual cost of purchasing and setting the private cloud infrastructure.

Bastian et al [Bastian et al., 2010] came up with a concept of SDI Spatial Data Infrastructure based on cloud computing paradigm and presented a real world

Table 2.2: Public and Private Cloud Environment

Item	**Desktop**	**Cloud VM**
Physical CPU	Four Intel six-core XEON E52620 2.0 GH	N/A
Virtual CPU [min]	One for map VM and four for reduce VM (One VCPU = 2.0 GHz 2007 Xeon processor)	One for map VM and four for reduce VM (One VCPU = 2.0 GHz 2007 Xeon processor)
Physical Memory	64 GB	N/A
Virtual Memory	3.75 GB for map VM and 15 GB for reduce VM	3.75 GB for map VM and 15 GB for reduce VM
Physical Network	1 Gbpbs	N/A
Virtual Network	1 Gbpbs for all VMs	Medium for map VM and high for reduce VM
Physical Storage	4 TB	N/A
Virtual Storage	410 GB for map VM and 80 GB for reduce VM	410 GB for map VM and 80 GB for reduce VM
OS	CentOS 6.4 10	CentOS 6.4
VMs	10 map and 1 reduce VMs	10 map and 1 reduce VMs computation

use case as a proof of concept which benefits from the scalable cloud infrastructure as a service model. Bastian et al identified the current obstacles facing SDI development as upfront costs, mass market requirements and legally binding performance allowances. Hence, cloud computing is considered as a convenient solution to face these challenges. However, it could be argued that even approaching cloud computing paradigm can't solve the upfront costs since it depends on the type of the implemented cloud solution whether private cloud or public one. As a real world use case, Bastian et al implemented a scenario of public risk management system to asses a fictive fire threat in Tasmania to create highly scalable solution using in-situ-sensor data analysis. Amazon Web Services are used with OGC Web Processing Service (WPS) to offer calculating

buffer and intersection processes. The service was deployed using EC2 instances and the following rules were applied:

- Only one instance is running continuously
- 12 is the maximum number of instances to run simultaneously
- If CPU workload is less than 20% in 30 seconds interval, the number of running instances will decrease by one
- If CPU workload reaches more than 50% in 30 seconds interval, the number of running instances will increase by one

The purpose behind setting the above rules is to test the scalability features of Amazon EC2. Moreover, stress test is used to evaluate the peak load time by increasing the number of concurrent requests on 2 different infrastructure environments, cloud-based SDI and a local machine hosting the same service.
Figure 3 shows when the number of requests increases from 1 to 200 on top of both infrastructures. It is obvious that the normalized response time grows linearly on top of the local non-cloud WPS while stays nearly constant using the cloud based SDI. The EC2 automated scalability option here prove that cloud computing is a convenient option to be adopted with SDIs.
Nonetheless, authors here paid attention to spatial and in-situ-sensor data only without mentioning big data or utilizing the real power of computing that the cloud offers. The point here was the latency in response time from the WPS and the server depends also on how the Apache Tomcat server configured more than the computing power and scalability. Especially, they evaluated the cloud based SDI using just 200 requests which is still not considered heavy enough load.
Yunqin et al [Zhong et al., 2012] proposed a framework (VegaCI) to integrate raster and vector Geospatial data using cloud based infrastructure and distributed data storage system to process massive geospatial data sets.
In line with current evolution of geospatial and remote sensing data size, Yunqin

et al designed scalable cloud-based architecture to overcome data storage and processing challenges. The system utilizes distributed storage and parallel processing techniques like HBase and Hadoop to handle more than 930GB of vector and raster datasets to perform processing tasks e.g. ANN, kNN, RNN. Vector data structured as WKT and WKB and covering 218,611,357 POINT, 58, 149,873 LINE and 9, 097,126 POLYGON objects while raster datasets contain 89,372, 583 tiles including 6 map scales with maximum resolution of 1:5000. Yunqin et al configured the system environment with 9 nodes, each node consisting of two quad-core Intel CPU 2.13GHZ, 4GB DDR3 RAM, 15000r/min SAS hard disk driver, 300GB. And software configuration includes CentOS5.5, JDK1 ȯ.0 _ 20, MySQL- 5.1 .49, PostgreSQL-9.0.5, PostGIS- 1.5.3, Oracle Database 11g Release 2 and HBase-0.90.3 to make comparison with different types of clusters like PostgreSQL 9.0 and Oracle Database 11G.

Figure 2.2 shows the differences in performance between PostgreSQL, Oracle clusters and the proposed cloud based architecture (VegaCI) in performing ANN, kNN k=5, kNN k=10, rNN algorithms using 5 nodes configured as mentioned above. It is noticeable that VegaCI has the least spent time to process all proposed algorithms compared with PosgreSQL and Oracle clusters.

On the other hand, to check the scalability of the proposed architecture, they used LoadRunner to check the load balance and applied another experiment by increasing the number of users/requests from 50 to 300 in 30 minutes duration (refer to Fig. 2.3).

Similarly, Angel et al [Ferrn et al., 2013] agreed that satellite images nowadays are massive and need advanced processing tools to handle those huge datasets. Accordingly, they presented a web-based system for classification of remote sensing data to allow inexperienced users to perform unsupervised classification. The system architecture relies on 3 layers as follows, Client, Server and Map layer.

Map layer implemented using Google maps API (Application Programming Interface) to let the user choose which scene to be processed. From processing

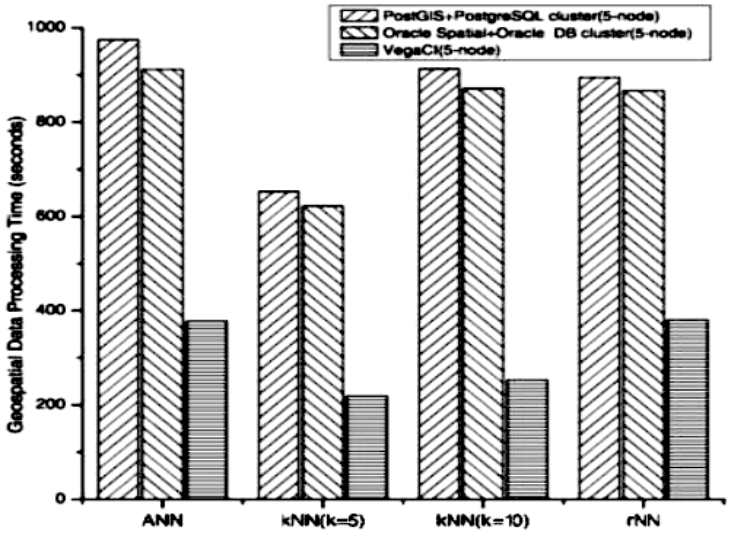


Figure 2.2: Comparison of geospatial data processing performance by [Zhong et al., 2012].

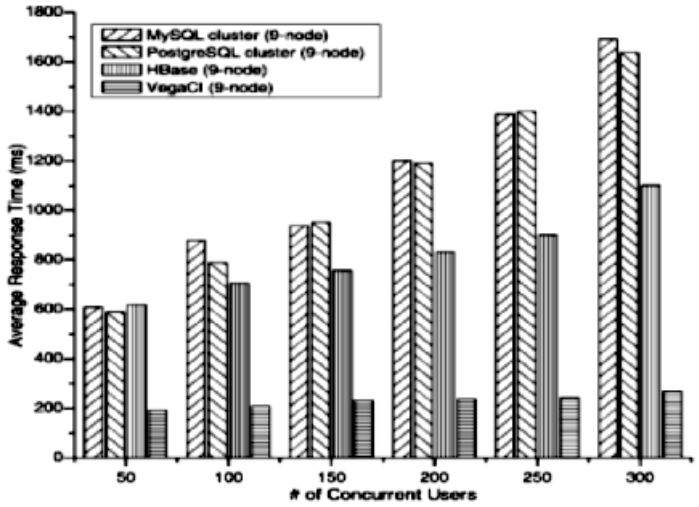


Figure 2.3: Scalability evaluation.

perspective, K-means and ISODATA algorithms are supported.

They proposed a system works as follows:

A client initiates an HTTP request via WMS/map layer. The system captures the URL associated with input parameters that will be used in data processing on the server. The system will access Google maps repository to retrieve the requested images in order to be processed. Once the server finished processing, the results will be presented to the user on the browser with a link to download results on their local machines (See Figure 2.4).

However, the presented system works only with limited spectral-bands data like Google map images in which, simple classification algorithms like K-means and ISODATA were sufficient.

Almeer [Almeer, 2012] compared between utilizing cloud computing and using single PC to apply different image processing algorithms. Image processing tasks including Sobel filtering, image resizing, image format conversion, auto contrasting, image sharpening, picture embedding, text embedding, and image quality inspection are evaluated. In order to evaluate the performance, two

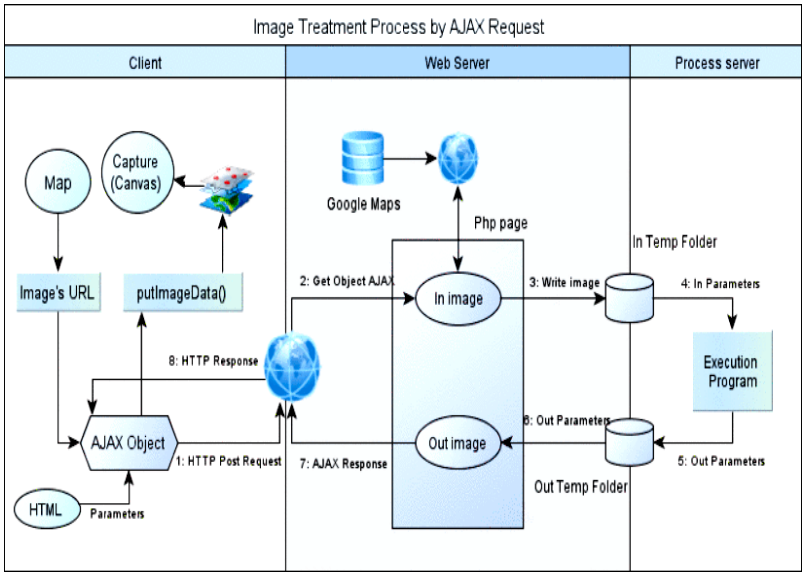


Figure 2.4: Angel et al [Ferrn et al., 2013] system architecture.

different environments were configured to serve that purpose. First environment was Apache Hadoop [Foundation, 2018] cluster based on IBM BladeCenter cloud infrastructure equipped with 112 physical cores and 7 TB of storage. Hadoop cluster was configured with 1 Name Node and 8 Data Nodes and every machine configured to use 2x 2.5 GHz CPUs, 2 GB of RAM and 130 GB of disk storage. In addition, all the computing nodes were running on Red Hat Linux 5.3, Hadoop 0.20.1, and Java 1.6 were installed. Second environment was configured as standalone personal computer with Intel Core 2 Duo CPU, 2.27 GHz, 4 GB of RAM and 130 GB disk space.

Algorithms were applied to Landsat images with 16669 x 8335 pixels in TIF format and 1GB size per image. Although Hadoop is a framework which is designed to allow distributed processing of large data sets across clusters of nodes, it was originally built to process text. But Almeer customized the source code to allow Hadoop work with different input format like TIF images. Almeer considered the elapsed processing time as the sole performance measure in his experiments and he compared the time taken by the single PC with the cluster to observe the speedup factors and finally analysed the results.

Almeer applied very simple algorithms related to image enhancements like: sobel filter and image sharpening, also he focused more on processing time than the number of images processed. However, Hadoop MapReduce framework is designed to split big files into chunks to utilise parallel computation across MapReduce tasks. Conversely, Almeer eliminated splitting function and extended MapReduce default behaviour to deal with the satellite image file as a whole which could affect Hadoop performance.

Similarly, Zeqiang et al [Chen et al., 2012b] implemented a Web Processing Service (WPS) on top of Hadoop cloud environment to process Moderate Resolution Imaging Spectro-radiometer (MODIS) data. The main objective of this paper was to group WPS with cloud computing to process Earth Observation Data (EOD). Zeqiang et al designed a system allowing users to calculate Normalized Difference Vegetation Index (NDVI) for MODIS data on the cloud.

Three processing services including daily NDVI, weekly NDVI and coordinates converter were implemented to test the framework. Although the processing tasks were limited to just simple algorithms like NDVI calculation, the feasibility of integrating cloud computing platforms with Earth Observation Data (EOD) processing services was validated.

Similarly, Huang et al [Huang et al., 2013] used cloud computing Infrastructure As A Service IAAS to build dust storm forecasting system using NMM-dust model. Huang et al presented a comparison study between using High Performance Computing (HPC) and cloud computing to host the developed model. The comparison included computing capacity and cost aspects between Amazon Elastic Compute Cloud (EC2) and traditional HPC cluster. Table 2.3 shows the computing environment setup for both EC2 and HPC clusters.

EC2 cluster has unlimited number of computing nodes with 2.93 GHz per CPU, every single node has 2 processors and every processor has 4 cores while the traditional HPC cluster limited to 28 nodes with 2.33 GHz CPU. Every node has 2 processors and every processor has 4 cores. To compare between EC2 and HPC clusters performance, 15 forecasting tasks run simultaneously on both of systems. And the results show that Amazon EC2 cluster has a better performance

Table 2.3: EC2 and HPC computing environments [Huang et al., 2013]

Items	**EC2 cluster compute instances**	**HPC cluster**
Nodes	theoretically unlimited	28
CPU	2.93 GHz	2.33 GHz
Number of processors	2	2
Number of cores/processors	4	4
Support hyper-threading	Yes (resulting in 16 CPU cores in total)	No
Total memory	23 GB	16 GB
Network bandwidth	10Gbps	1Gbps
Virtualization	hardware-based virtualization	N/A

than the traditional HPC. From computing capacity perspective, Fig. 2.5 shows NMM-Dust execution time of both EC2 and HPC clusters.

It is obvious that EC2 consumed less time than HPC cluster which means that cloud computing has high probability to take over from traditional HPC and servers. From economical perspective, its observed that HPC cluster running cost per hour is much higher than EC2 cloud solution (896 times!).

In [Mandal et al., 2018], Google Earth Engine cloud platform (GEE) [Gorelick et al., 2017a] was used to build a processing chain to recognize different stages of rice plantation. The authors indicated how the integration between the intensive computing power and earth observation big data was worthwhile. Google's platform as a service (Earth Engine) is equipped with many EO datasets e.g. Sentinel, Landsat and MODIS. This allows users to access the datasets directly without the need to download them locally.

Similarly, [Chen et al., 2017] used Google Earth Engine to process nearly 3600 Landsat-8 scenes to map glacial lake changes in Tibetan Plateau. Given the vast amount of data and processing power required to achieve the study goals, authors in [Chen et al., 2017] reported the inevitable need for cloud computing.

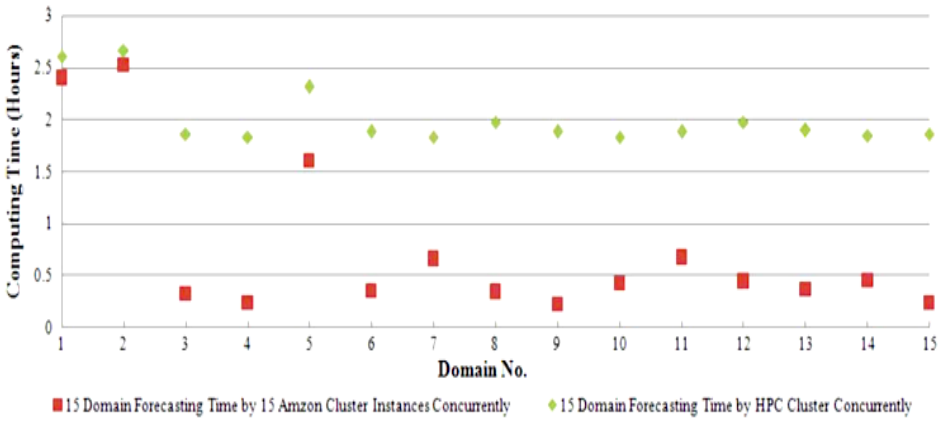


Figure 2.5: Execution time for 15 forecasting tasks on Amazon EC2 Vs. HPC cluster in [Huang et al., 2013].

Likewise, [Shelestov et al., 2017] et al utilised GEE to explore the efficiency of cloud computing capabilities in crop classification tasks. Several algorithms were used to map crops in Ukraine which required a large amount of EO data as reported by the authors. GEE enabled the accessibility to remote sensing products and overcame the big data problem using powerful computational resources.

On the same line, [Mateo-Garca et al., 2017, Saranya and Muralidharan, 2017, Celik, 2018, Xu and Bai, 2015] listed many reasons to take GEE as a platform for building their processing services as follows:

- The GEE platform broke down the computation burden of building intensive processing tasks on multiple Petabyte satellite datasets.
- Users are not required to download datasets to local storage and data can be directly used from the cloud storage bucket.
- GEE provides several programming libraries to allow users to process the hosted datasets in addition to visualising them.
- The flexibility to upscale and downscale the processing cores and allocated memory according to the requirements of the task

In [Long et al., 2018], Long et al followed the same line and utilized GEE to build an automated global burned area mapping approach using Landsat-8 dataset. The authors referred to GEE as a huge EO data catalogue with the ability to run high performance computing tasks. A global scale of landsat-8 coverage from dense time-series data was used to build the system which was considered as high resolution when it comes to global scale monitoring. As explained in the manuscript, GEE was used for two reasons, the data accessibility and the computing capacity.

Azzari and Lobell [Azzari and Lobell, 2017] took advantage of GEE to classify

landcover using Landsat-8 dataset. Random Forest [Ho, 1995] algorithm was applied on two different datasets which are driven from Landsat-8 bands. The authors indicated that GEE was ideal tool for accessing wide pool of satellite imagery in addition to the scalability of the computational resources.

In [Patel et al., 2015], GEE platform was used to extract urban areas from Landsat8 imagery. The authors made use of the large stored datasets by harnessing the computation scalability options to achieve accurate population mapping output. Patel et al concluded that GEE-driven applications capable of boosting accuracy limits in the reported results.

Table 2.4 summarises the most relevant papers which have targeted remote sensing big data processing. It shows how the evolution of computing capabilities and the availability of remote sensing data contributed to several application domains. However, there wasn't any unified framework or data model to be followed regarding data pre-processing, processing or post-processing stages.

Table 2.4: Review summary

Reference and Year	Application Domain	Cloud Computing	Algorithm	Platform
[Ye et al., 2013]	Big data, Data mining, Cloud Computing, Clustering	Yes	K-means	RHadoop
[Cavallaro et al., 2015]	Big data, Data mining, HPC, Classification, Parallel processing, Spatial analysis, support vector machines (SVMs)	No	SVM	N/A
[Zhang, 2010]	Geospatial Computing, High-Performance Computing	Yes	Geo-Weighted Regression	private cloud, Nvidia CUDA
[Plaza et al., 2011]	Cluster Computing, FPGAs, GPUs, High Performance Computing, hyperspectral remote sensing	No	Hyperspectral image processing (un-mixing)	N/A

[Chavarr et al., 2012]	High Performance Computing, Parallel Computing	No	N/A	N/A
[Xiaoqiang and Yuejin, 2010]	Geographic Information Services, Cloud Computing	Yes	MapReduce	private cloud, Hadoop Distributed File System, Bigtable
[Kiemle et al., 2016]	Earth observation big data processing	Yes	N/A	private cloud
[Gançarski, 2014]	Earth observation big data, Data analysis	Yes	N/A	N/A
[Almeer, 2012]	Cloud computing, Hadoop, HPC, Image processing, Map reduce	Yes	Interpolation Algorithms (Color Sharpening, Sobel Filter, Auto-Contrast)	private cloud

[Yang, 2011]	GIS, Geodynamics, CyberGIS, Spatial analysis, HPC, Geospatial Cyberinfrastructure	Yes	N/A	private cloud
[Wang, 2011]	Cloud computing, Virtualization, Grid computing, Intrastructure as a Service, Parallel computing	Yes	Distributed Improved Splitting-and-Merging Cluster (ISMC) algorithm	OpenNEbula
[Padarian et al., 2015]	Super-computing, Cloud computing, Global Soil Map	Yes	Rifle Serial Classifier	Google Earth Engine
[Huang et al., 2010]	Cloud Computing, Virtualization, Amazon EC2, GEOSS Clearinghouse	Yes	N/A	Amazon Elastic Cloud Computing (EC2)

[Golpayegani and Halem, 2009]	Satellite image processing	Yes	Image gridding	Hadoop on a cluster of IBM PowerPC blade clusters
[Pan and Zhang, 2013]	Cloud computing, Distributed file system	Yes	MapReduce	private cloud, Hadoop
[Chen et al., 2012b]	Cloud computing, web processing services	Yes	N/A	private cloud, Apache Hadoop
[Wang et al., 2013]	Satellite image processing, Cloud computing,	Yes	MLC (Maximum likelihood classification)	private cloud, MapReduce, HDFS
[Gorelick et al., 2017b]	Cloud computing, Big data, Analysis	Yes	N/A	Google Earth Engine
[Mascolo et al., 2014]	Remote sensing data retrieval, Big data	Yes	N/A	N/A
[Marc Ferrer1, 2014]	Remote sensing big data	Yes	N/A	N/A
[Goor, 2014]	Big data	No	N/A	N/A

[Yu et al., 2016]	Cloud computing, Earth Observation, Environment monitoring	Yes	N/A	N/A
[Kristof et al., 2014]	Remote sensing big data, point cloud visualisation, object detection and extraction	Yes	N/A	N/A
[Almeida et al., 2014]	Sentinel data Sandbox Service, cloud computing	Yes	N/A	N/A
[Febrier and Montmory, 2014]	Computer vision, Remote sensing data processing	Yes	N/A	N/A
[Xing et al., 2014]	Image segmentation, Cloud computing	Yes	K-means	private cloud
[Zhong et al., 2012]	spatial cloud computing, cloud infrastructure, data management	Yes	N/A	private cloud

[Ferrn et al., 2013]	Remote sensing data processing, satellite/airborne image classification, web-based system	No	kmeans, ISODATA	N/A
[Chen et al., 2012a]	Web processing services	Yes	NDVI	private cloud with Hadoop
[Mandal et al., 2018]	Land-cover classification, Google Earth Engine (GEE)	Yes	kmeans	Google Earth Engine
[Chen et al., 2017]	Object detection, Google Earth Engine	Yes	Non-local active contour	Google Earth Engine
[Shelestov et al., 2017]	Crop classification, Google Earth Engine	Yes	Multi-Layer Perceptron (MLP)	Google Earth Engine
[Mateo-Garca et al., 2017]	Time series analysis, object detection, cloud masking, Google Earth Engine (GEE)	Yes	N/A	Google Earth Engine (GEE)

[Saranya and Muralidharan, 2017]	Google Earth Engine, Vegetation Indices	Yes	M5P	Google Earth Engine
[Celik, 2018]	Change detection, Urbanisation	Yes	N/A	Google Earth Engine
[Xu and Bai, 2015]	Change detection, Google Earth Engine	Yes	Random Forests	Google Earth Engine
[Long et al., 2018]	Google Earth Engine, Time-series analysis, change detection	Yes	Random Decision Forests	Google Earth Engine (GEE)
[Azzari and Lobell, 2017]	Land-cover classification, Change detection, Big data, Machine learning	Yes	Random forests	Google Earth Engine (GEE)

2.3 Conclusion

In this chapter, the most relevant articles were reviewed to explore the current status of using earth observation big data with cloud computing infrastructure. This review confirms that there wasn't any unified model for geo-spatial data processing in general. Even though applications and algorithms were identical in some papers, still the implemented processing chains were different. The contribution of this chapter from the thesis is to answer the following questions:

- **Given the recent advances in EO systems, what are the recent applications which utilised cloud computing paradigm?**

  The literature reviewed a large variety of research done in the field which made use of the EO data burst and integrated with cloud computing. The published work vary between raster and vector data processing while there are some cases integrating between both data types.

  Raster data processing included simple algorithms like K-means [Ferrn et al., 2013], kNN [Zhong et al., 2012], ISODATA [Ferrn et al., 2013] and Random Forest [Azzari and Lobell, 2017] for classification purpose and simple calculations like NDVI and NDWI [Yu et al., 2016] indexes. However, the reviewed papers and research done in the field are still at an early stage as we can see from the achieved work.

- **What are the most used cloud computing platforms for geo-processing tasks?**

  The above literature and relevant background explored the most recent developments on cloud computing platforms. AWS and GEE platforms are being used by most of the remote sensing researchers and developers nowadays. According to the requirements of the application, users are split between GEE and AWS.

  AWS showed an impressive performance in terms of flexibility. It grants the user all the required privileges to form the framework as needed. While on the other hand, GEE serves an end-to-end platform as a service to let the user utilise massive amount of hosted satellite data in addition to the computing power. At the early stage of the integration between cloud computing and remote sensing data, Microsoft Azure released ModisAzure project [Ghaffar and Vu, 2015] which provided a processing pipeline for remote sensing imagery with on-demand scalability options.

  The project was a big step towards breaking the limits of usual desktops and opened more initiatives towards remote sensing on the cloud projects.

However, Microsoft Azure platform was not involved actively in the research and applications of remote sensing as before. Overall in the field of EOD processing, AWS was dominating till 2016 until GEE appeared. The application needs directed some of the research and developers towards GEE. Noteworthy to mention the massive datasets Google offered recently and directly accessible on their platform.

- **What features are important to consider when deciding which cloud computing platform to be used for geo-processing?**[1]

  From satellite image processing perspective, we can conclude that three main factors can decide which platform to choose.

  - A. Flexibility

    As an essential factor, flexibility here refers to how customizable, scalable and variable is the level of virtualization afforded by cloud computing providers. Based on fact that cloud computing rely on virtualization, it is substantial not to restrict the client to specific operating system, hypervisor, API or programming language. Moreover, readiness to host remote sensing data and the flexibility of data volume since this may affect the productivity and the reliability of the proposed framework. The reviewed projects and published papers shows a general orientation towards AWS when it comes to a complicated structures and workflows. While the same happens with GEE when simple algorithms and calculations are required. The GEE provides ready to use APIs using Python and Javascript languages which are popular among developers and researchers.

  - B. Scope and Performance

    The aim here is to make sure that the vendor is supporting the

[1]This question was answered by published paper as: 'Cloud computing providers for satellite image processing service: A comparative study', Moataz Ahmed and Tuong Thuy Vu, International Conference on Space Science and Communication (IconSpace), 2015.

required hardware and software to run computer vision and deep learning algorithms. For example, graphical processing units (GPU) and load balance tools to monitor performance of the application if required.

  - C. Service Management and Pricing

    It is important for the users to have a user friendly control panel to deal with the cloud infrastructure and different services and tools. The number of services introduced by cloud providers is exponentially increasing by the time and especially since big data era started. For instance, computing, storage, databases, data migration, networking, monitoring, security, analytics, AI and many more services are hosted by AWS nowadays compared to just compute, storage and networking when just started their business. The explosion of services also has an impact on how users can manage their spending on cloud services. The pricing models differed from hour to minute to second recently.

- **Are there any specific advantages from using cloud computing platforms to deploy EOD processing services?**

  Employing cloud computing to accommodate geo-processing services is of vital importance. Space agencies such as NASA and ESA harnessed cloud computing storage services to facilitate the process of data acquisition and processing. This step accelerated the usage pattern of cloud computing by remote sensing scientists. The afforded computational capacity combined with the unprecedented amount of earth observation data empowered remote sensing scientists to apply complicated algorithms such as deep learning. Moreover, cloud computing providers are currently supporting the most recent processing units such as GPUs and TPUs which are perfect match with deep learning needs. In addition, the pay-as-use model which is favoured by most of cloud computing providers can afford sufficient computing power at minimum cost to run very complicated models.

At the end of this chapter and after considering all the aforementioned factors, AWS IAAS was chosen to build our work-flow utilising its several services. The next chapter will explain our proposed conceptual data model which can be used

to unify data processing pipelines on cloud-based infrastructure in general and AWS particularly. In addition, we demonstrate a proof-of-concept example for satellite image landcover classification as a service which was deployed using the proposed model.

Chapter 3

Integrated cloud-based framework for remote sensing big data processing

As explored in the chapter 2, cloud-based applications emerged as a general direction in EO data processing. This being said, chapter 3 explains a novel conceptual data model utilising cloud computing and EO big data. The selection of architecture, cloud services and processing tools was based on a survey disseminated among 51 participants from both research and industry backgrounds. The conceptual model harnesses the power of cloud computing architectures with Earth Observation Data (EOD) archives to derive useful information about the earth. The main focus in this chapter is to explore how to orchestrate several cloud computing components, data, tools and frameworks to produce a remote sensing data processing service rather than assessing specific accuracy results. The conceptual model is followed by a proof of concept case study for Landsat-8 supervised classification using an SVM algorithm [Cortes and Vapnik, 1995]. Moreover, chapters 4 and 5 will utilise the developed model to automate the creation of deep learning super resolution datasets.
It is noteworthy that part of this chapter is based on a published paper as:

"An Integrated Cloud-based Framework for Remote Sensing Data Processing", Moataz Ahmed, Tuong Thuy Vu, Tomas Maul., International Journal of Geoinformatics, Vol 12-2,2016.

3.1 Introduction

The recent advances in remote sensing technologies resulted in acquiring unprecedented amounts of Earth surface details with multi-spatial, temporal and spectral resolutions. As a result of those improvements, adopting new approaches to process such big data is of vital importance. Cloud computing emerged as a scalable, elastic and reliable solution to serve that purpose. Well-known space agencies such as National Aeronautics and Space Administration (NASA) and European Space Agency (ESA) supported the transition and became pioneers in cloud based processing and archiving services especially for scientific research purposes.

NASA Earth Exchange (NEX) [NASA, 2016] is one of the initiatives which aims at accumulating earth observation data for scientific collaboration and knowledge transfer. The number of captured scenes has been doubling each year with continuous support for new launched satellites. Following the same direction, ESA opened Sentinel-1,2,3 and 5p data for users at no cost. AWS [AWS, 2018] and SciHub [ESA, 2016] platforms are used to store public datasets and distribute them for scientific usage.

Although the move was a big step towards massive utilisation of EO big data, still researchers and scientific communities are just scratching the surface of EOD usage. This is due to the main challenges represented of bandwidth limitation, processing speed and data size which are not tackled by the proposed initiatives yet.

The recent developed Google Earth Engine (GEE) [Google, 2018] helped in providing Platform As A Service (PAAS) and several papers utilised it as we mentioned in chapter 2. However, the limitations of using specific programming

languages to process the data and relying on a specific vendor are considered the main drawbacks of the platform.

Similarly, [Sinergise Ltd, 2018] afforded an Application Programming Interface (API) to deal with Sentinel and Landsat data through Open Geospatial Consortium (OGC) standards. However, the free API is used to access data only and with a limited number of requests and bandwidth.

Taking advantage of the aforementioned wave and following the same direction, we disseminated a survey among researchers, private companies and governmental agencies to assess the current situation of cloud computing usage in remote sensing data processing in Malaysia.

3.2 Remote Sensing and Cloud Computing Survey

As cloud computing technology becomes more accessible to users, it is important that the design and implementation of services will also be able to meet the expectation of the users. Hence, a market survey was carried out to evaluate the acceptance of this technology by experts from the field of remote sensing in Malaysia. To find the appropriate participants, we disseminated the survey among Institution of Geospatial and Remote Sensing Malaysia (IGRSM). IGRSM supports and facilitates development of geospatial and remote sensing technologies in Malaysia with more than 170 members representing several sectors and specialisations. The survey aims to analyse users preferences when using image processing/analysis applications and understand user perspectives on cloud computing as a service for remote sensing applications in addition to defining the most used datasets by the community and experts. Moreover, survey results can help in shaping the services in order to maximise how useful they can be to current and future users. The outcomes from this survey will be used to draw an architecture of a conceptual design which aims at harnessing cloud computing capabilities with EO big data.

3.2.1 Methods

A total of 51 participants from the remote sensing user community in Malaysia participated in this online survey. The online survey consisted of 12 questions where one of the questions was to identify the respondent's area of specialisation while other questions were mainly designed in order to identify which organisation respondents represented (researchers/academicians, private sector / NGOs, governmental organisation).

The remaining questions are related to the user knowledge on using remote sensing applications and understanding of cloud platforms.

Participants were told that the purpose of this study was to understand users preference using an image processing/analysis program and their perspective on using cloud computing as a service for remote sensing applications.

All the participants are from field of geographical information systems and remote sensing applications, and have various area of specialisations. This includes areas such as ecology, forestry, urban mapping, hydrology, environmental studies, and research and development of remote sensing techniques.

The proportion of participants from the survey was made up of 68% students/academicians; 22% private sector/non-governmental organisations (NGOs); and 10% from governmental organisations. In order to statistically analyse the survey results and given the fact that we had non-probability sampling results, conclusions were only representing Malaysian case and may not be generalised all over the world. However, the developed conceptual data model in section 3.3 is designed to be generic and flexible. The survey was distributed via a customised online Google survey form. The participants were informed they only needed 3 minutes to complete the survey and their responses would be anonymous. The results of the survey are explained in the following sub-sections.

Important aspects to evaluate when choosing satellite image processing tools

This section aims at defining what are the most important factors which are taken into consideration to decide whether to use a satellite image processing tool or not. The chosen aspects included learning curve ease, the presented functionality, the variety/range of afforded tools, the performance of the tool, the simplicity of usage/operation and "other aspect". A chi-square test of goodness-of-fit was performed to determine participant's perspectives on the required aspects of an image processing analysis. The test was found to be statistically significant, X^2 (5, N = 139) = 27.49, $p < .001$. The result indicates that the important aspects of image processing preferences are not equally distributed. It shows that functionality (n = 36) is the most important aspect of an image processing tool in comparison to processing performance (n = 27), range of tools (n = 26), easy learning curve (n = 24), simple to operate (n = 24) and unspecified other aspects (n = 2) (refer to Fig. 3.1).

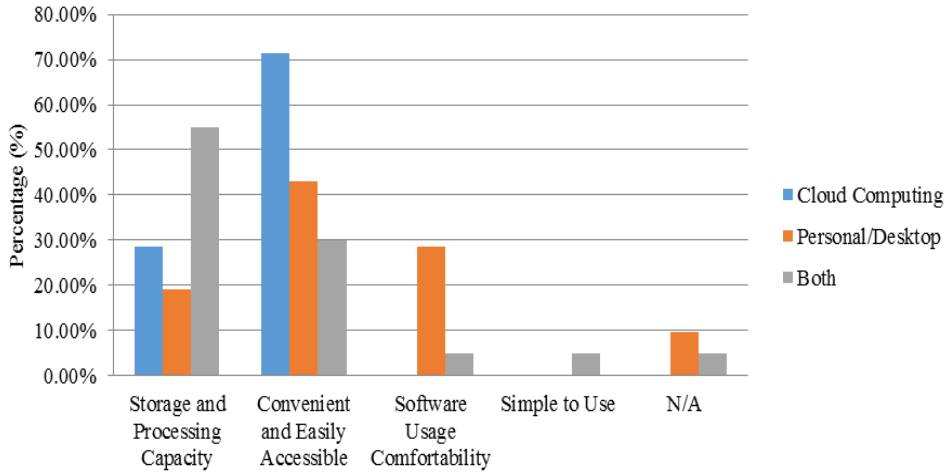


Figure 3.1: Aspects to consider before using a satellite image processing service

User Groups Understanding of Cloud Computing

This section measures the level of understanding of the cloud computing model between survey groups. The choices were given as (high, moderate, low and never heard about it before). A chi-square test was performed and showed that there was a significant difference between a user group's understanding of cloud computing, $X\,(1, N = 51) = 13.86$, $p = 0.037$. The result indicates that the majority of developers (44%) have higher understanding on cloud computing, whilst 69% of analysts and 61.5% of users have moderate understanding of cloud computing (refer to Fig. 3.2).

Types of Platform Choices for Future Image Processing Usage

The following analysis aimed to explore the preference of EOD processing platforms for future tasks. The choices included cloud computing platforms, personal desktops, both or neither. A chi-square test of goodness-of-fit was performed to determine participant preferences on the type of platform usage for

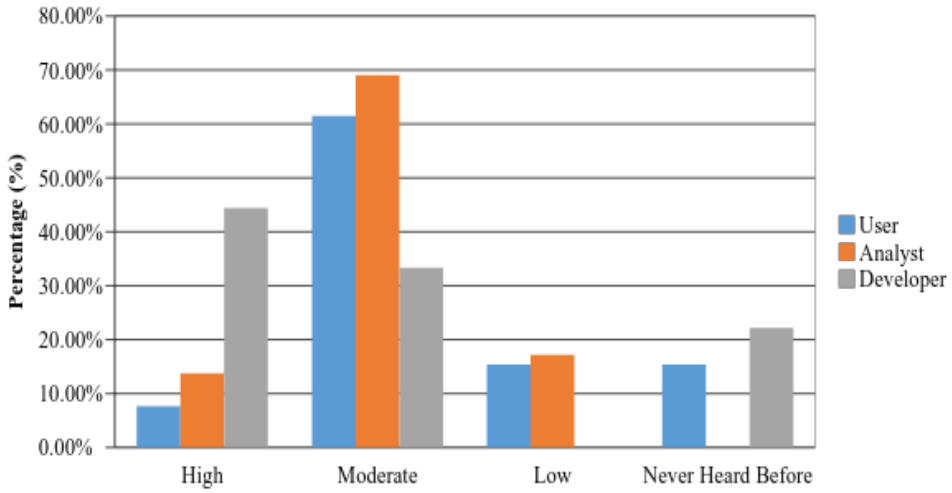


Figure 3.2: The level of understanding cloud computing models among survey groups (users, analysts and developers).

their future image processing needs. The test was found to be statistically significant, X (3, N = 51) = 19.51, p < .001. The result indicates that the category of personal/desktop platform (n = 21) and the category of both (cloud computing and personal/desktop) platforms (n = 20) are highly preferred choices for future usage of image processing compared to only using the cloud computing platform (n = 7). There were only n = 3 participants who chose neither platforms for future usage of image processing (refer to Fig. 3.3).

Reasons for choosing the types of platform for Future Image Processing Usage

This section aims at analysing the previous section to understand the reasons behind every choice. The choices were defined as follows: storage and processing capacity, convenient and easy access, software usage restrictions, simplicity and others. To analyse the answers, a chi-square test was conducted to assess the participant's reason for choosing a particular platform (either Cloud Computing or Personal/Desktop) or both platforms together. The results were significant, X (15, N = 51) = 44.11, p < .001.

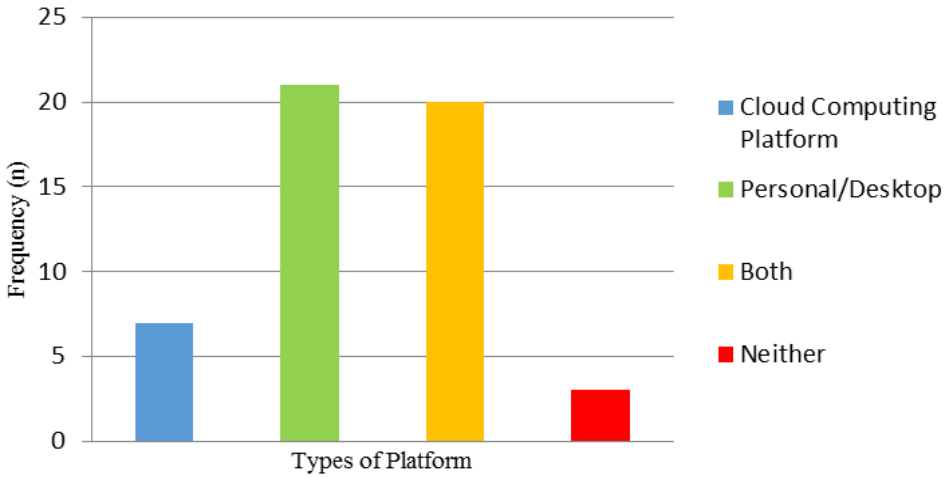


Figure 3.3: Platform preference for future EOD processing tasks

It shows that participants who opted for the personal/desktop platform have chosen ”convenient and easily accessible” (42.9%) as the main reason of their platform choice, followed by the ”software usage comfort/ability” (28.6%) and ”storage and processing capacity benefits” (19%).

Participants who preferred the cloud computing platform chose the platform more for its ”convenience and easy accessibility” (71.4%), than the benefits of ”storage and processing capacity” (28.6%).

Lastly, participants who chose both platforms have selected ”storage and processing capacity benefits” (55%) as the main reason for their choices (refer to Fig. 3.4).

The usefulness of Cloud Computing Platform for Image Processing/Analysis

This section aims at defining the participants' perspectives regarding the usefulness of cloud computing in satellite image processing. A chi-square test of goodness-of-fit was performed to determine the usefulness of the cloud computing platform by the participants. The test was found to be statistically

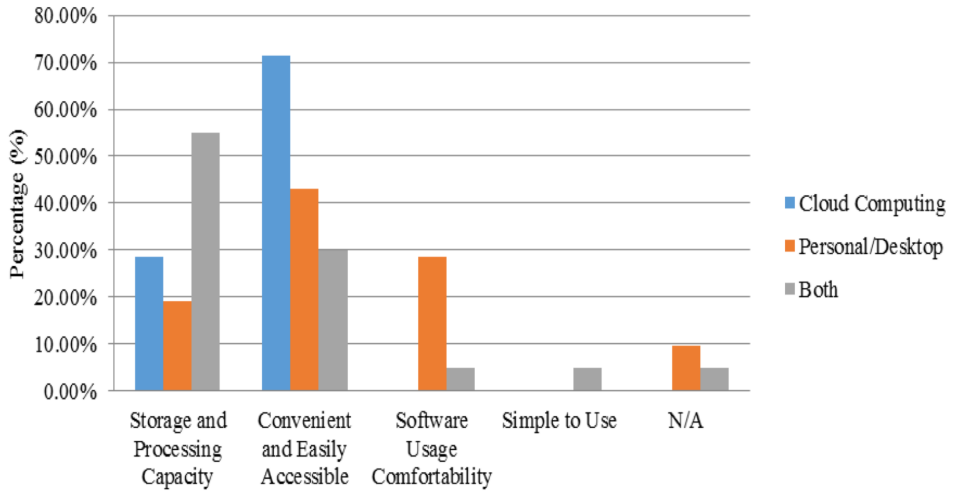


Figure 3.4: Reasons to choose between cloud computing and personal desktops for satellite image processing tasks.

significant, X^2 (1, N = 51) = 21.35, p $<$ .001. The result indicates participants did not randomly decide the usefulness of the cloud computing platform for image processing. The majority appears majority of the participants voted yes (n = 42) compared to no (n = 9). It is generally agreed that the cloud computing platform is useful for image processing (refer to Fig. 3.5).

Level of Competency in Handling Image Processing

In order to understand the competency level of the target market for cloud computing applications, participants were categorised into various levels as user, analyst or developer. User-level is categorised as users who utilise the basic functions of image processing tools such as exploration and simple mapping tasks. The analyst-level comprises of users who utilise image processing tools for the purpose of extracting useful information. The developer-level refers to users who are involved in the development of advanced EOD processing techniques.
A chi-square goodness-of-fit test was calculated to examine if there is a difference in level of competency in handling image processing tasks. The test

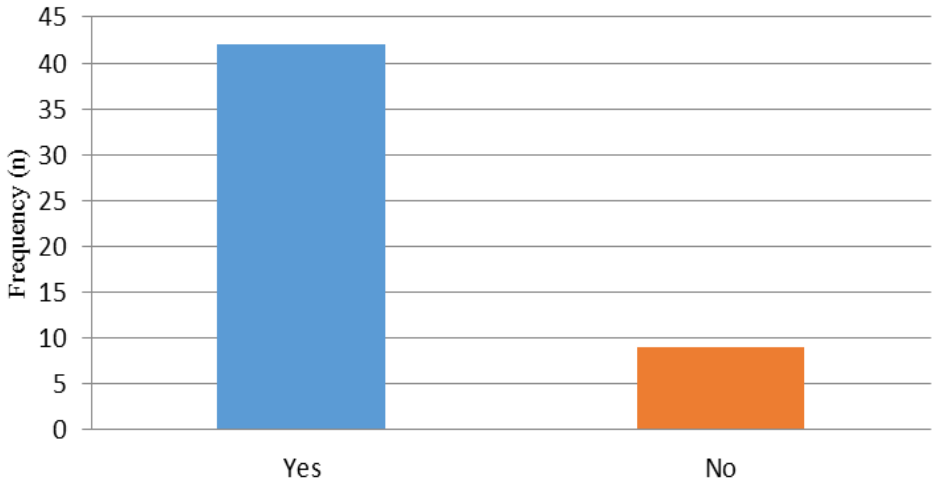


Figure 3.5: Participants perspective regarding the usefulness of cloud computing models in EOD processing

was found to be statistically significant, X^2 (1, n = 51) = 14.07, $p < 0.01$. The results suggest that the frequencies of the levels of competency are not equally distributed and are statistically different from what would be expected by chance. The majority of the participants have competency level of an analyst (n = 27), whilst there are 13 users and 9 developers (refer to Fig. 3.6).

The association between processing type and the used platform

In order to evaluate the association between object and pixel-based processing types from one side and cloud and desktop-based from the other side, a Chi-square Test-of-Independence was applied with degree of freedom of 1. X^2 obtained 8.386 which is greater than critical value for α of 5% (3.841) and α of 10% (2.706). The null hypothesis was rejected and the X^2 showed a clear association between the followed processing methodology and the used platforms.

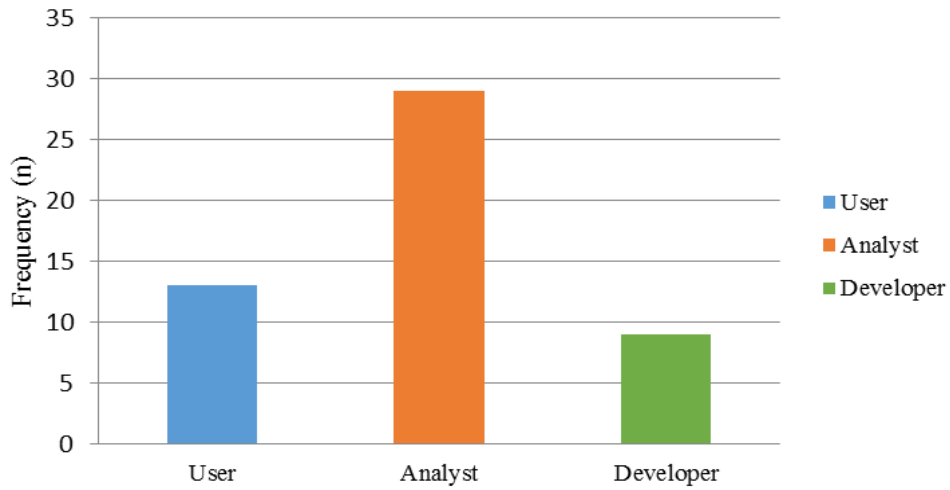


Figure 3.6: Level of earth observation data usage among survey participants

The relation between processing type and cloud computing usefulness for geo-processing

In this test, the relation between processing methodologies and usefulness of cloud computing was checked. A Chi-square Test-of-Independence test was applied to check which hypothesis will be rejected. A null hypothesis means that there is no relation between variables. X^2 obtained value of 3.88 which is greater than the critical value for α of 5% (3.841) and α of 10% (2.706). which rejects the null hypothesis with degree of freedom of 1.

The variety of used sensors

In this section, participants were requested to input what type of remote sensing datasets they are using currently. Choices included multi-spectral, hyper-spectral, radar, lidar, UAV or others. The result of chi-square goodness-of-fit indicates that frequencies of image source by types are not equally distributed among the participants and frequencies are statistically different from what would be expected by chance. The test was found to be statistically significant, X2 (5, n = 110) = 50.69, $p < 0.01$. Based upon the observed frequencies, it shows that the highest image source used was multi-spectral satellite images (n = 43), followed by LIDAR (n = 20), RADAR (n = 18), UAV (n = 14), hyper-spectral image (n = 12) and others (n = 2). The two identified image sources used in the others category are GPS and TRMM Microwave Imagery. A majority of participants uses multi-spectral images which might be justified as a result of the availability of free and open-source images from Landsat and Sentinel constellations as we mentioned in chapter 2 (refer to Fig. 3.7).

Spatial resolution accuracy of the currently used datasets

This section evaluates the level of spatial resolution accuracy of the used EOD. Spatial resolution was split as follows: less than 1 meter, 1 to 30 meters, 30 to 90 meters, 90 to 150 meters, 150 to 1000meters and greater than 1000 meters. The

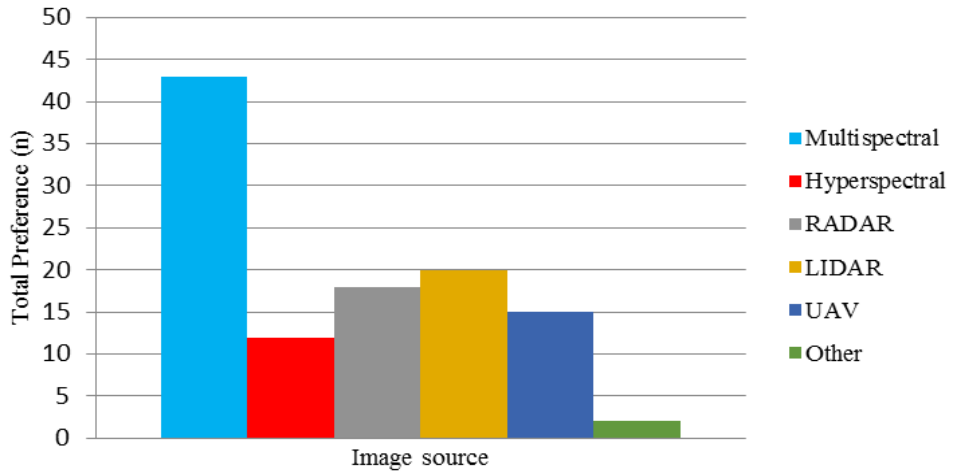


Figure 3.7: Types of remote sensing data used by participants

result of chi-square goodness-of-fit indicates that frequencies of image resolution usage are not equally distributed among the participants and that the frequencies are statistically different from what would be expected by chance. The test was found to be statistically significant, X2 (4, n = 90) = 37.89, $p < 0.01$. Based upon the observed frequencies, it shows that the 30m resolution is the most frequently used spatial resolution with n = 37, followed by <1m resolution (n = 20), 90m resolution (n = 12); the lowest usage frequencies corresponded to 150m (n = 8) and 1000m (n = 7) (refer to Fig. 3.8).

The majority of participants were using 30 meter spatial resolution images as it is a common resolution to analyse land-use and land cover change detection. Those who have chosen to use image resolutions of 1000m, the majority come from the backgrounds specialising in wildlife population, hydrology, geomatics and waste management applications which typically don't need high resolution data.

Types of Image Classification Method

In this section we try to identify which classification methodology is used among survey participants. Choices contained object-based, pixel-based or both pixel

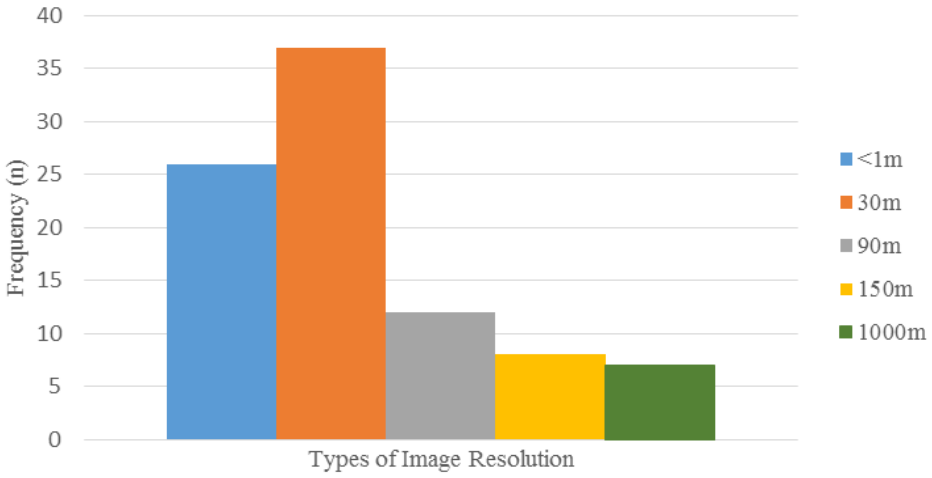


Figure 3.8: Spatial resolution accuracy

and object based image classification. A chi-square test of goodness-of-fit was performed to determine whether the three image classification methods were equally preferred. The test was found to be statistically significant, X (2, N = 51) = 20.24, $p < .001$. The result indicates that the frequencies of image classification methods are not equally distributed and frequencies are statistically different from what would be expected by chance. It is clearly noticed that pixel-based classification methodology (n = 29) is used more often than object-based classification (n = 19) and the both types of classification option (n = 3). (refer to Fig. 3.9)

Geo-spatial processing tools preference

This part highlights user preferences regarding the geo-processing tools which are used to handle EOD. The choices were categorised to include proprietary, open-source and both options. Results were classified according to the category of participant (user, analyst, developer). A chi-square test was performed and it shows a significant difference between user groups and preference of software/tool used, X^2 (1, N = 51) = 13, p = 0.029.

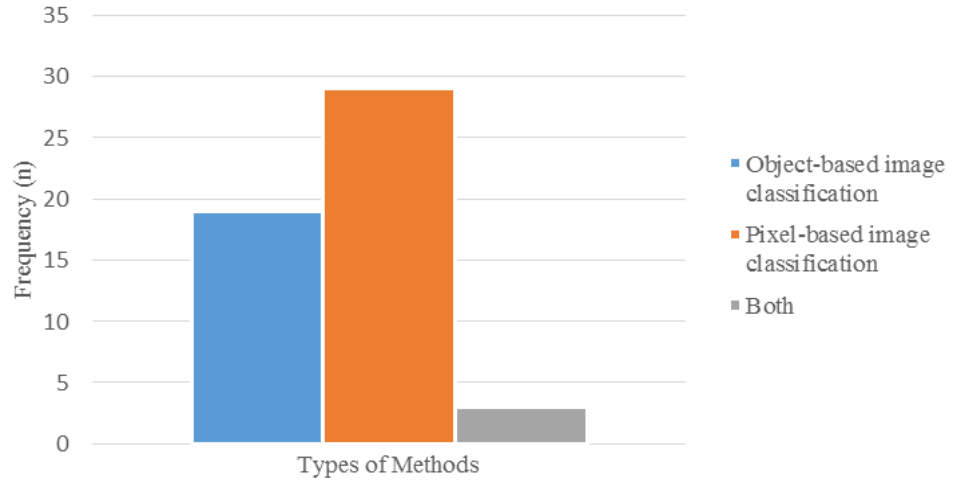


Figure 3.9: The most applied image classification methodology

The result indicates that usage of commercial software is most popular among users (84.6%) and analysts (55.2%) whilst open-source is favourably used by developers (33.3%). In general, usage of both platforms is highest among the developers (44.4%). (refer to Fig. 3.10)

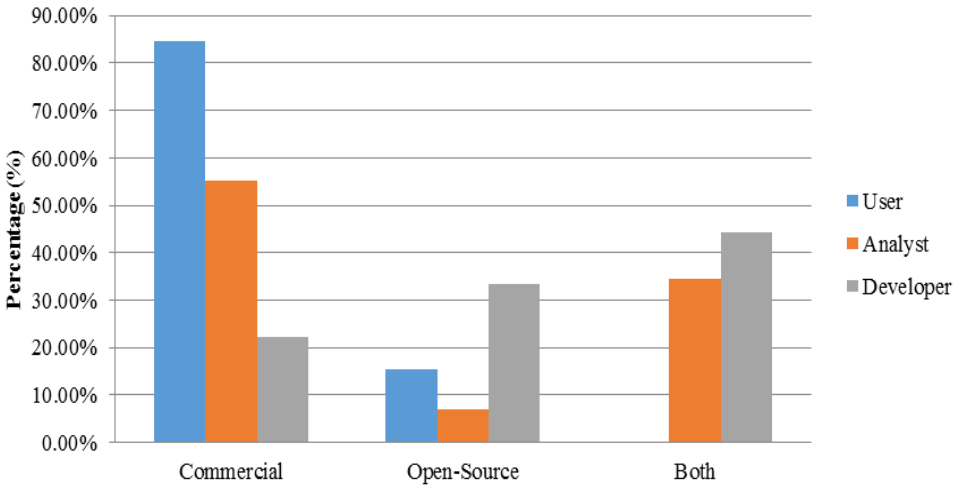


Figure 3.10: Open-source vs proprietary geospatial processing tools among users, analysts and developers groups

3.2.2 Conclusion

Cloud computing services are growing exponentially in the technology industry. It was estimated that the revenue for the worldwide cloud IT market amounted to US$180 billion in 2015 [Mark Brinda, 2018] and it is predicted to increase to US$390B in 2020, attaining a Compound Annual Growth Rate (CAGR) of 17%. According to Asia Cloud Computing Association (ACCA), Malaysia is ranked 8th among the 14 Asian countries that are cloud ready, and Malaysian businesses are more cloud-ready than their neighbouring counterparts in Singapore [Computing, 2018]. The overall adoption of cloud computing services across all general industries in Malaysia has grown 100% since 2015 [Malaysia, 2018] and at least 77% of the government services are already using a digital platform based on the 11th Malaysia Plan 2016-2020 [EPU Malaysia, 2018].
The aforementioned insights alongside our survey indicate that the Malaysian market is ready to utilise cloud computing for satellite image processing applications. The survey helped in identifying the needs of remote sensing experts from different usage categories.
A set of conclusions and outcomes can be summarised as:

- Multi-spectral datasets are being used by the majority of EOD users compared to other data types. This conclusion can help in defining what datasets need to be integrated first with cloud infrastructure to deploy a PAAS.
- Medium resolution datasets such as Sentinel-2 and Landsat-8 are being favoured by remote sensing communities alongside Very High Resolution (VHR) data. Sentinel-2 and Landsat-8 datasets can be used for many types of applications such as object detection and classification tasks.
- Pixel-based classification is the most applied classification methodology in remote sensing applications as we can see from the survey results. This can be reflected in the design of training datasets and model architectures (as we will demonstrate in chapter 4 and 5).

- The market is dominated by proprietary software vendors and this might be caused by the support service and technical training provided. This can reflect the level of usability users can expect form EOD cloud processing services.
- Cloud computing is not far from the remote sensing community as many responses indicated.
- A relatively narrow range of users accepted replacing personal desktop platforms with cloud-based ones to process EOD.
- The main reason behind preferring personal desktops in EOD processing was the easiness of access to processing tools. This concern can rely mainly on the followed cloud computing model (SAAS, PAAS or IAAS) as a user friendly PAAS model can represent an acceptable solution to replace desktop-based geo-processing tools.
- Users demonstrated how important cloud computing is for EOD processing by more than 90% votes favoring a ”yes” response as explained in the last question.

Given the aforementioned results and considering the survey analysis, the next section explains our developed conceptual data model which employs cloud computing with EO big data. The survey results are taken into consideration in the architectural design, workflow, datasets, output presentation, tools and usability.

3.3 Conceptual Data Model Design

In order to make use of the aforementioned wave of EOD and facilitate processing tasks to derive near real-time products, we propose a conceptual data model design which allows data acquisition, processing and output visualisation tasks to be executed on the cloud. The design considered flexibility options

which can facilitate data-flow during all ingestion/processing/visualisation stages. In addition, it was taken into consideration not to restrict model components with any cloud computing service provider. Figure 3.11 shows the architecture of the model starting with receiving data from the sensor until producing the final output.

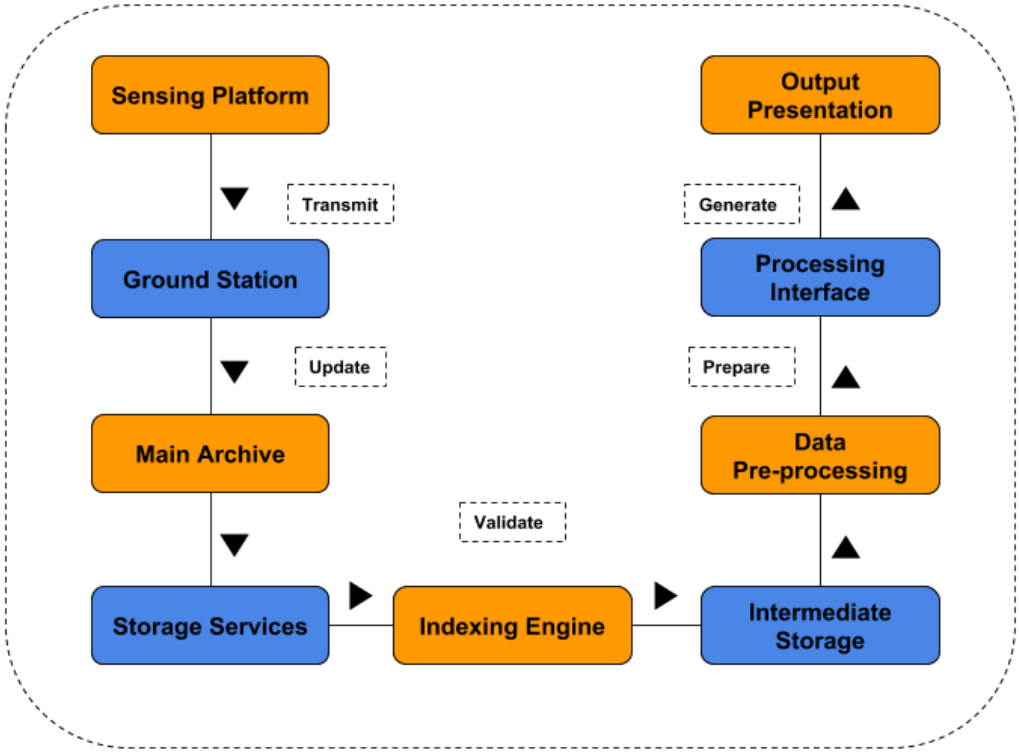


Figure 3.11: Conceptual Data Model.

3.3.1 Receiving and Indexing Data

The proposed data model is meant to be generic enough to handle any kind of remotely sensed imagery data. The process of publishing satellite data can be described as follows:

1) The captured scenes are transmitted to the ground stations for processing and data conversion steps.

2) Ground stations are linked with the main archiving mirrors which are considered the data hub for that specific satellite.

3) The main data hub is updated periodically according to the temporal resolution of the satellite itself.

Storage services are being adopted nowadays as a convenient solution especially after the eruption of EO data as mentioned in chapter 2. Storage services allow different types of data analysis to measure the data statistics such as number of downloaded and uploaded objects, speed analysis, and total execution times. The proposed design doesn't require using any specific storage service provider. However, Amazon S3 and Google Cloud Storage are chosen by EO agencies like ESA or NASA to host EO data.

Once the imagery data are downloaded, we propose using indexing engines. Indexing services can be used to build searching schema according to the derived meta-data from the downloaded products. Meta-data text/xml files are mandatory to be included with all satellite imagery data. Indexing engines can use the meta-data to build searching schema which can be used for querying, mapping and ranking data. Many indexing services are built for analytic and searching purposes such as [Elastic Co, 2018] and [Apache Foundation, 2017b]. Reaching this step, the data are well organized and accessible via the intermediate storage server.

3.3.2 Data Processing

In this section, all processing phases are covered starting from accessing the indexed data from the previous phase up to producing the processing output. A series of pre-processing steps might be applied to prepare data for information extraction. Processing interface here refers to the allowed protocols to deal with EO data whether in vector or raster formats. Remote sensing communities and

consortiums have been working to define a common standard way of communication and dissemination of geospatial data. The Open Geospatial Consortium (OGC) [OGC-Consortium, 2018] offers a large varieties of services to handle different types of geo-data. Web Map Service (WMS), Web Processing Service (WPS), Web Feature Service (WFS) are the most used interfaces in many frameworks. Depending on the target output, the processing interface is expecting pre-processed input data to be received. The processing node is expected to support a large variety of geo-processing tools and scripts chained together with automated workflow engines such as Apache Airflow [Apache Foundation, 2017a] and Luigi framework luigi. To overcome the expected load on processing units, queuing systems and distributed processing frameworks are expected to be used in all processing tasks. This helps in avoiding failures in processing nodes and gaining more capacity for executing more tasks in parallel.

3.3.3 Information Retrieval

The proposed model is designed to adapt to any kind of geo-processing service which accepts raster or vector data as input. It is suitable to allow an infinite number of algorithms to be deployed on top of the cloud infrastructure. According to the processed data, the expected output can be retrieved using several channels. Moreover, the framework allows downloading an output or visualizing it in a browser via different OGC services such as WMS.
In the next section, a fully automated Landsat-8 landcover classification as a service is presented applying the proposed conceptual data model to explore the benefits of using cloud computing services alongside EO big data flow.

3.4 Landsat 8 Imagery Classification As A Service

Until the time we published [Ghaffar et al., 2016], few libraries were developed to deal with Landsat-8 data archive [Ian, 2018, USGS, 2017]. The solution in [Ian, 2018] is a command line based tool which helps users to download

landsat-8 scenes directly from AWS S3 storage. The developed tool however makes the job of downloading imagery more complicated and time consuming because of being CLI based in addition to having limited criteria to choose from while downloading scenes. Around the same time, [USGS, 2017] offered a graphical user interface (GUI) to download imagery with few selection criteria e.g. cloud coverage. Hence, we present an automated system that allows downloading and processing Landsat-8 data according to a wide scope of criteria that relies on the attached meta-data files with each product. The developed framework handles Landsat-8 data once received by ground stations while the pre-processing and processing steps are are done subsequently according to the quality of the ingested products. Following the aforementioned model description, Figure 3.13 specifies an implemented proof of concept to present a best practice of Landsat-8 landcover classification as a service. The data-flow is categorised into 3 steps as explained in the following sections.

3.4.1 Data acquisition and indexing

Since Landsat-8 data became freely open for everyone to use, earth observation and monitoring applications production increased rapidly especially change detection, ecological monitoring and biodiversity conservation [Young et al., 2017] .

Following the architecture of the cloud computing paradigm as shown in Figure 3.12, the Software As A Service (SAAS) model is targeted to present the final output to the user. The SAAS model provides all the required processing capabilities relying on the assigned quota per user/account. Based on the literature in chapter 2, the AWS cloud provider is chosen to host the service. The flexibility and scalability afforded by AWS and the freedom to use any programming language or processing tools to deal with raster and vector data supported that decision. Accordingly, we managed to submit a research proposal for AWS mentioning the details of our workflow and the used datasets and technologies. We succeeded in securing a 10,000 USD grant from Amazon AWS

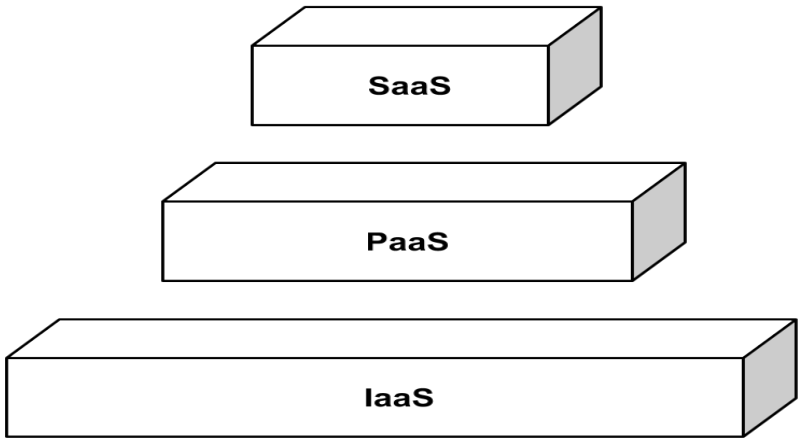


Figure 3.12: Cloud computing architecture

in the form of cloud credit to use any service they offered.

Figure 3.13 shows the workflow of the designed model, where steps 1-4 show the data acquisition and indexing methodologies.

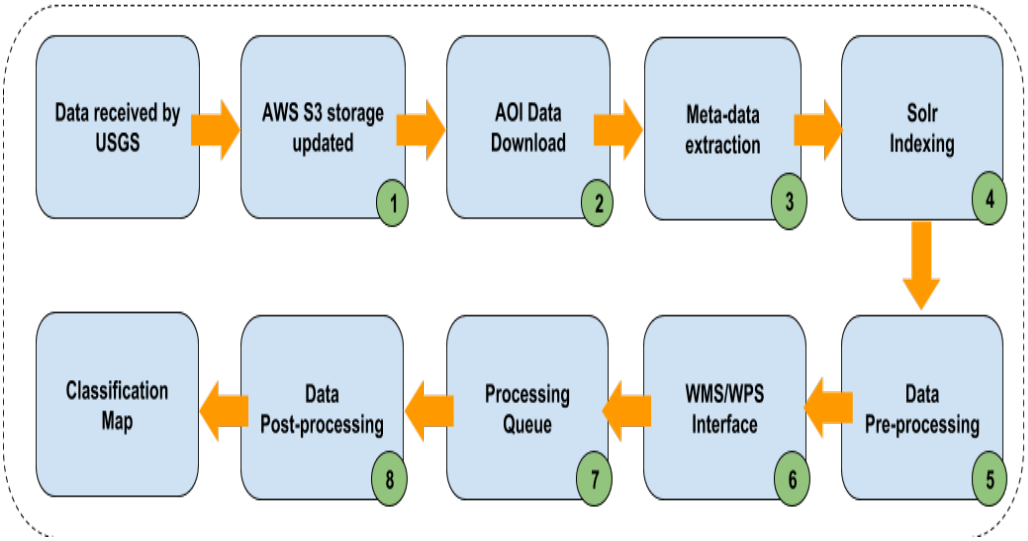


Figure 3.13: Landsat-8 landcover classification model

Table 3.1: Landsat-8 Processing Levels

Pre-collection	Collection-1	Description
L1T	L1TP	Radiometrically calibrated and orthorectified using ground control points and digital elevation model (DEM) data to correct for relieft displacement. These are the highest quality Level-1 products suitable for pixel-level time series analysis.
L1GT	L1GT	Radiometrically calibrated and systematic geometric corrections applied using the spacecraft ephemeris and DEM data to correct for relief displacement.
L1G	L1GS	Radiometrically calibrated with systematic geometric corrections using the spacecraft ephemeris data.

Step 1: Once the scene is captured by the satellite sensors, ground stations receive the signal and transfer it to the mission control facilities for processing and systematically generate and archive Level 0 and 1 products [ESA, 2018a, USGS, 2018a]. At the time we started this study in March 2015, the most recent and highest accuracy freely available dataset was Landsat-8 on AWS storage objects.

Table 3.1 shows different processing levels of Landsat-8. AWS S3 stores a global scale of Landsat-8 data within hours of production with public accessibility for downloading and archiving data once available. However, changes to original datasets are not allowed on the hosted archive.

Step 2: Built on top of the AWS EC2 micro machine, cron jobs are set to run landsat-util [Development Seeds, 2017] to download and archive a specified AOI according to the user configuration. Inspecting the Landsat-8 product contents, the Operational Land Imager (OLI) and Thermal Infrared Sensor (TIRS) instruments deliver 11 bands as shown in table 3.2. The product zip file contains the bands in TIF format in addition to meta-data text files. The metadata includes a lot of details which are useful for data interpretation and processing as mentioned in the next step.

Table 3.2: Landsat-8 OLI and TIRS bands

Landsat-8 Bands	Wavelength(mm)	Resolution (meters)
Band 1 - Ultra Blue (coastal/aerosol)	0.435 - 0.451	30
Band 2 - Blue	0.452 - 0.512	30
Band 3 - Green	0.533 - 0.590	30
Band 4 - Red	0.636 - 0.673	30
Band 5 - Near Infrared (NIR)	0.851 - 0.879	30
Band 6 - Shortwave Infrared (SWIR) 1	1.566 - 1.651	30
Band 7 - Shortwave Infrared (SWIR) 2	2.107 - 2.294	30
Band 8 - Panchromatic	0.503 - 0.676	15
Band 9 - Cirrus	1.363 - 1.384	30
Band 10 - Thermal Infrared (TIRS) 1	10.60 - 11.19	100 * (30)
Band 11 - Thermal Infrared (TIRS) 2	11.50 - 12.51	100 * (30)

Step 3: All the downloaded Landsat-8 products contain metadata text files (MTL) which are beneficial for building systematic searching and archiving mechanisms. Apache Solr [Apache Foundation, 2017b] emerged as a great support for indexing data. Out of the box, Apache Solr enables location-aware search parameters. Complex spatial data polygons, longitude, latitude and bounding boxes are all supported for filtering and searching throughout the data. Additionally, different data formats like WKT and GeoJSON are accepted and can be utilised. Apache Solr is used here to extract all the meaningful search parameters to present an interface for the user to specify which scenes to download/process.

Step 4: In our proposed framework, we use the metadata files to create an index for the imagery once received at the S3 storage. Parameters such as Landsat_scene_id, Collection_number, File_date, Cloud_cover and Image_quality are used to allow users to select scenes with very specific conditions to fit with the study purpose. The developed framework offers a GUI interface to access and download the data as shown in figures 3.14, 3.15 and 3.16. A user can select specific band, scene creation date, cloud coverage margin, collection number, processing level and minimum quality for data to be downloaded/processed.

In the next section, we explore the pre/processing phases.



Figure 3.14: Available criteria for the searching mechanism

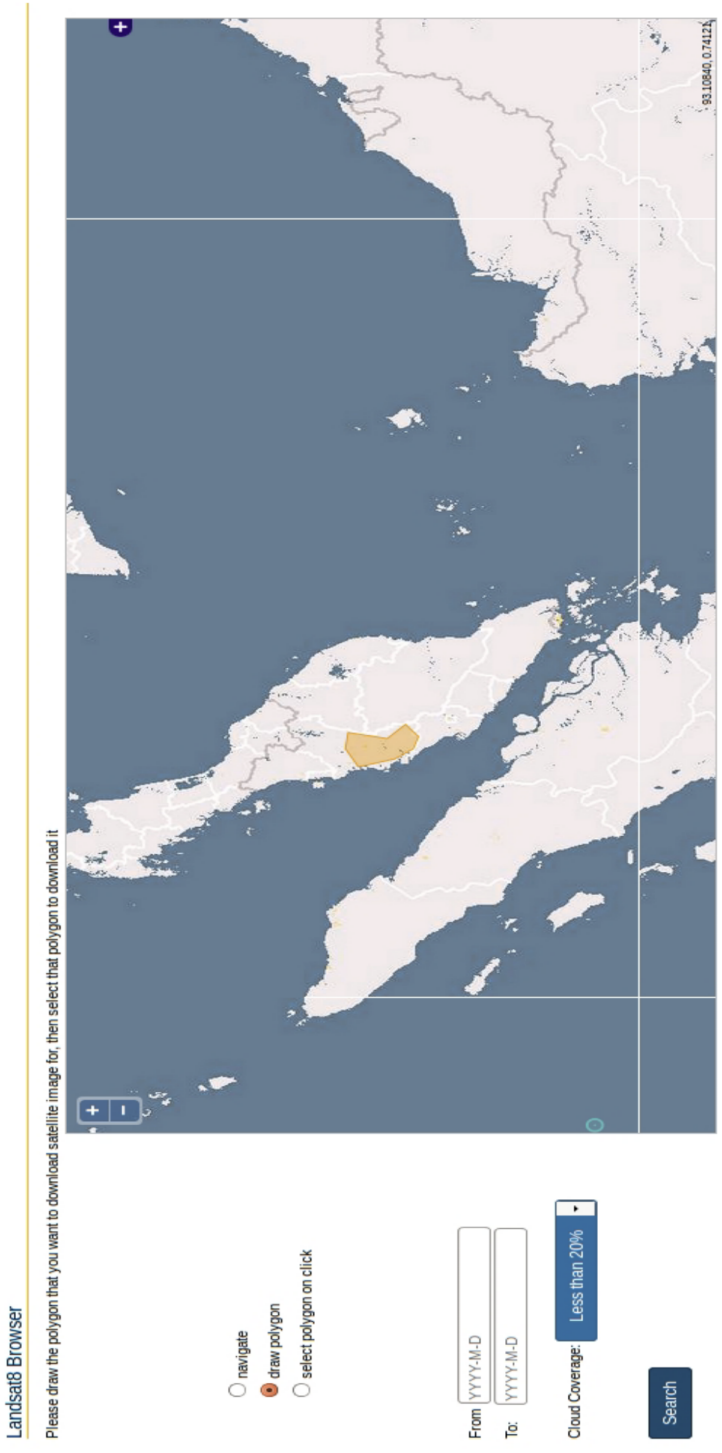


Figure 3.15: Search interface.

Figure 3.16: Results interface.

3.4.2 Data processing

Step 5: Before using Landsat-8 scenes for certain applications, it is necessary to pre-process data. In order to allow a large variety of processing tools for users, GDAL [Contributors, 2018] and OTB [Grizonnet et al., 2017] tools are deployed on an EC2 machine for processing purposes. Airflow [Apache Foundation, 2017a] processing chains are designed to run concurrently for dataset preparation once new captured scenes are made available such as segmentation, cropping samples or atmospheric correction.

Step 6: Processing interfaces are provided to help users in communicating with the model. HTTP, WPS and WMS services are supported to allow sending upload, download and processing requests to EC2 processing machines. However, multiple requests are expected to be received simultaneously which needs to be handled with some queuing mechanism.

Step 7: In order to avoid failure in processing nodes, queuing tasks is of vital importance in this case. RabbitMQ [Pivotal, 2018] is used as a task broker to queue processing requests/tasks to meet high-availability/scalability needs while Celery [Celery-Project, 2018] is used to execute tasks asynchronously in the background or synchronously. In terms of tasks/functions, SVM was used here but the user is not restricted to implement/deploy any specific processing algorithm such as Random Forest, KNN, K-means or ANN. Input and output data for such algorithms are defined via HTTP, WMS and WPS tasks on EC2 machines. The next section illustrates how to obtain the final results/output from the designed model.

3.4.3 Information retrieval

Step 8: Following the queuing system, RabbitMQ notifies the user regarding the progress of running tasks. Depending on the processing algorithm, the output is expected to have a pre-defined format. Land-cover classification tasks are expected to produce classification maps. The results are published via

OGC [OGC-Consortium, 2018] standards as WMS, WCS or WFS services for ease of access. In our proposed model, WMS is used to visualize the area of interest (AOI) before and after processing.

3.5 Conclusion

In this chapter, a novel conceptual model for a satellite data processing pipeline which downloads, pre-processes and generates output in near real-time is presented. A case study of Landsat-8 supervised classification service using SVM was tested utilising the proposed conceptual model. The selection of Landsat-8 data and SVM pixel-based classification was determined based on the survey. The accuracy of the output results whether for a simple or complicated algorithm is not taken into consideration in the scope of this chapter. The contributions added through the designed model can be summarised as follows:

- The designed model doesn't force users to use any specific scripting/programming language to handle remote sensing data.
- A modular design which offers flexibility to choose any vendor for any particular functionality.
- Providing quick access to the most recent captured scenes/satellite data without bandwidth limitation.
- A unified interface for any kind of pre-processing required before analysing data.
- Near real-time indexing of satellite data with optimisation for any high volume traffic.
- Advanced filtering capabilities for satellite imagery data based on all the ingested parameters in metadata files.

- Location-aware searching capabilities powered by indexing engines to facilitate finding AOIs.
- Resilience of data-flow starting from the input process until receiving the output.
- Obtaining near real-time processed products once scenes are captured by the satellite.

The proposed model can be adopted to automate any processing chain dealing with satellite data. The given flexibility through different cloud services allows receiving, processing and deriving information from any kind of intermittent data.

In this study, the proposed model was employed to automate two processing tasks as follows:

1) Creating a training data-set to be used with a deep learning algorithm for spatial resolution enhancement.

2) Producing near real-time land-cover classification service for Landsat-8 data.

Given the afforded flexibility in this model and the tremendous processing capabilities of cloud computing, in the next chapter we explore more complicated processing tasks to be presented as a cloud-based service. Particularly, spatial resolution enhancement techniques were reviewed in order to define the state-of-the-art methodologies. Based on the developed conceptual data model, the next chapter explains how to harness cloud-based data processing pipelines with deep learning techniques to enhance spatial resolution of Landsat-8 and Sentinel-2 data.

Chapter 4

Satellite Image Resolution Enhancement using Deep Learning

In this chapter we explain how deep learning techniques, EO big data and cloud computing can be used to enhance spatial resolution of satellite images. Various spatial resolution enhancement approaches were explored in detail with particular focus on super resolution using deep learning techniques. The terminology Super Resolution is a sub-category of resolution enhancement techniques and it can be applied using several approaches as we will demonstrate in this chapter.

Inspired by SRCNN [Dong et al., 2016], we demonstrate how to re-train and re-design a convolutional neural network which was designed originally for super-resolving conventional photos to fit with satellite image super resolution purposes. SRCNN is one of the state-of-the-art algorithms for super-resolving conventional photos. The differences between conventional photos and satellite image's characteristics in addition to the required adaptation on SRCNN's architecture to fit with satellite images perspective were explored. Moreover, we explain how to utilise the proposed conceptual data model in chapter 3 to automate the process of generating training datasets for the satellite image super-resolution task.

It is noteworthy that part of this chapter is based on a published paper as:

"Multi-modal Remote Sensing Data Fusion Framework", Moataz Ahmed, Tuong Thuy Vu, Tomas Maul, The International Archives of the Photogrammetry, Vol XLII-4/W2, FOSS4G-Europe 2017.

4.1 Resolution Enhancement Introduction

Spatial resolution is one of the most important aspects to evaluate the significance of a satellite image [Demirel and Anbarjafari, 2010]. Applications utilising satellite images to extract useful information depend on how accurate the details in captured scenes are. Expressed in meters, spatial resolution refers to the pixel size in a satellite image. Over the years, spatial resolution has gradually increased, in tandem with advances in remote sensing technologies. Table 4.1 shows different resolutions for multi-spectral sensor loaded satellites from 1999 till 2017. It shows clearly a significant improvement in the accuracy of the spatial resolution which unlocked a new set of applications that were infeasible with previous satellites. On the other side, resolution enhancement from a software perspective is being pursued by remote sensing communities and computer scientists to find cheaper and faster methodologies to obtain better spatial resolution.

Satellite image resolution enhancement can be achieved using different approaches. We categorise these approaches as interpolation based, fusion based and learning based methodologies as explained below.

Table 4.1: Spatial resolution improvements from 1999 to 2017

Satellite	**Year**	**Spatial-Resolution**
Modis-Terra	1999	250-500 meter
Landsat-8	2013	30 meter
SPOT-5	2015	10 meter
Sentinel-2A	2015	10 meter
WorldView-4	2016	1.2 meter

4.1.1 Interpolation based

In this type of resampling, simple equations are applied to satellite imagery. The main purpose of applying such equations is to enhance resolution and obtain better visualization. Bilinear and bicubic interpolation methods are the most well known types to be applied on remote sensing data. Bilinear interpolation works by calculating the weighted average of the nearest four input pixels to generate a smoother output. Bilinear interpolation is commonly used in satellite image processing to estimate missing values and artifacts. Similarly, bicubic interpolation considers the nearest 16 pixels to resample an image. The generated output is smoother with less interpolation distortion compared to bilinear interpolation output. Following the same methodology, the nearest neighbour algorithm is considered as one of the simplest approaches to interpolate an image. Rather than calculating the average value using a weighting criteria or generating an intermediate value based on specific rules, this method simply assigns the unknown pixel value an intensity similar to its neighbouring pixels. The interpolation-based methods are simple but are widely reported to produce outputs containing artifacts and distortions [Titus et al., 2013].

4.1.2 Fusion based

Pansharpening is one of the most applied spatial resolution enhancement in the field of remote sensing data processing. Panchromatic bands generated by satellites carrying panchromatic sensors are always having higher resolution than the spectral sensors. Landsat-8 as an example has a 30 meter multi-spectral band resolution while it has 15 meter panchromatic band resolution. Remote sensing scientists fuse the spectral characteristics from the multi-spectral bands with the spatial characteristics of the panchromatic band to generate 15 meter pan-sharpened images. Several algorithms can be used to transform spectral characteristics from the multi-spectral bands. The Principal Component Analysis (PCA) approach has been widely used in pansharpening process [Vivone et al.,

2015]. PCA is used to transform a set of observations which might be correlated to a set of linearly uncorrelated variables (Principal components).

In pansharpening applications, PCA aims to extract the spatial information in the first component (PC-1) while spectral information of each band are accounted by other components (PC-2,3,..). The first component PC-1 is then replaced with the panchromatic band so that spectral information from other components can be fused with it.

However, the fusion part has to be carefully considered as spectral distortion can be expected according to the applied fusion algorithm [Thomas et al., 2008]. The dissimilarities between multi-spectral and Pan images are due to the effects of the environmental physics and the challenging process of geometric registration. These dissimilarities are more frequent when images were captured from different platforms. In [Blanc et al., 1998], it was proven that the quality of pixel-to-pixel fusion process can easily get affected by geometric distortion less as 0.1 pixel.

4.1.3 Super Resolution

Super resolution aims at recognizing local features from input low-resolution images and retrieve the high-frequency information to construct the missing details in a high resolution output. The terminology appeared in 1984 [Tsai and Huang, 1984] referring to the process of constructing high resolution image from single or multiple low resolution image by recovering additional information using signal processing techniques. SR can be categorised according to the number of input low resolution images used to retrieve the high resolution output [Khizar, 2017] as follows:

Single-Image SR

In which a HR output is constructed from a low resolution image by estimating the underlying high resolution missing pixels [Khizar, 2017]. Being an ill-posed

problem, it is expected that several HR versions of output can be derived from the input image [Hui et al., 2018]. Single-Image SR can be divided into learning-methods and construction-methods as follows:

- **Learning Methods**
  The learning based methods which can also be referred to as example-based methods employ machine learning techniques to estimate the high resolution details of the output image. This process of estimation can be achieved either per pixel or patch-wise [Bevilacqua, 2014]. The pixel-wise procedure infers the HR output image singularly per pixel using statistical learning methods [Zhang et al., 2012] [He and Siu, 2011]. On the other hand, the patch-wise procedure relies on a corresponding dictionary of LR and HR patches which is generated to relate LR patches to their most-likely HR version. It is noteworthy to mention that the accuracy of the relation process depends on the goodness of the created dictionary [Freeman et al., 2002].

- **Reconstruction Methods**
  Reconstruction based methods aim at building the missing high frequency details via interpolating the LR input [Li and Orchard, 2001]. In contrast to learning-based methods, training datasets and dictionaries are not employed in the reconstruction based methods. Instead, constraints are set for the target HR image to enhance the quality of the reconstruction process. Constraints such as regularisation [Aly and Dubois, 2005] or edge-directed interpolation [Tappen et al., 2003] are typically adopted in this approach.

Multi-Frame SR

Conversely to single-image SR techniques, multi-frame SR is applied only when several LR images for the same scene are available [Borman and Stevenson, 1998]. The idea behind this approach is to capitalise on slightly different

perspectives of the same scene. New information/details can be extracted from these differences if sub-pixel shifts are found in the LR input images [Park et al., 2003].

In the next section, satellite image super resolution methodologies and the latest research in this field are explained in detail.

4.2 Satellite Image Super Resolution

In line with progress in sensor accuracy, data processing techniques are continually being developed and refined. Due to its ability to form useful hierarchical representations of complex data, deep learning has made significant contributions to the field of image processing [Huang et al., 2015]. Deep learning algorithms have been used in several remote sensing applications such as classification [Liu et al., 2017] [Kussul et al., 2017], feature selection and extraction [Zhang and Wang, 2015] and recently super resolution (SR) [Liebel and Körner, 2016]. It is a perfect match to big data [Schmitt and Zhu, 2016] and it has shown high performance levels in classical computer vision problems such as SR [Dong et al., 2016]. As we mentioned in section (4.1.3), from a methodological perspective SR using deep learning techniques can be achieved either using multi-frame or single-image approaches. With reference to satellite image super resolution, the multi-frame method can be interpreted as utilising the overlapping areas between scenes to be fed as low resolution input for the algorithm, e.g., scenes 127,057 and 127,058 as shown in figure 4.1. The aforementioned method can exploit useful new information from the different perspectives and sub-pixel shifting of the same spot that could be used to form the high resolution output image [Bevilacqua, 2014]. An alternative way of implementing multi-frame super resolution algorithms might be by utilising satellite image pixel shifts which are introduced by positioning errors [Wang et al., 2018a].

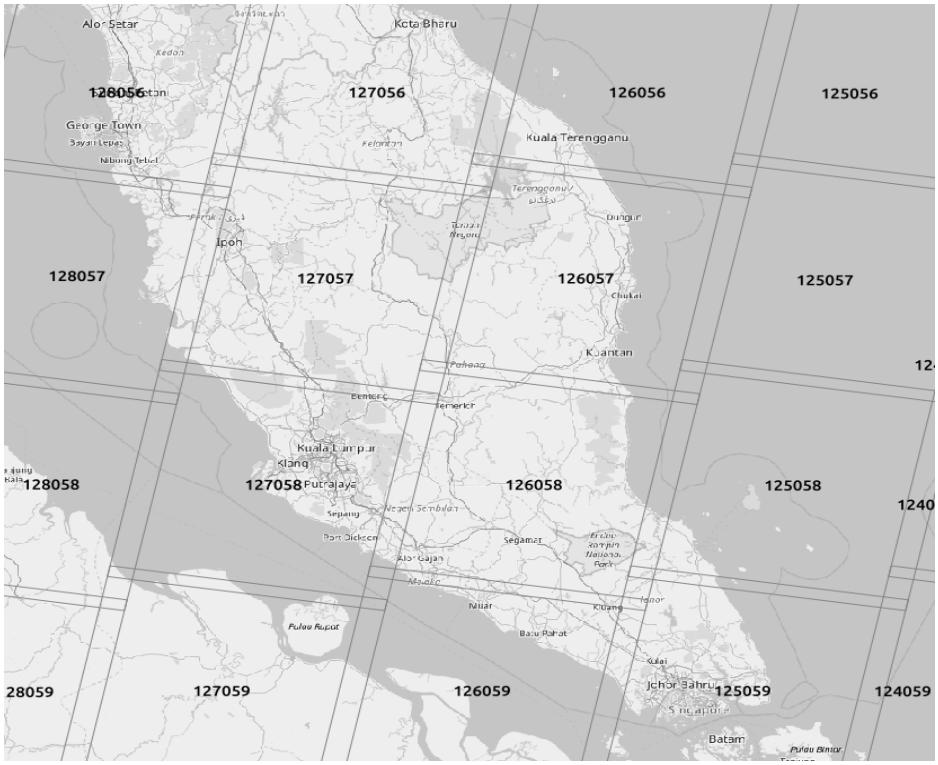


Figure 4.1: The overlapping areas between scenes.

In [Wang et al., 2015], a novel geostatistical model was proposed to generate 250 meter spatial resolution bands from Moderate Resolution Imaging Spectroradiometer (MODIS) [NASA, 2018c] coarser bands (3,4,5,6,7). The MODIS instrument carries sensors with 500 and 250 meter resolutions such as bands 1 and 2 which can be used in a wide range of applications such as global monitoring of deforestation. The proposed idea aims to extract the fine spatial details from 250 meter products using regression modelling and applying area-to-point kriging (ATPK) to up-sample the coarse residuals from the regression. The reported results show that ATPRK-based methodology preserved spectral characteristics of the original coarse MODIS data in addition to outperforming fusion methods based on Principal Component Analysis (PCA), wavelets, High-pass Filter (HPF) and Kriging with External Drift (KED) for

upsampling purposes.

Following the same direction, in [Wang et al., 2016] a Sentinel-2 data-set was used to implement a set of fusion methodologies to upsample bands (5,6,7,8a,11,12) from 20 to 10 meters using bands (2,3,4,8). Authors compared between few data fusion models which can be used with downscaled versions of bands (2,3,4,8) to generate higher resolution outputs (10 meter). Both Component Substitution (CS) and Multi Resolution Analysis (MRA) fusion methodologies were applied and compared with the recently developed At The Point Regression Kriging (ATPRK) [Wang et al., 2015] to evaluate the accuracy and provide recommendations for Sentinel-2 data fusion tasks. The ATPRK approach is an extension for regression kriging and ATPK. Regression kriging is a hybrid interpolation technique which uses regression on covariates and kriging to interpolate residuals of the regression model. The authors used evaluation metrics such as Correlation Coefficient (CC), Spectral Angle Mapper (SAM) and Relative Dimensionless Global Error (ERGAS) which are frequently used to evaluate fusion accuracy processes. The results show that the ATPRK based methodology outperformed CS and MRA based methods. Although the aforementioned papers didn't achieve any progress beyond the maximum resolution the same sensor can produce, the results were still considered as a step forward towards satellite image super resolution. In addition, the results were heavily reliant on the At The Point Regression Kriging (ATPRK) [Wang et al., 2015] methodology which was introduced for the first time in 2015 and was applied to MODIS data.

In [Lanaras et al., 2018], the authors reported a super resolution algorithm which is based on a fusion methodology denoted as SUPer-REsolution for multispectral Multiresolution Estimation (SupReME). The reported methodology targets satellite sensors capturing multiple spatial resolution products such as Sentinel-2 which acquires scenes at 10, 20 and 60 meter spatial resolutions. The aim of this

methodology is to upscale spectral bands to the highest spatial resolution of the satellite products. For instance, super-resolving Sentinel-2 20 meter bands (B5, B6, B7, B8a, B11, B12) to 10 meters. SupReME relies mainly on the observation model of blurring and down-sampling HR bands to generate LR samples. SupReME utilises the textural information from HR bands to encode the cease of the data in LR bands. It propagates the spatial information to LR bands using regularization technique which assumed that spatial information discontinuities are likely to be found at same area across all LR bands. By inverting the blurring/down-sampling observation model, LR bands can be super-resolved to match the maximum resolution of HR bands. The proposed method contributes to environmental and climate applications as it targets upscaling bands within the infrared spectrum. In [Lanaras et al., 2018], the authors reported that their approach SupReME outperformed the state-of-the-art approaches. However, this approach was only limited to infrared bands while visual bands (B2,B3,B4,B8) were disregarded. Moreover, the performance of the designed approach depends on the resolutions of the attached sensors and there wasn't any test to validate the possibility of applying the same methodology with different satellite such as Landsat-8. Moreover, as stated by the authors, 60 meter bands were upsampled to 10 meters but with accuracy similar to 20 meters.

Although the aforementioned papers achieved good progress in the satellite image resolution enhancement domain, deep learning techniques weren't employed in any of them.

In [Liebel and Körner, 2016], the authors took advantage of deep learning based super resolution work published by Dong et al. [Dong et al., 2016] to super-resolve generic photos using an architecture named Super Resolution Covolutional Neural Network (SRCNN). SRCNN represents a feed-forward neural network which reformulates sparse-coding super resolution methods in a deep learning architecture/algorithm based approach. SRCNN proposed an

end-to-end architecture which maps low-resolution images to high-resolution ones using convolutional layers as explained in section 4.3. In terms of super resolution methodology, SRCNN resides under the single-image super resolution category. In [Liebel and Körner, 2016], an SRCNN architecture was employed to super-resolve Sentinel-2 data band by band separately. The authors designed the network to upscale red, green and blue bands separately using a single band layer input and a single band layer output. As reported by the authors, the experiments showed poor results when the network was tested with bands other than the one used in training. Moreover, the authors concluded that combining RGB bands is of little value compared to single bands and the original luminance and chrominance channels reported in [Dong et al., 2016].

Apart from satellite imagery, the problem of super resolution using deep learning has been intensively studied. However, real-world applications have been mostly limited to conventional/generic image resolution enhancement compared to being applied in practice to satellite imagery data [Kawulok Michałand Benecki et al., 2018]. This can be understood from the number of research works presented up to the end of 2018 as we explored in this section. Inspired by the aforementioned research, in this study we focus on single satellite image super resolution using a deep learning approach. The architecture of SRCNN was extended to match the specificity of satellite imagery data. Both Landsat-8 and Sentinel-2 datasets were used to test the accuracy of the architecture after modifications. A detailed description of the architecture is explained in section 4.4.1.

The following section demonstrates how to create a training dataset following the aforementioned conceptual data model in chapter 3. Following the rule-of-thumb in creating training datasets for single-image super resolution purposes, the original high-resolution image/sample was considered as high resolution target/label and a synthesised version is generated to represent the lower resolution sample. The process of creating the low resolution sample relies on down-sampling the high resolution target/label first and then up-sampling it again using the same down-sampling factor.

This results in having an original high resolution sample in addition to a synthesised low resolution copy with the same dimensions. The following section explains this process in detail using the proposed conceptual model in chapter 3.

4.3 Creating training dataset for single-image super resolution

Building training datasets for deep learning algorithms is a problematic process that can affect the accuracy and speed of processing and value prediction [Castelluccio et al., 2015] [Gardner Daniel, 2017], and satellite images are no exception. Likewise in any deep learning task, the pre-processing step is of vital importance however, it is usually difficult to build datasets of the scale/size required by deep learning. In general, datasets created for super resolution tasks contain instances representing low and high resolution representations. Section 4.1.3 introduced multiple ways of creating pairs of low and high resolution training instances. However, the aforementioned methodologies were targeting fusion techniques instead of deep learning to enhance spatial resolution.

In order to build a training dataset for deep learning based super-resolution purposes, 2 freely available satellite imagery datasets with different spatial resolutions were used to test the algorithm including Landsat-8 (30 meters) and Sentinel-2 (10 meters).

The pre-processing steps including data acquisition phase are implemented following the proposed data model in chapter 3 as follows:

- Task 1. Create shapefiles to be used in scene cropping.
- Task 2. Assign coordinate reference system (CRS) to the shapefiles.
- Task 3. Crop scenes according to the created shapefiles.

- Task 4. Downscale generated patches by 2x.
- Task 5. Upscale samples by 2x (Bicubic).
- Task 6. Split data between training, validation and testing portions.

Task 1 Refers to the process of creating shapefiles with specific dimensions. The shapefiles will be used to crop samples from the downloaded AOI scenes. The uploaded area of interest is converted to a bounding box and a grid of polygons with defined dimensions (64x64 pixels) will be created inside that bounding box. The input of this task originates from the intermediate storage as we mentioned in chapter 3 while the output is be generated as a set of shapefiles to be passed to the next task. Figure 4.2 explains the workflow of task 1 while Figure 4.3 shows an example of the created footprints.

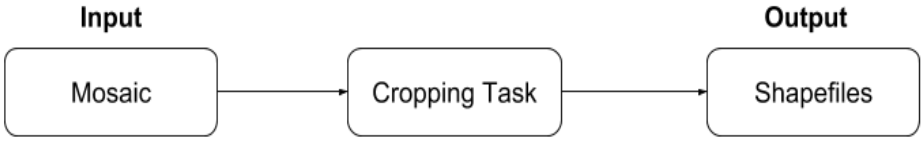


Figure 4.2: Task 1 takes a mosaic of AOIs and generates footprints for training instances.

Task 2 receives the input from task 1 as shapefiles however after the cropping process, the generated shapefiles need to be assigned a reference system per sample. The main function of this task is to assign a Coordinate Reference System (CRS) per shapefile so that when raster data is cropped, the positions can be matched correctly. The output from this task is a set of reprojected shapefiles which can be used as footprints in the raster cropping task (refer to Fig. 4.4).

Task 3 uses the output from the reprojection task and feeds it as input to the warping tool which crops the training samples according to the projected shapefile dimensions. As an output from this step, training samples are created as 64x64 patches which are then ready for the low-resolution synthesizing process.

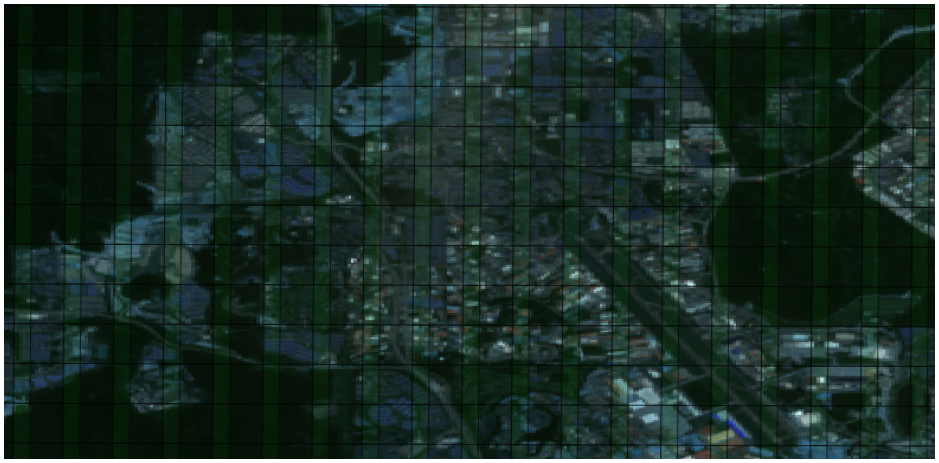


Figure 4.3: Example of task 1 after creating (64x64 pixels) training footprints for AOI over Kuala Lumpur.

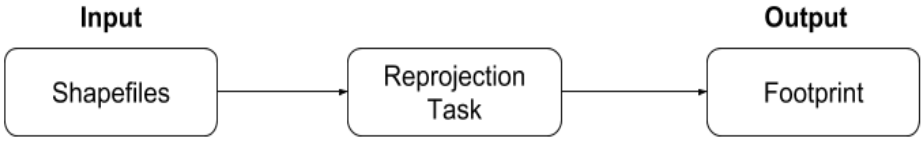


Figure 4.4: Task 2 receives shapefiles as input and assigns projection per polygon.

Figure 4.5 shows the workflow to produce a projected training sample while Figure 4.6 shows an example of the output.

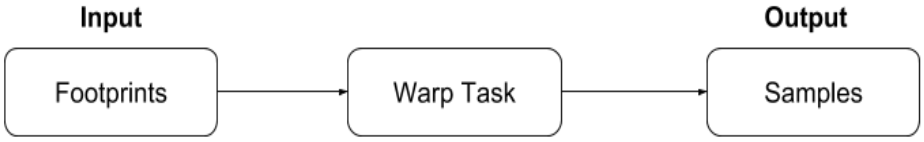


Figure 4.5: Task 3 matches the projected footprint with the mosaic (AOI) and subsets the training samples.

Regarding tasks 4 and 5, in order to create a low-resolution versions from

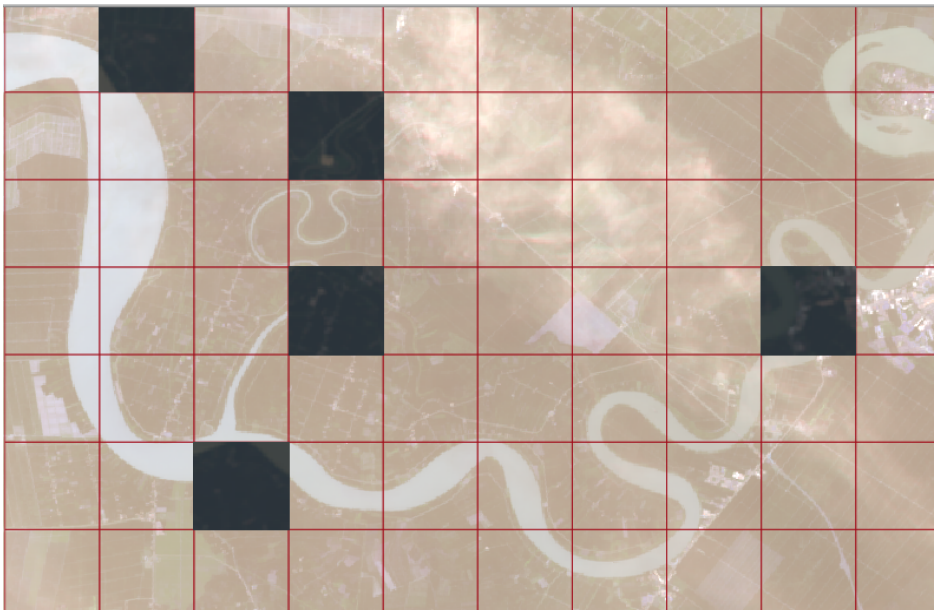


Figure 4.6: Example of task 3 after warping a projected footprints.

original high resolution training samples, the generated samples are down-sampled by a factor of 2 and then up-sampled by the same factor so that we keep the same dimensions and at the same time generate a low-resolution version from the same sample/location. This step ensures that we have a ground-truth high resolution sample (original sample) and a synthesised low-resolution version with the same dimensions.

Figure 4.7 shows the workflow to generate a synthesised low-resolution training sample while Figure 4.8 shows an example of the created low-resolution training sample.

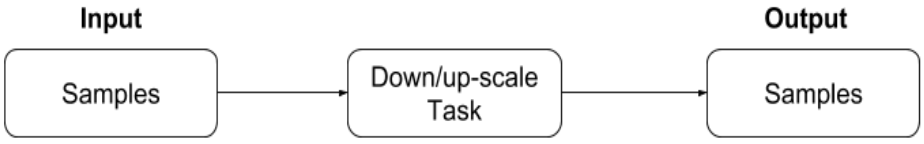


Figure 4.7: Task 4 and 5 synthesis the low resolution training samples through down and up scale of instances.



Figure 4.8: Example of synthesised low-resolution training sample after down/up-scaling process in task 4 and 5.

Task 6 splits the generated training samples into training, validation and test datasets. As a rule of thumb, the percentage of division can be 70% training, 20% validation and 10% for testing. It is of vital importance to ensure the divergence of the data in terms of separating training samples from validation and testing so that the model can learn without bias (refer to Fig. 4.9).
Once the processing pipeline has accomplished task 6, the dataset is ready for the training process.
Both Landsat-8 and Sentinel-2 datasets were fed into the processing pipelines to create super resolution datasets. The area of interest included peninsular Malaysia in addition to the east side of Malaysia. Figures 4.10 and 4.11 show training areas of interest. The number of created training instances reached 20,000 with 64x64 pixels per instance. Task 6 assigned 14,000 instances for training, 4000 for validation and 2000 for testing.

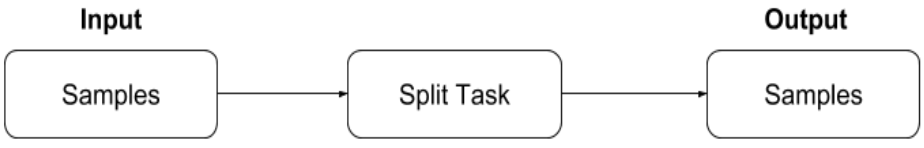


Figure 4.9: Task 6 splits dataset into training, validation and test sets.



Figure 4.10: Training area from peninsular Malaysia.



Figure 4.11: Training area from east side of Malaysia (Sarawak)

The next section explains how SRCNN works and is followed by the proposed changes to fit with the satellite imagery domain.

4.4 SRCNN

Convolutional Neural Networks (CNNs) are intended for processing data that exhibit topological regularities and which are shaped in multi-dimensional arrays such as images [LeCun et al., 1990]. Currently, CNNs are extensively adopted by computer vision scientists for classification tasks [LeCun et al., 2015], but have yet to receive the same amount of attention for SR tasks, especially in the domain of satellite images.

In 2016, Dong *et al.* [Dong et al., 2016] outperformed the state-of-the-art of published methodologies pertaining to deep learning single-image SR for the generic/conventional photography domain. Despite the simplicity of the presented SRCNN model, the demonstrated performance was good enough to score an average of 36.66 dB PSNR [Joshi et al., 2016] when applied to the Set5 dataset [Bevilacqua et al., 2012a]. Figure 4.12 shows examples from Set5 datast. The accuracy achieved by SRCNN inspired us to utilise the same model and build over the proposed architecture to adapt it to the satellite imagery domain.

Similar to an auto-encoder approach [Cui et al., 2014], the designed model intends to map the high resolution (HR) features directly from the low resolution (LR) ones.

Figure 4.13 shows the SRCNN model architecture which contains 3 layers as follows:



Figure 4.12: Set5 dataset examples.

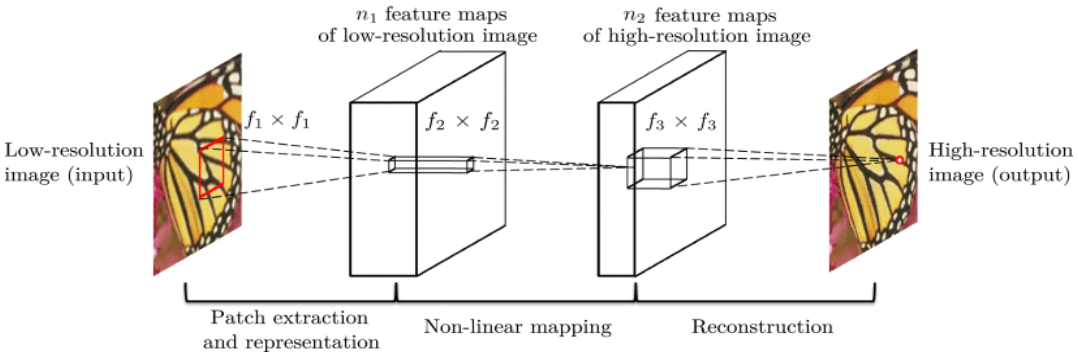


Figure 4.13: SRCNN architecture by [Dong et al., 2016].

- Low-resolution feature extraction. Given the input as an RGB image, the first step is to extract low-resolution features according to a specified number of filters. The first operation $F_1(\mathbf{Y})$ can be represented as proposed by [Dong et al., 2016] in Equation 4.1:

$$F_1(\mathbf{Y}) = \max(0, W_1 * \mathbf{Y} + B_1) \tag{4.1}$$

  Where *W* represents n_1 number of filters of shape (*number of channels* $\times$ *filter size* $\times$ *filter size*). B_1 corresponds to biases while '*' refers to the convolution operation. This is followed by the ReLU function *max(0, X)* [Nair and Hinton, 2010], which is useful for minimizing training time [Dong et al., 2016, Nair and Hinton, 2010]. The output from this operation is a collection of low-resolution feature maps that will be used as input to the next layer.

- Non-linear mapping. In this phase, the generated feature maps from the first layer are mapped to high resolution features that will be used later to construct the high resolution image. The second operation is denoted as follows:

$$F_2(\mathbf{Y}) = \max(0, W_2 * F_1(\mathbf{Y}) + B_2) \tag{4.2}$$

Where W_2 refers to n_2 filters of shape ($n_1 \times$ *filter size* $\times$ *filter size*), which are applied to the output of F_1, after which biases B_2 are added, followed by the ReLU function.

- Output construction. The final layer combines the high resolution representations from the second layer to produce the final output high resolution image through a convolutional layer. The generated output has the same resolution as the original image before the downscaling process. This operation is denoted as:

$$F(\mathbf{Y}) = W_3 * F_2(\mathbf{Y}) + B_3 \tag{4.3}$$

Where W_3 refers to three (RGB) channels shaped as (n_2 *x filter size x filter size*), F_2 is the output from the second layer and B_3 represents biases.

4.4.1 SRCNN Adjustments

Given the complexity/dimensionality of satellite imagery compared to conventional photos [Ma et al., 2015], the architecture of SRCNN required several adaptations to fit with this complexity. SRCNN converts image channels to different color space (YCbCr). In YCbCr color space, channels are represented as luminance/brightness (Y) in addition to two color difference channels, Cb which is blue minus luminance (B-Y) and Cr which is red minus luminance (R-Y). The process of converting RGB bands to another color space is not favoured for satellite data [Liebel and Körner, 2016] especially that this conversion will decrease the information/size of the image by factor of 3 or more, so the RGB composite was used instead. Moreover, near infrared bands were employed alongside RGB to explore any potential accuracy boost.
In addition, the size of the receptive field, activation functions, number of layers and number of feature maps were changed to fit with the characteristics of satellite images.

Detailed explanations of all experimental setups according to the proposed changes are described in the next section.

4.5 Results

In order to evaluate the performance of SRCNN with the aforementioned adjustments, a set of experiments were carried out to verify the usefulness of the approach in the satellite image super resolution domain. In order to save processing time, every reported experimented was included based on 2 preceding small and medium sized datasets to measure success or failure before running the experiment on the large scale dataset. As demonstrated in chapter 3, the proposed processing pipelines were employed to generate multiple scale datasets as follows:

- Small scale dataset containing 2,000 instances (50 epochs)
- Medium scale dataset containing 10,000 instances (100 epochs)
- Large scale dataset containing 32,000 instances (250 epochs)

The number of epochs was proportional to the size of the dataset given that the overall complexity of the learning problem increased for the larger datasets.

4.5.1 Experiment 1

The methodology in SRCNN [Dong et al., 2016] was built on training the network on the YCbCr color space version of the Set5 [Bevilacqua et al., 2012b] training dataset. The authors reported one experiment using RGB however they concluded that RGB was of little value as it added only .07 dB to the PSNR accuracy of the YCbCr color space. Contrarily to this assumption, satellite images are greatly affected by this property of SRCNN. The characteristics of the luminance channel compared to both Cb and Cr are dissimilar as the luminance channel measures the intensity of the brightness while Cb represents the blue

chroma component and Cr corresponds to the red chroma component.

Also from a dimensionality reduction perspective, SRCNN super-resolved the Y channel only relying on the fact that it has the majority of the usable information. This assumption cannot be validated for satellite image super resolution [Liebel and Körner, 2016] although it can be applied in the segmentation domain as explained in [Packyanathan et al., 2015].

In this experiment the YCbCr color model was changed to natural color combination to be tested with both Landsat-8 and Sentinel-2 datasets. Bands 4 (Red), 3 (Green) and 2 (Blue) were used to form RGB bands combination. In addition, training samples of size 64x64 were considered in this experiment to measure the effects of feeding different input dimensions to the network.

Results were evaluated quantitatively using Peak-Signal-to-Noise-Ratio (PSNR) and qualitatively by visualising random test samples after the super-resolving process. Both msiSRCNN in [Liebel and Körner, 2016] and bicubic interpolation methodologies were considered as baselines to compare our proposed changes against.

Table 4.5.1 shows a comparison between the proposed change in the input dimensions to be 64x64 instead of 33x33 pixels as implemented in both SRCNN and msiSRCNN. It is clearly noticed that a 9-1-5 architecture with 64x64 outperformed the baseline methodologies. The results obtained by msiSRCNN in [Liebel and Körner, 2016] were better due to reducing the dimensionality of the input layer to a single channel instead of 3 (RGB). However, reducing the dimensions of the input layer by using a single channel training approach with multispectral satellite imagery datasets dropped a lot of cross-band information which can be useful for training the model as we explain in experiment 2.

In [Liebel and Körner, 2016], msiSRCNN was experimented against RGB color combination however the reported results had significant difference between the minimum (36.235) and maximum (68.583) achieved PSNR and it wasn't possible to reproduce the same results using our small, medium and large datasets. Moreover, after reviewing the papers which have cited [Liebel and

Table 4.2: Comparison between PSNR values of 64x64 input dimensions against msiSRCNN and bicubic interpolation 33x33 in logarithmic decibel dB.

Dataset	64x64	msiSRCNN	Bicubic Interpolation
Landsat-8	44.768 dB	43.956 dB	38.928 dB
Sentinel-2	44.827 dB	43.912 dB	38.771 dB

Körner, 2016], we found a similar approach in [Mei et al., 2017] which has reported an accuracy of 32.479 dB using msiSRCNN approach with Hyper-Spectral Images (HSI) dataset. On the other hand, our methodology obtained a minimum of (38.548 dB) and maximum of(47.125 dB) among 2,000 test samples which were never exposed to training process.

4.5.2 Experiment 2

In this experiment, the SRCNN architecture was extended to adapt to the diversity of sensors attached to orbiting satellites. Both Sentinel-2 and Landsat-8 satellites are carrying near-infrared sensors producing 10 and 30 meter spatial resolution scenes respectively. Bands 5, 6 and 7 representing near and short-wave infrared in Landsat-8 scenes were merged in addition to RGB (4,3,2) bands to form a 6 channels input layer while band 8 representing near-infrared channel in Sentinel-2 was merged with RGB (4,3,2) bands to form a 4 channels input layer.
Taking advantage of the flexibility of the SRCNN architecture, the network design was altered to accept 6 and 4 channels input samples while preserving the output construction layer's output as 3 channels (RGB). We proposed feeding in near and shortwave infrared bands to the network so that it could learn from the cross-bands information if found.
Table 4.3 shows the gained accuracy from appending additional IR and NIR to both Sentinel-2 and Landsat-8 RGB training samples. The additional bands granted useful information to the model which helped in inferring high frequency details in the output layer. The appended channels can be considered as a specific type of data augmentation for satellite image super resolution neural networks as

Table 4.3: Comparison between RGB against RGB+IR/NIR bands and msiSRCNN

Dataset	RGB	RGB+IR/NIR	msiSRCNN
Landsat-8	44.768	45.125	43.956
Sentinel-2	44.827	45.221	43.912

we explain in next chapter.

4.5.3 Experiment 3

In this experiment, the size of receptive fields, type of activation functions, number of layers (model depth) and number of feature maps were examined and fine-tuned with reference to the characteristics of satellite images. Different model configurations were tested to determine which could be extended to the SRCNN architecture to add value to the model.

Receptive Field

In convolutional neural networks, receptive fields refer to the region in the input layer that a feature/kernel is looking at. When design a neural network, the receptive field dimensions aren't generally following any specific rule. The decision typically depends on experience or on manually trying different dimensions until getting the highest accuracy.

In tasks such as image segmentation or super resolution where we predict a value for every single pixel, it is of vital importance to confirm that every pixel has a large enough receptive field so that no significant information was disregarded while making predictions.

The importance of understanding the effects of receptive field dimensions on CNN performance gained more attention recently. In [Luo et al., 2017] receptive fields were diagnosed to study their impact on CNN outputs. It was clearly stated that not every pixel in the receptive field contributes equally to the generated output. This motivated us to measure the effects of enlarging receptive fields in

satellite image super resolution tasks.

In this experiment, receptive fields were increased by introducing new layers to the model in addition to enlarging kernel size. (See Tables 4.4, 4.5, 4.6, 4.7 and 4.8 for experimental setups).

The number of training parameters in every experiment can be obtained using the following equation:

$$NP = (F_{\mathrm{h}} * F_{\mathrm{w}} * C + 1) * n \tag{4.4}$$

where F_{h} is kernel height, F_{w} is kernel width, C represents the number of channels in the input layer and n is the number of features.

Table 4.9 reflects how different architectures affected the accuracy of super resolving the Sentinel-2 dataset. It shows that the best results were achieved using larger receptive fields as introduced in experiment 3A. In experiment 3E, a new layer was added as a third level (1x1 convolution) which increases the non-linearity in the model. The added value from such type of layer is to tune the model complexity (in this case it increases the complexity of the model). However, adding too much complexity to the model can produce over-fitting while over simplified models might under-fit data samples.

Table 4.4: Experiment 3A using kernels of size 9x9 Level1, 1x1 Level2, 5x5 Output, n_1 = 128 and n_2 = 64.

Layer (type)	**Output Shape**	**Param #**
input_1 (InputLayer)	(None, 64, 64, 3)	0
level1 (Conv2D)	(None, 64, 64, 128)	31232
level2 (Conv2D)	(None, 64, 64, 64)	8256
output (Conv2D)	(None, 64, 64, 3)	4803
Total parameters: 44,291 **Trainable parameters: 44,291**		

Table 4.5: Experiment 3B using kernels of size 9x9 Level1, 1x1 Level2, 5x5 Output, $n_1 = 64$ and $n_2 = 32$.

Layer (type)	**Output Shape**	**Param #**
input_1 (InputLayer)	(None, 64, 64, 3)	0
level1 (Conv2D)	(None, 64, 64, 64)	15616
level2 (Conv2D)	(None, 64, 64, 32)	2080
output (Conv2D)	(None, 64, 64, 3)	2403
Total parameters: 20,099 **Trainable parameters: 20,099**		

Table 4.6: Experiment 3C using kernels of size 7x7 Level1, 1x1 Level2, 5x5 Output, $n_1 = 128$ and $n_2 = 64$.

Layer (type)	**Output Shape**	**Param #**
input_1 (InputLayer)	(None, 64, 64, 3)	0
level1 (Conv2D)	(None, 64, 64, 128)	18944
level2 (Conv2D)	(None, 64, 64, 64)	8256
output (Conv2D)	(None, 64, 64, 3)	4803
Total parameters: 32,003 **Trainable parameters: 32,003**		

Table 4.7: Experiment 3D using kernels of size 7x7 Level1, 1x1 Level2, 5x5 Output, $n_1 = 64$ and $n_2 = 32$.

Layer (type)	**Output Shape**	**Param #**
input_1 (InputLayer)	(None, 64, 64, 3)	0
level1 (Conv2D)	(None, 64, 64, 128)	9472
level2 (Conv2D)	(None, 64, 64, 64)	2080
output (Conv2D)	(None, 64, 64, 3)	2403
Total parameters: 13,955 **Trainable parameters: 13,955**		

Table 4.8: Experiment 3E using kernels of size 9x9 Level1, 1x1 Level2, 1x1 Level3, 5x5 Output, $n_1 = 64$, $n_2 = 32$ and $n_3 = 16$.

Layer (type)	**Output Shape**	**Param #**
input_1 (InputLayer)	(None, 64, 64, 3)	0
level1 (Conv2D)	(None, 64, 64, 64)	15616
level2 (Conv2D)	(None, 64, 64, 32)	2080
level3 (Conv2D)	,(None, 64, 64, 16)	528
output (Conv2D)	(None, 64, 64, 3)	1203
Total parameters: 19,427 **Trainable parameters: 19,427**		

Table 4.9: A comparison between different architectures and their effects on accuracy.

Experiment	**Average PSNR**	**Number of Parameters**	**Number of Layers**
EXP-3A	44.301	44.291	2
EXP-3B	44.253	20.099	2
EXP-3C	44.277	32.003	2
EXP-3D	44.264	13.955	2
EXP-3E	44.359	19.427	3

4.6 Conclusion

In this chapter, various resolution enhancement techniques were demonstrated. The proposed conceptual model in chapter 3 was employed to generate 2 training datasets based on Landsat-8 and Sentinel-2 satellite images. The created training datasets were fed into the SRCNN model which was originally designed to super-resolve conventional photos. We explained the differences between conventional photos and satellite images and how it might affect the model architecture. The SRCNN architecture was modified and re-trained using the created training datasets. A set of experiments was carried out showing the accuracy gains from applying such modifications.

The contributions added through this chapter can be summarised as follows:

- Reviewing various types of satellite image spatial resolution enhancement approaches.
- Introducing how cloud-based geo-processing can be used to automate the process of generating training datasets for satellite image super resolution purposes.
- Providing an alternative approach to enhance satellite image spatial resolution in case of absence of panchromatic sensors.
- Evaluating the possibility of using deep learning super resolution algorithm which was originally tested in conventional photos domain in satellite image super resolution domain.
- Extend state-of-the-art super resolution architecture SRCNN to exploit satellite image multispectral characteristics.
- Fine tuning the SRCNN model to perform better with satellite images.

Chapter 5

Boosting accuracy using data augmentation techniques

In this chapter, we explore the possibility of increasing the SRCNN accuracy using augmentation techniques from remote sensing data perspective. Traditional data augmentation techniques were reviewed and tested to quantify their effect on the SRCNN network. Moreover, we propose a novel fusion-based augmentation technique which can support the model with useful data representations at early stage of training. We prove that the performance of the proposed data augmentation technique exceeded traditional augmentation methodologies.

It is noteworthy that this chapter will be presented in Living Planet Symposium, 2019 as:

"Data Augmentation Techniques for Deep Learning Based Satellite Image Super-resolution", Moataz Ahmed, Tomas Maul, Tuong Thuy Vu.

5.1 Introduction

Data augmentation is a well known technique that is frequently used in machine learning tasks to increase the number of training instances and hence decrease model over-fitting. In this chapter we propose a data augmentation technique that can further boost the performance of satellite image super resolution tasks. A super-resolution convolutional neural network (SRCNN) was adopted as a state-of-the-art deep learning model to test the proposed data augmentation technique. Different augmentation techniques were studied to investigate their relative importance and accuracy gains. We categorized the augmentation methods into instance based and channel based augmentation methods. The former refers to the standard approach of creating new data instances through applying image transformations to the original images such as adding artificial noise, rotations and translations to training samples, while in the latter we add auxiliary channels (or custom bands) to each instance, which helps the model learn useful representations. Adding auxiliary derived channels to a satellite image RGB combination can be seen as a spectral-spatial fusion process as we explain later. We propose an edge-focused feature extraction to be stacked with training samples in addition to contrast enhanced channels. Several experiments were carried out to evaluate the efficacy of the proposed channel augmentation/fusion approach compared with traditional data augmentation techniques such as rotation, flip and noisy training inputs. The reconstruction quality of the high resolution output was quantitatively evaluated using Peak-Signal-To-Noise-Ratio (PSNR) and qualitatively through visualisation of test samples before and after super-resolving.

5.2 Background

Massive advancements have been witnessed in Remote Sensing technologies recently. Whether improving sensors or processing techniques, these advancements are reflected in terms of the 5Vs of big data [Yang et al., 2016a], i.e.: volume, velocity, variety, veracity and value. The spatial, spectral and temporal resolutions of Remote Sensing data, are core contributors to the volume factor. Moreover, very high spatial resolution (VHR) datasets are increasingly emerging as superior solution components that cover the needs of various geospatial and remote sensing applications [Romero et al., 2016]. For example, sub-metric spatial resolution has been reached by recently launched satellites such as WorldView-4 [Digital Globe, 2017]. Nevertheless, VHR datasets are still expensive and only low to mid resolution datasets such as Landsat and Sentinel [AWS, 2017a, AWS, 2017b] are open for free use and download. For this reason, there is a current need for enhancing the freely available, lower resolution datasets.

In line with progress in sensor accuracy, data processing techniques are continually being developed and refined. Due to its ability to form useful hierarchical representations of complex data, deep learning has made significant contributions to the field of image processing [Huang et al., 2015]. Deep learning algorithms have been used in several remote sensing applications such as classification [Liu et al., 2017, Kussul et al., 2017], feature selection and extraction [Zhang and Wang, 2015] and super-resolution (SR) [Liebel and Körner, 2016]. It is a perfect match to big data [Schmitt and Zhu, 2016] and it has shown high performance levels in classical computer vision problems such as SR [Dong et al., 2016]. From a methodological perspective, SR using deep learning techniques can be achieved either using multi-frame or single-image approaches. The former relies on building a model which is capable of learning how to enhance spatial resolution through learning features from multiple scenes from different perspectives/angles of the same spot. With reference to satellite image super resolution, the multi-frame method could be interpreted as

super-resolving the overlapping areas between scenes e.g. scenes 127,057 and 127,058 (refer to Fig. 4.1). The aforementioned method can exploit useful new information from the different perspectives and sub-pixel shifting of the same spot that could be used to form the high resolution output image [Bevilacqua, 2014]. The single-image approach, on the other hand, relies on recovering a high resolution image from a single lower resolution image [Dong et al., 2016]. The original high-resolution image corresponds to the target and a synthesized version is generated to represent the lower resolution source by a down-sampling process applied to the target, followed by an up-sampling of the target image using the same down-sampling factor.

Unlike trivial image interpolation processes (e.g. bicubic or bilinear filtering) which rely mainly on magnifying the existing details of the input image, SR targets the prediction of details that were missing from the input low resolution image [Bevilacqua, 2014].

In this study we focus on single satellite image super resolution using a deep learning approach. Building training datasets for deep learning algorithms is a problematic process that can affect the performance and speed of classification or regression values [Castelluccio et al., 2015] [Gardner Daniel, 2017], and satellite images are no exception. It is usually difficult to build datasets of the scale required by deep learning. Data augmentation is frequently reported to mitigate the problem of data scarcity in many domains [Ding et al., 2016]. The technique also reduces over-fitting, which can occur when applying the model to closely related data instances [Wang and Perez, 2017] and over-complex models. However, unfortunately not much work has been reported in the domain of satellite image super-resolution with data augmentation techniques[1].

In [Pouliot et al., 2018], the authors tested satellite image super resolution using deep and shallow convolutional neural networks to demonstrate the effects of

[1]Searching Scopus and Google Scholar databases for papers published from 2012-2018 with the phrase ”satellite image” AND ”augmentation” AND ”super-resolution” OR ”super resolution” returned only 32 results and majority of them mentioned data augmentation as a technique to increase the number of training samples.

tuning the training model depth on the accuracy. The authors used SRCNN methods to super resolve Landsat-8 and Landsat-5 images using Sentinel-2 data as a target/label. Although the authors explained the importance of data augmentation techniques, they stated clearly that no data augmentation approaches were used except for Landsat-5 data to cover the lack of training samples.

In [Liebel and Körner, 2016], SR was applied on Sentinel-2 [AWS, 2017b] 13 spectral bands without mentioning any usage of data augmentation techniques. The same applies to [Wang et al., 2018b], where super-resolution convolutional neural networks (SRCNNs) were applied to super-resolving aerial images. Both papers reported relatively high levels of accuracy.

In this chapter, we demonstrate how to apply channel and instance augmentation/fusion techniques to super-resolution problems in order to achieve higher accuracy. Inspired by [Cirean et al., 2012] and [Ahn et al., 2015] data augmentation approaches for classification and restoration problems, we formed a spatial-spectral fusion at feature level which can boost satellite image super resolution accuracy. We also compare the performance of the proposed fusion technique against standard instance augmentation approaches encapsulated by rotated, flipped and noisy inputs.

This study aims to answer the following questions:

1. Does data fusion via channel augmentation boost accuracy of satellite image super resolution?
2. What are the most useful additional bands to be fused with input training samples?
3. Does traditional instance augmentation based on mirror flips, rotation, and noise, add value to the model?
4. What type of noise is most useful for instance augmentation for satellite image SR?

Section 5.3 provides a detailed description of the methodology, including the convolutional neural network, dataset, data augmentation techniques and experimental design adopted. Section 5.4 summarizes the main results obtained and section 5.5 provides several conclusions and guidelines for future work.

5.3 Methodology

Data Augmentation

Data augmentation aims at enlarging the dataset in order to address gaps in data representation and to minimize the problem of over-fitting. This leads to improved model performance and prevents imbalanced learning. In case of the image classification domain, both satellite and conventional images have benefited from several augmentation techniques [Ding et al., 2016, Wang and Perez, 2017]. In satellite image classification, clipping, rotating, flipping, shifting and translating are the most commonly used image transformations [Ding et al., 2016, Yang et al., 2016b], whereas in the context of satellite image super-resolution, materials weren't available to form a strong opinion on which augmentation techniques were more useful. Moreover, we assume that the statistical properties of satellite images are sufficiently different from generic photographs, thus affecting the effectiveness of SR solutions, and justifying a study that focuses on data augmentation techniques specifically in the satellite image super resolution domain.
We categorize augmentation techniques in 2 main groups as follows (refer to Fig 5.1):

Instance-based augmentation

This refers to all well-known geometric, coloring, noise, deformation, translation, brightness and smoothing image transformations which have been used in scene classification and conventional image super resolution tasks to

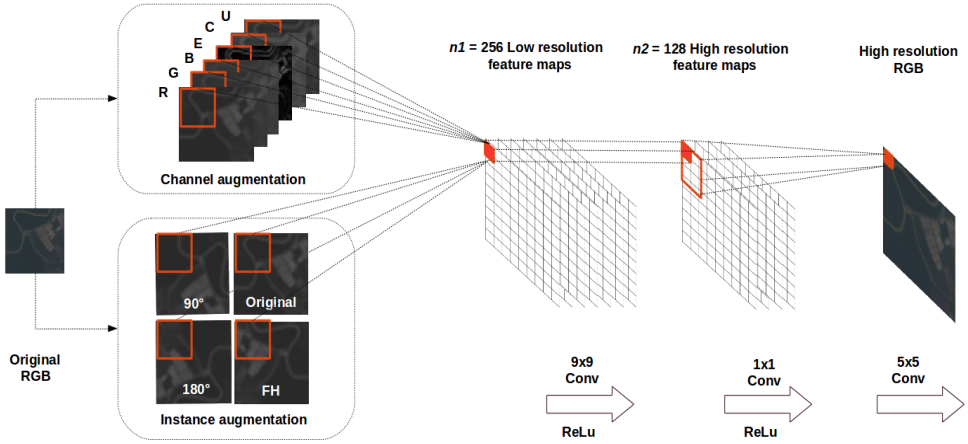


Figure 5.1: SRCNN architecture including the proposed data augmentation methods at the input layer where E refers to edge detection layer, C contrast enhanced layer and U unsharp mask layer.

increase the number of samples/instances in a dataset.

Fusion-based augmentation

This represents stacking additional bands that might add supplementary beneficial observations (or perspectives) to the model that contribute towards improving model accuracy. In other words, we add a set of derived channels to be fused with input data which increases the dimensionality of the data rather than the number of training instances.

Since there are many types of kernels that can be applied to images to derive meaningful features, in the next section we focus on some of the most relevant to denoising, sharpening and resolution enhancement, as we believe that such features might be useful to the model. Although deep architectures traditionally aim to automated the feature extraction process, we prove quantitatively and qualitatively that fusing manually extracted features with training samples adds useful representation to the model which can boost super resolution accuracy.

The proposed added features include edge detection, unsharp masking and contrast enhancement. We argue that adding such features to the input will prevent the network from learning irrelevant kernels in addition to emphasizing the edge-focused and sharpening features. At the same time, this can help in boosting the overall model performance. A detailed description of each channel and how it gets fused with the input layer is explained in the following sections.

- **Edge Detection**

  In general, any kind of convolutional neural network attempts to find useful representations of data via edges, corners, textures and many other features. At the beginning of a neural network, kernels extract simple features such as edges while the extraction becomes much more complex and abstract when it goes deeper through the network. Since edges are very important features in CNNs in general and particularly in super resolution, it motivated us to study the effect of fusing manually generated edge features on super resolution accuracy.

  In order to derive edge features form satellite images, we converted an RGB combination to grayscale first and hence we were able to create different types of edges features. Edge kernels such as Sobel, Touzi and Gradient are the most used ones in satellite image analysis applications. However, a gradient-based approach was adopted based on several experiments as we explain later in the results section.

  Gradient edge detection uses derivatives to detect large intensity changes in an image [Katiyar and Arun, 2014] using the magnitude and direction of vectors. Magnitude and direction can be calculated through equations 5.1 and 5.2 respectively where $\boldsymbol{F}$ refers to the image function, and $\boldsymbol{x}$ and $\boldsymbol{y}$ are directions axis.

$$\|\bigtriangledown I\| = \sqrt{(\frac{\delta F}{\delta x})^2 + (\frac{\delta F}{\delta y})^2} \tag{5.1}$$

$$\theta = \tan^{-1}[\frac{\delta F}{\delta y}/\frac{\delta F}{\delta x}] \tag{5.2}$$

In order to measure the effects of fusing the gradient edge feature with SRCNN, it was necessary to inspect the output feature maps of a training sample stacked with gradient features against the same training sample with only RGB color combination to evaluate the resulting representations.

Fig. 5.2 shows a sentinel-2 training sample containing an aircraft (A) and the results of convolving (A) with and without fusing edge feature after 1 epoch during first layer (9x9) of the SRCNN architecture. The convolution process was followed by non-linear activation function Rectified Linear Unit (Relu). The resulting feature map (C) was strongly affected by fusing gradient edge features as clearly seen from the number of activated neurons. We hypothesised that fusing such features at an early stage of training might assist the model by presenting useful representations.

The edge detection derived channel was fused with the RGB color combination to enforce the model to learn and extract edge-focused features in addition to preserving details of complex image structures that could be beneficial to construct the HR output. Quantitative results using Peak-Signal-to-Noise-Ratio metric show the gains of fusing such features



Figure 5.2: Difference between convolution output of manually added gradient edge feature (C) and convolution output for same training sample without adding gradient edge feature (B) while original training sample is (A).

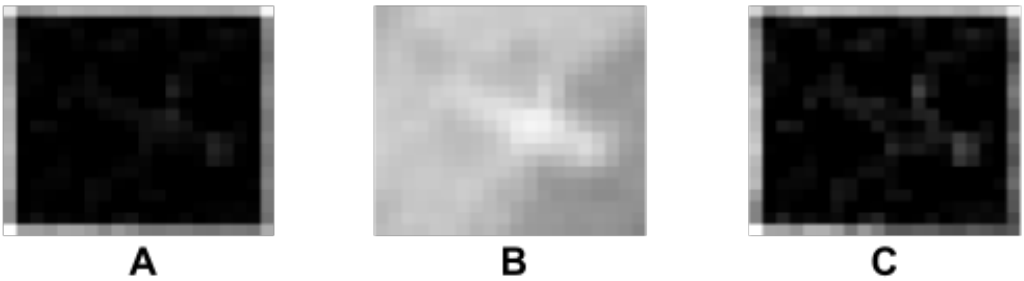


Figure 5.3: Difference between convolution output of manually added contrast enhanced feature (C) and convolution output for same training sample without adding contrast enhanced feature (A) while original training sample is (B).

in the results section.

- **Contrast Enhancement**
  From an image enhancement perspective, contrast enhancement is used to improve the disparity between the objects in a scene and their background [Ernest, 1979]. We assume that enhancing contrast can expose several hidden but relevant image details, which can help in extracting significant features for SR. Among contrast enhancement methodologies, histogram equalisation is the most used algorithm in remote sensing image manipulation [Fu et al., 2015]. Histogram equalisation aims to derive the intensity mapping that will as best as possible equalise the image histogram.

  As depicted in Fig. 5.3, the fusion of a contrast enhanced channel using histogram equalisation algorithm with the RGB color combination helped in representing more details in (C) which were not so apparent in the original training sample (A).

- **Unsharp Masking** As a simple method of increasing details in an image, unsharp masking consists of adding a mask to the original image [Maheshwari and Pati, 2014] which is created by subtracting a blurred version of the original image from the original one as follows. Let

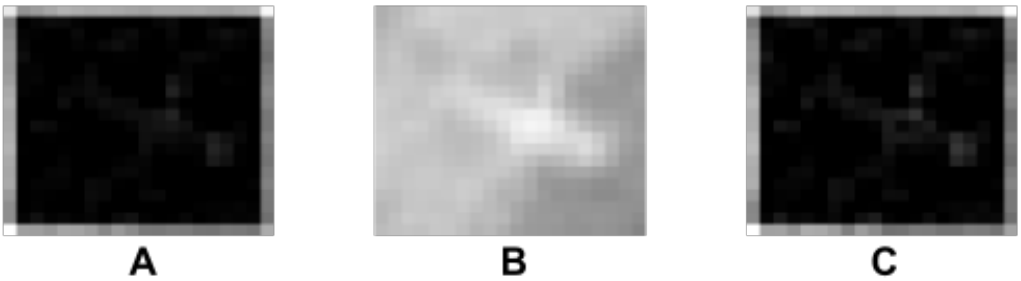


Figure 5.4: Difference between convolution output of manually added unsharp mask feature (C) and convolution output for same training sample without adding unsharp mask feature (A) while original training sample is (B).

A be the original image, B the blurred version, *mask* = *B* - *A*. The created mask is then combined with the original image to produce a sharpened version. We presume that adding such channel will highlight the deblurring features to be extracted during training. Following the same approach of visualising gradient edge feature, Fig. 5.4 shows the difference between applying the same convolution process on training sample (B) with manually added unsharp mask feature (C) and without adding in (A). Although it shows less added value than the gradient edges feature this might be justified as early layers in CNNs tend to focus on edges.

In the next section, we explain how datasets were created to test the proposed augmentation methods on both Landsat-8 and Sentinel-2 products.

Dataset

Creating a balanced training dataset for deep learning tasks is an important prerequisite to having an unbiased model. In remote sensing, hundreds of scenes are being captured and sent to ground stations for publishing and ingestion. Starting from late 2008, Landsat-8 [AWS, 2017a] data became open for download by all users free of charge and within a few hours of scene capture.

The 11-band spatial resolution is 30m for visible and infrared bands and 15m for panchromatic data.

On the other hand, the European Union adopted an open data policy for the Copernicus programme [ESA, 2018b]. Sentinel-2 data contains 13 bands with spatial resolution varying from 10, 20 to 60 meter bands which serves a wide range of applications related to the Earth.

The study area consists of the western side of Malaysia which is covered by paths 126, 127 and rows 57 and 58 as shown in Fig. 4.1 for landsat-8 Worldwide Reference System (WRS) Path/Row. Regarding Sentinel-2, the same region was covered by granules 47NQE, 47NQD, 47NRE and 47NRD.

Given an image sample size of 64x64 pixels, 12k samples were created from the selected scenes with a stride of 8 pixels. 8400 samples were allocated for training while 3600 were allocated for validation. Training samples were divided into X and Y, where Y consists of the original samples representing the high resolution target, and X refers to the corresponding synthesized low resolution version of the original samples, obtained by downscaling and subsequent upscaling (with a corresponding scaling factors).

Experimental design

This section explains the achieved experiments to evaluate the efficacy of adding fusion-based data augmentation compared to traditional data augmentation techniques. In addition, utilising the flexibility of the SRCNN architecture, we evaluate using SRCNN in new domains such as denoising and dehazing using synthesised noise and haze effects.

Dataset preparation

In order to evaluate the proposed augmentation methods on Landsat-8 and Sentinel-2 datasets, a grayscale scene was created to derive the unsharp mask, contrast enhanced, and gradient edge bands, in addition to bands 4 (red), 3 (green) and 2 (blue). The selected scene channels were then stacked prior to cropping patches of size 64×64. The created patches were cropped through a

grid of vector polygons designed with a stride of 8 pixels. The raw dataset of 12,000 samples was divided into 70%, 20% and 10% portions to form non-overlapping training, validation and test sets respectively for both Landsat-8 and Sentinel-2 products. A set of experiments were designed with the following core conditions:

Super-Resolution RGB with instance-based augmentation:

- Bands 4,3,2 in addition to instance augmentation including (flipping, rotating, noise and smoothing).

Super-Resolution RGB with fusion-based augmentation:

- Bands 4,3,2 fused with gradient edge detected feature
- Bands 4,3,2 fused with unsharp masking feature
- Bands 4,3,2 fused with contrast enhanced feature
- Bands 4,3,2 in addition to near and shortwave infrared bands
- Bands 4,3,2 fused with gradient edge detected, contrast enhanced and unsharp masking features

Moreover, additional augmentation methodologies were tested in different domains such as denoising and dehazing as follows:

Denoising:

- Bands 4,3,2 with noise effects (salt-and-pepper).

Dehazing:

- Bands 4,3,2 with synthesised haze effects.

In the next section, we demonstrate how the results of SRCNN are influenced by our proposed augmentation method compared with traditional instance-based augmentation. Moreover, the SRCNN was tested against denoising and dehazing

tasks. As an example of synthesised noise, salt-and-pepper effect was added as augmented samples. In addition, to simulate the haze effect, red, green and blue bands were split to modify the contrast of every channel separately. The effect of haze is obviously noticed in blue bands and less in red and green bands as mentioned in [Qin et al., 2018]. Although haze effects are usually not following a uniform distribution especially that it depends on atmospheric scattering models [Qin et al., 2018], this experiment aimed to approach the haze problem from contrast deterioration perspective.

The assessment of image restoration can be measured through Peak Signal to Noise Ratio (PSNR) metric. PSNR can be denoted as:

$$\text{PSNR} = 10 \cdot \log_{10} \frac{C^2}{\text{MSE}} \tag{5.3}$$

where C^2 represents the maximum value a pixel can have and MSE refers to Mean Squared Error which can be obtained using equation 5.4.

$$MSE = \frac{1}{n} \sum_{i=1}^{n} ||\mathbf{Y}_i - \mathbf{X}_i||^2 \tag{5.4}$$

where Y represents the predicted high resolution output and X is the ground truth sample.

5.4 Results

Taking advantage of the flexibility of the SRCNN design, various channels have been merged to test the effectiveness of fusion-based augmentation methodologies compared to instance-based ones.

In addition, we introduce the SRCNN architecture to new problems such as denoising and dehazing. The results are shown in table 5.1 and figures 5.5, 5.6 and 5.7, where we can observe the following:

Table 5.1: A comparison between different augmentation approaches testing results

Training strategy	Average PSNR in dB
RGB	**44.768**
RGB with instance augmentation	**45.224**
RGB fused with CE	45.254
RGB fused with UM	45.023
RGB fused with ED	45.605
RGB fused with (CE,UM,ED)	**45.788**
RGB + NIR + SWIR I + SWIR II	45.125

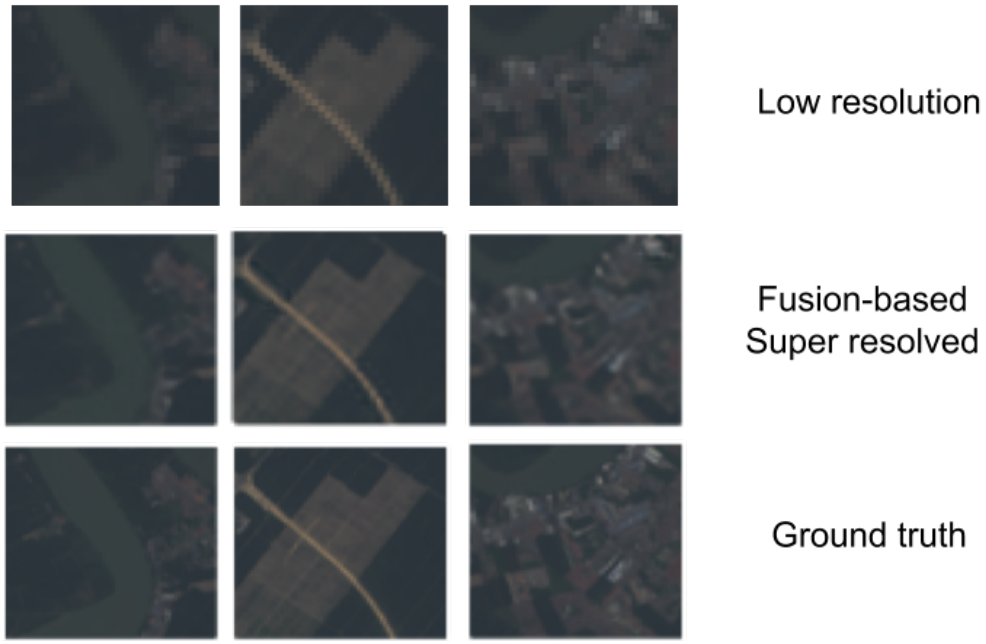


Figure 5.5: Examples from test set results of the proposed fusion-based augmentation compared with ground truth samples.

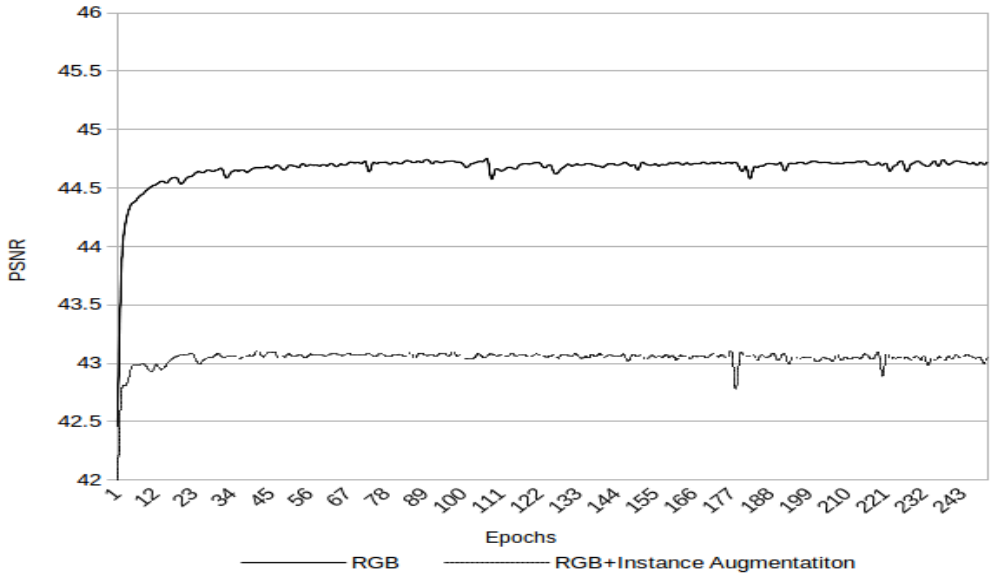


Figure 5.6: Comparison between RGB channels with and without instance augmentation learning convergence.

(i) insignificant performance improvement when instance augmentation including flipping and rotating have been applied to the RGB channels; (ii) it is noteworthy that gradient edge detection provides the most useful fused feature compared to contrast enhanced and unsharp mask features; (iii) adding edge detection, contrast enhancement and unsharp masking channels to the visual bands improved the performance more than any other augmentation method we experimented with SRCNN; (iv) RGB is improved to some extent by instance augmentation and infrared channels, but more significantly by the proposed channel augmentation.

On the other hand, figures 5.8 and 5.9 show the denoised and dehazed samples. The proposed augmentation approaches to simulate noise and haze effects didn't work as expected and the results show spectral distortions throughout test samples.

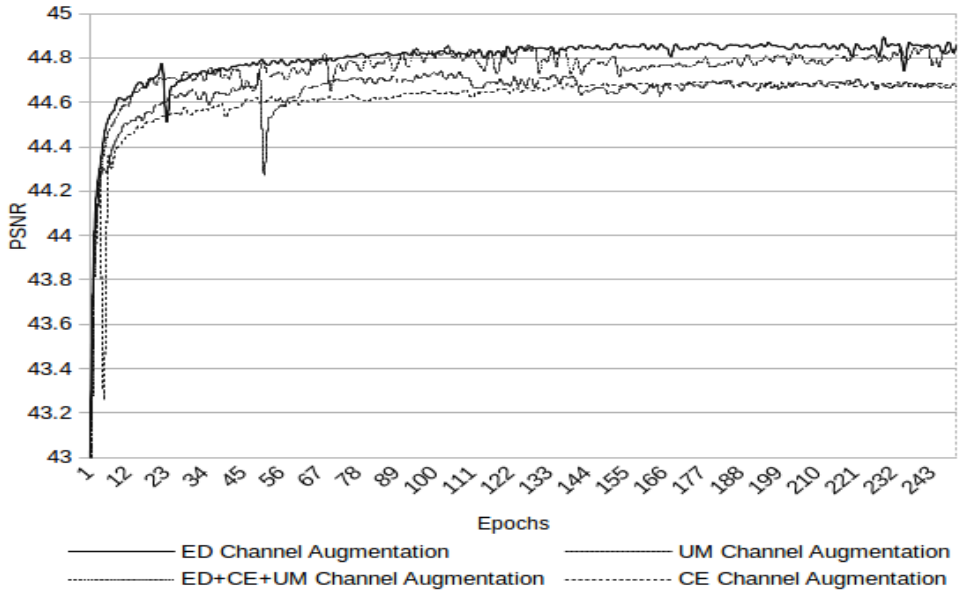


Figure 5.7: Comparison between the learning convergence of different channel augmentations added to RGB channels.

5.5 Conclusions

In this chapter, we presented data augmentation methods that help boost super resolution accuracy in the satellite image domain. The proposed data augmentation methodology integrates the power of SRCNN for learning nonlinear mappings between low and high resolution images, with the flexibility to incorporate additional feature representations via fusing additional input channels with input data. A selection of additional channels was experimented with, that provided alternative training strategy which contributed to the construction of more accurate high resolution outputs. Following the rule of thumb of evaluating image structure similarity, the PSNR metric was used to numerically assess the super resolved images by comparing them against the original ground truth high resolution images. The experimental results showed

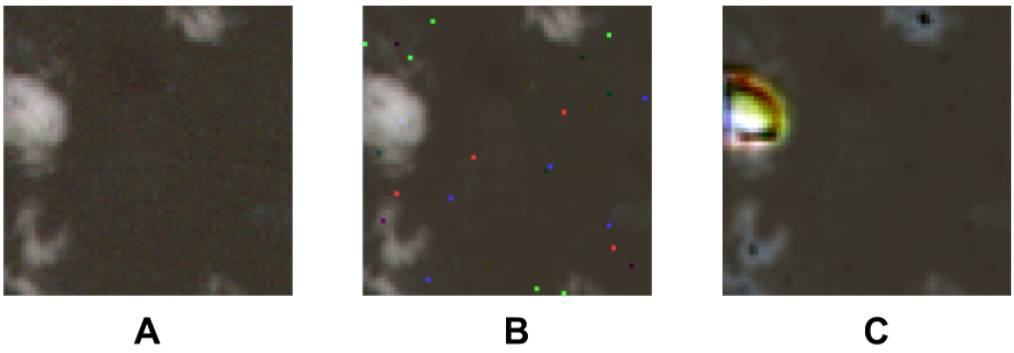


Figure 5.8: Example of denoise process where A represents the original sample, B represents the added salt-and-pepper noise and C is the result.

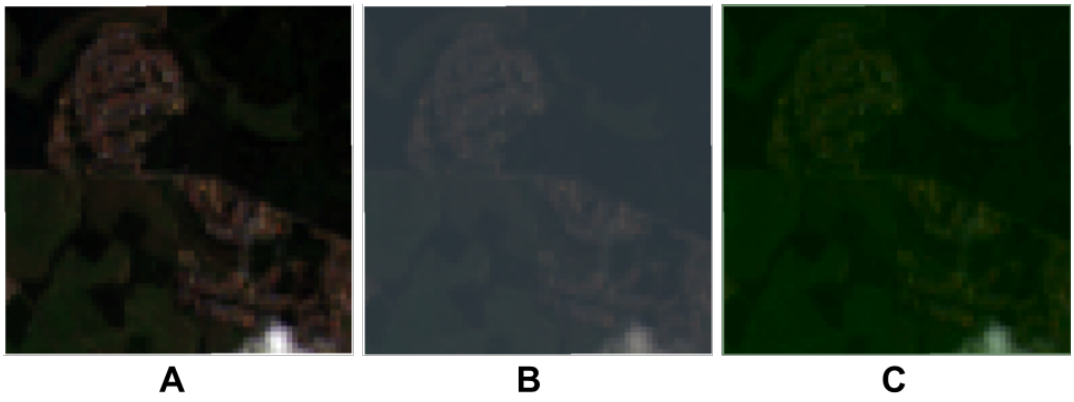


Figure 5.9: Example of dehaze process where A represents the original sample, B represents the synthesised haze and C is the result.

the effectiveness of our proposed fusion-based augmentation approach compared with standard instance augmentation methods. However, limitations were highlighted when augmentation was introduced to different problem domain such as denoising and dehazing. Since it is out of the scope of this thesis, in future work we aim to explore the required changes to adapt the model to denoise and dehaze problems since haze is one of the risks facing Malaysia recently.

In the next chapter, we evaluate the effects of satellite image super resolution on landcover classification accuracy with particular focus on Landsat-8 data to derive more frequent landcover products which can be integrated with Sentinel-2 data.

Chapter 6

Evaluating Super Resolution Accuracy via Landcover Classification Tasks

This chapter aims to provide a more practical use-case of super resolution evaluation. In order to confirm that the quantitative evaluation can be reflected on the operational conditions and the super resolution performance was sufficiently mature enough to enable real-life applications, we propose using landcover classification as a test field. Particularly, Landsat-8 test samples were super-resolved and compared with both Sentinel-2 and crowd-source data captured using Google Earth Engine.

6.1 Introduction

Although the novelty of deep learning based super resolution approaches in the satellite image domain might push forward the capabilities of remote sensing applications, still real-life applications are not common yet. One could argue that the reason behind this is the absence of appropriate evaluation metrics which can truly measure the quality of reconstructed outputs [Benecki et al., 2018].

In learning-based single-image super resolution methodologies, the process of creating the training dataset relies on a degradation model to derive the low resolution samples from the original high resolution sample. The original sample is considered as the high resolution target output so that during the training process it can be used as a reference to measure the error/cost between low and high resolution predicted outputs. The differences in spectral and spatial characteristics of any higher resolution satellite data restrain the idea of using it as target/reference high resolution output for measuring quality of reconstruction. In addition, the differences in the timing of scenes capturing will always reflect changes in the structure of the images.

Having said that, the majority of satellite imagery super resolution methodologies were evaluated using metrics such as Peak-Signal-to-Noise-Ratio as followed in [Liebel and Körner, 2016], Structural Image Similarity Index (SSIM) as followed in [Huang et al., 2017b] or Image Quality Index (IQI) as followed in [Nguyen et al., 2018].

However, still the aforementioned metrics might be misleading especially in the field of remote sensing applications. For instance, Fig. 6.1 shows an example of original sample compared with both contrast changed version having the same spatial resolution (24.54 dB) and low resolution blurred version (31.83 dB). The PSNR was significantly affected although the spatial resolution wasn't changed in the contrast changed sample while a better PSNR value was obtained in low resolution example. This can be understood as the way PSNR works doesn't put enough weight towards the contrast/brightness differences compared to the changes in high frequency details in an image.

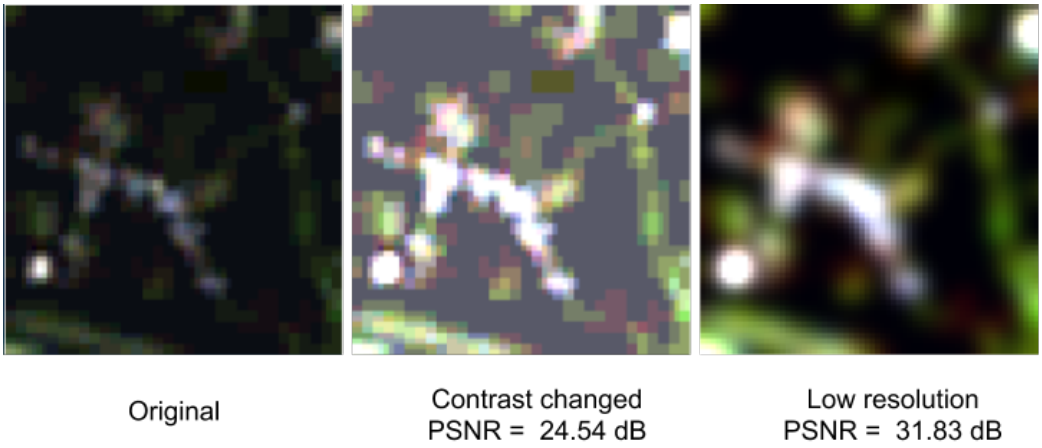


Figure 6.1: Difference in contrast affects the PSNR accuracy.

In order to move the satellite image super resolution domain towards real-life applications, we propose an integrated approach which can harness super-resolved Landsat-8 and Sentinel-2 products alongside crowd-sourced data to derive continuous monitoring of the Earth at refined spatial and temporal resolutions.

The Sentinel-2 mission consists of 2 satellites S2A and S2B which can cover the whole Earth every 5 days. In addition, Landsat-8 is able to revisit the same spot of the Earth every 16 days.

Deriving timely global monitoring is of vital importance for a wide range of applications such as deforestation, urbanisation studies, vegetation phenology and many change detection based applications.

Taking advantage of the proposed data model in chapter 3, we extended the framework to allow the generation of landcover classification maps using the super-resolved Landsat-8 products to be compared with Sentinel-2 data. By accumulating the final output from both sources, up to 8 landcover classification products might be generated for the same region per month. (6 from Sentinel-2 and 2 from super-resolved Landsat-8). The next section explains the adopted methodology in detail.

6.2 Methodology

The proposed data model in chapter 3 was extended to align the acquisition of both Landsat-8 and Sentinel-2 data according to predefined dates of expected scenes. The orbiting paths for both satellites were used to extract the intersecting area of interest to download the targeted scenes/tiles. Sentinel-2 follows Universal Transverse Mercator (UTM) projection which divides the Earth into 60 zones , where each zone is of width 6°longitude and height 8°latitude. ESA allows downloading the Sentinel-2 tiling grid in Keyhole Markup Language (KML) format. On the other hand, Landsat-8 uses the Worldwide Reference System 2 (WRS-2) which divides the whole Earth into 233 paths (longitude) and 248 rows (latitude). The WRS-2 grid is accessible via the ESRI polygon shapefile format.

By combining both grid systems and specifying a date range, Landsat-8 and Sentinel-2 products for the same AOI within a specific time window can be obtained.

In order to have ground-truth data which can be used as a reference for all levels of the designed experiments, crowd-sourced data were used to compare between original Sentinel-2 land-cover classification accuracy against super-resolved Landsat-8 land-cover classification outputs to measure the accuracy of the gained details of the super resolution process. A set of 200 random points were located within the study area using Google Earth [GoogleEarth, 2018]. Google Earth allows accessing historical data which enabled acquiring the proper land-cover at a specific time-line.

6.2.1 Study area

The study area was located north of Kuala Lumpur city and it covers approximately 250 km^2. The land-cover in this area consisted mainly of vegetation, bare-land, built-up and water. In order to match between Sentinel-2 and Landsat-8 orbiting paths, an area of interest (AOI) was generated as a

polygon to find the intersection between the area and Sentinel-2 grid system and Landsat-8 path/row footprints. The resulting footprints were identified as T47NQE for Sentinel-2 and 127/057 for Landsat-8 (Refer to Fig. 6.2). In order to obtain appropriate scenes from both satellites, two correlated factors where considered while querying the datasets as follows:

- Cloud coverage: Both clouds and cloud shadows can limit a sensor's view of the Earth. The existence of clouds in satellite images might reduce the accuracy of land-cover classification or change detection based analysis. Hence, it was important to acquire scenes with minimal percentage of cloud coverage in both datasets.

- Sensing date: Alongside the cloud coverage, having scenes which were captured over a long span of time might increase the possibility of having changes in land-cover , which can reduce classification accuracy when compared to each other.

Taking into consideration the aforementioned factors, Sentinel-2 product id: S2A_OPER_MSI_L1C_TL_SGS__20151231T084903_A002732_T47NQE_N02.01 and Landsat-8 scene id LC81270572016009LGN00 were used for this study. Cloud coverage in both scenes was less than 14% and the difference between sensing days was 9 days. The next section demonstrates how the acquired data were used to evaluate the accuracy of super resolution in terms of land-cover classification.

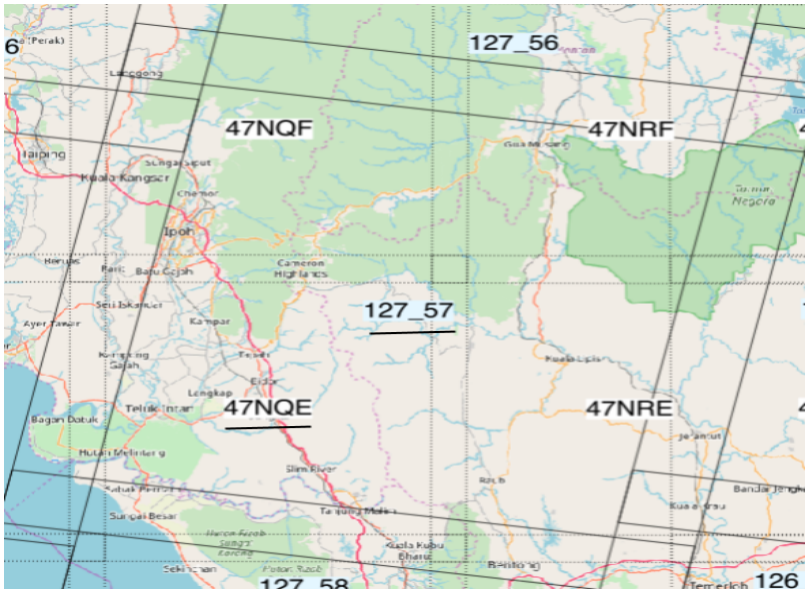


Figure 6.2: Study area showing intersection between Sentinel-2 zone T47NQE and Landsat-8 127/057 path/row footprints.

6.3 Evaluation Methodology

Inspired by the published work [Wu et al., 2012] which aimed at associating Hyperion data [Hyperion, 2018] with ALOS data [ALOS, 2018] to evaluate super resolution mapping accuracy, we propose using classification products of both Landsat-8 and Sentinel-2 to validate super resolution accuracy. However, in [Wu et al., 2012] the main objective was modelling land-cover classes at sub-pixel level. The contribution of the super resolution process towards land-cover classification accuracy in addition to validating super resolution results using ground-truth data were measured through 3 experiments. The experiments were designed as follows:

- **Experiment 1:** Generate super resolved versions of Landsat-8 AOI samples and compare classification product with ground-truth Landsat-8 samples
- **Experiment 2:** Generate super resolved versions of Sentinel-2 AOI

samples and compare classification products with ground-truth Sentinel-2 samples.

- **Experiment 3:** Generate super resolved versions of Landsat-8 and compare classification products with Sentinel-2 classification products as a ground-truth reference.

It is noteworthy that the accuracy of the reported classification results in these experiments weren't the main target. The experiments were setup identically to use super-resolved data against ground-truth to highlight the differences in land-cover classification accuracy regardless of fine-tuning classification algorithms.
For the sake of simplicity, a Random Forest supervised classification algorithm was used to differentiate between super-resolved and ground-truth data. The number of training samples, classes and the used libraries were identical to maintain equity and emphasize the differences in data representation.
The next section explains in detail the results achieved for individual experiments.

6.4 Experiments and Results

6.4.1 Experiment 1: Landsat-8

The super-resolved test dataset from scene id: LC81270572016009LGN00 was generated using vector polygons of dimensions (64x64) to be classified among 4 land-cover classes as vegetation, bare-land, water or built-up. A total number of 100 samples (64x64) were used to be classified using a Random Forest algorithm on both the original high resolution image against super resolved samples in experiment1-A and B respectively.
Figure 6.3 shows samples of classification maps for both super-resolved and ground-truth regions. It is noteworthy that the proposed super resolution process helped in highlighting some features which were not classified in the

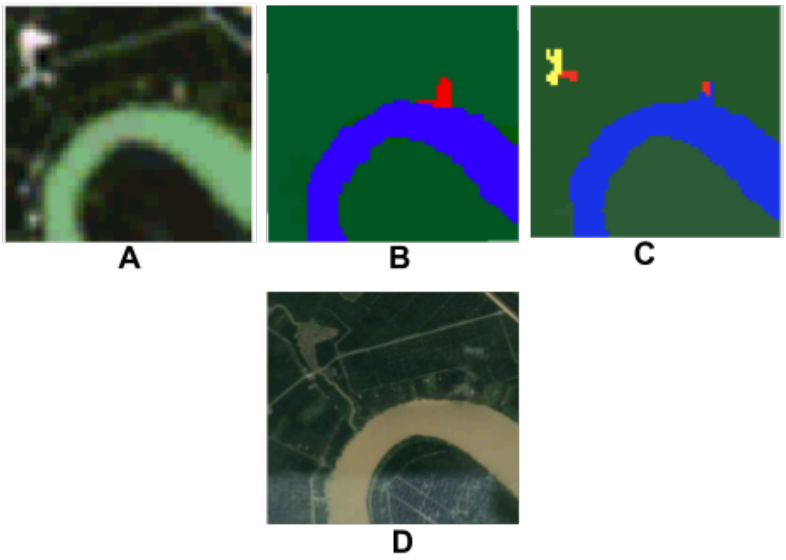


Figure 6.3: Landsat-8 test sample (A) with classification map of original high-resolution version (B) and classification map of super-resolved sample (C) and land-cover ground-truth sample (D) while colors (red = built-up, green = vegetation, blue = water and yellow = bare-land).

ground-truth classification sample.

For instance, bare-land region towards the north west corner was identified in the super resolved sample (C) while being unidentified in the original high-resolution classification map (B). While on the other side, less representation of built-up land-cover in the north east corner was identified in the super resolved version (C) compared to original high-resolution classification map (B). Ground-truth sample (D) was extracted using Google Earth to validate/visualise differences between (B) and (C).

In order to evaluate classification accuracy quantitatively, table 6.1 shows error metrics for original high resolution classification results (Experiment1-A) while table 6.2 shows error metrics for super resolved classification results. The ground-truth/reference data for both experiments were generated randomly by allocating 200 points over the study area. The overall accuracy reached 83.50%

Table 6.1: Error matrix for experiment 1-A

Error Matrix	**Ground-truth**				
Classification	Vegetation	Built-up	Water	Bare-land	Total
Vegetation	**55**	1	2	3	61
Built-up	4	**38**	2	0	44
Water	10	0	**34**	0	44
Bare-land	6	1	4	**40**	51
Total	75	40	42	43	**200**
Overall Accuracy: 83.50%					
Water	**Producer's Accuracy: 80.95%** **User's Accuracy: 77.27%**				
Bare-Land	**Producer's Accuracy: 93.02%** **User's Accuracy: 78.43%**				
Built-up	**Producer's Accuracy: 95.00%** **User's Accuracy: 86.36%**				
Vegetation	**Producer's Accuracy: 73.33%** **User's Accuracy: 90.16%**				

in Experiment1-A while classification of super resolved samples (Experiment 1-B) scored 87.00% (Refer to Table 6.2). In order to demonstrate the differences, producer's and user's accuracy (PA and UA) were derived per class as follows:

- Producer's Accuracy = Number of correctly classified reference points divided by total number of reference points. Producer's accuracy measures how often are real features on the ground correctly shown on the classified map or the probability that a certain land cover of an area on the ground is classified as such.

- User's Accuracy = Number of correctly classified reference points divided by total number of classified points. The user's accuracy essentially tells us how often the class on the map will actually be present on the ground.

Super-resolved data scored the best in built-up class with 92.5% compared to 86.36% in experiment1-A. Moreover, both water and bare-land classes obtained

Table 6.2: Error matrix for experiment 1-B

Error Matrix	**Ground-truth**				
Classification	Vegetation	Built-up	Water	Bare-land	Total
Vegetation	**64**	0	4	6	74
Built-up	2	**37**	1	0	40
Water	5	1	**36**	0	42
Bare-land	4	2	1	**37**	44
Total	75	40	42	43	**200**
Overall Accuracy: 87.00%					
Water	**Producer's Accuracy: 85.71%** **User's Accuracy: 85.71%**				
Bare-Land	**Producer's Accuracy: 86.04%** **User's Accuracy: 84.09%**				
Built-up	**Producer's Accuracy: 92.50%** **User's Accuracy: 92.50%**				
Vegetation	**Producer's Accuracy: 85.33%** **User's Accuracy: 86.48%**				

higher accuracy in super-resolved instances compared to experiment1-A while the vegetation class was better in experiment1-A.

6.4.2 Experiment 2: Sentinel-2

In this experiment, an identical setup to experiment1 A and B was applied to the Setinel-2 dataset. Tables 6.3 and 6.4 show error metrics for experiments 2-A and 2-B respectively. Like experiments experiment 1-A and B, super resolved samples were classified with accuracy higher than the original Sentinel-2 dataset.
However, the bare-land class was classified with higher PA and UA in the original dataset (experiment 2-A).

Table 6.3: Experiment 2-A error metrics

Error Matrix	**Ground-truth**				
Classification	Vegetation	Built-up	Water	Bare-land	Total
Vegetation	**71**	1	3	1	76
Built-up	1	**39**	1	1	42
Water	2	0	**35**	4	41
Bare-land	1	0	3	**37**	41
Total	75	40	42	43	**200**
Overall Accuracy: 91.00%					
Water	**Producer's Accuracy: 94.60%** **User's Accuracy: 93.42%**				
Bare-Land	**Producer's Accuracy: 97.50%** **User's Accuracy: 92.85%**				
Built-up	**Producer's Accuracy: 83.33%** **User's Accuracy: 85.36%**				
Vegetation	**Producer's Accuracy: 86.04%** **User's Accuracy: 90.24%**				

Table 6.4: Experiment 2-B error metrics

Error Matrix	**Ground-truth**				
Classification	Vegetation	Built-up	Water	Bare-land	Total
Vegetation	**68**	0	1	0	69
Built-up	2	**37**	2	1	42
Water	1	0	**39**	1	41
Bare-land	4	3	0	**41**	48
Total	75	40	42	43	**200**
Overall Accuracy: 92.50%					
Water	**Producer's Accuracy: 90.66%** **User's Accuracy: 98.55%**				
Bare-Land	**Producer's Accuracy: 92.50%** **User's Accuracy: 88.09%**				
Built-up	**Producer's Accuracy: 92.85%** **User's Accuracy: 95.12%**				
Vegetation	**Producer's Accuracy: 95.34%** **User's Accuracy: 85.41%**				

6.4.3 Experiment 3: Landsat-8 super-resolved using scale factor of 3 against Sentinel-2 as ground-truth

In this experiment, super-resolved Landsat-8 data samples were classified and compared with the Sentinel-2 original dataset. The comparison aimed to explain the feasibility of obtaining more frequent land-cover classification maps with comparable accuracy from different sensors with different spatial resolution. Landsat-8 data samples were super-resolved with a scaling factor of 3 and the results were compared to experiment 2-B in which Sentinel-2 (10 meter) ground-truth samples were classified.

Table 6.5 shows the overall accuracy of super-resolved Landsat-8 classification maps (86.50%). Although the achieved accuracy level didn't reach Sentinel-2 (91.00%), still super-resolved instances achieved comparatively high accuracy especially for the built-up class where UA exceeded Sentinel-2 samples (89.18 and 85.36 respectively).

Table 6.5: Experiment 3 error metrics

Error Matrix	**Ground-truth**				
Classification	Vegetation	Built-up	Water	Bare-land	Total
Vegetation	**65**	0	4	2	71
Built-up	3	**35**	3	1	42
Water	2	2	**33**	0	37
Bare-land	5	3	2	**40**	50
Total	75	40	42	43	**200**
Overall Accuracy: 86.50%					
Water	**Producer's Accuracy: 86.66%** **User's Accuracy: 91.54%**				
Bare-Land	**Producer's Accuracy: 87.50%** **User's Accuracy: 83.33%**				
Built-up	**Producer's Accuracy: 78.57%** **User's Accuracy: 89.18%**				
Vegetation	**Producer's Accuracy: 93.02%** **User's Accuracy: 80.00%**				

6.5 Conclusion

In this chapter, satellite image super resolution was evaluated using a land-cover classification application. The efficacy of super-resolving Landsat-8 and Sentinel-2 datasets was reflected in the classification accuracy as highlighted in experiments 1 and 2. The achieved boost in classification accuracy was employed to derive more frequent landcover classification maps after super-resolving Landsat-8 data (30 meter spatial resolution) combined with Sentinel-2 data (10 meter spatial resolution). Error metrics and accuracy measurements demonstrated how super resolution supported a simple classification algorithm such as Random Forests to separate between 4 classes (vegetation, bare-land, water and built-up).

Chapter 7

Conclusion

This chapter draws a conclusion of this thesis and the achieved work in all chapters followed by a list of contributions and future work to be done.

7.1 Deep learning and Remote Sensing

Data-intensive science is the paradigm shift being witnessed nowadays. Fortunately, we have entered era of remote sensing big data. Alongside remote sensing big data, machine learning techniques are becoming increasingly important. Particularly, deep learning has proven to be an extremely powerful tool in several fields of remote sensing applications especially after the increased availability of computational resources through cloud computing platforms. While majority of applications in the literature were focused on landcover classification, this thesis considered spatial resolution enhancement through deep learning and data augmentation techniques.

Moreover, the conducted research opens the field to investigate the role of data augmentation in improving deep learning algorithms for other remote sensing applications too.

Although most deep learning related researches are focused on object detection and classification, further applications are expected to solve more complicated physical models which are not well-understood. Given that remote sensing imagery data are direct product of physical processes such as scattering and reflection, fusing deep learning algorithms with physics-based modeling is expected to be a promising solution.

On the other hand, one of the major problems facing remote sensing deep learning applications is the limited number of annotated/labeled data. Remote sensing communities/scientists should tackle this issue through weak or semi-supervised learning based methodologies. An alternative method for solving this problem is to create synthetic labeled data using generative models such as Generative Adversarial Networks (GAN).

In this context, the remote sensing data are now big and available, the computational resources are much cheaper and powerful with cloud computing and deep learning frameworks are free and open-source, now is the right time to design deep learning algorithms which can be tailored to deal with remote sensing multi-modal and temporal aspects.

7.2 Summary

The conducted research aimed to cover multidisciplinary fields from remote sensing and computer science perspectives. The main concerned fields were cloud computing, remote sensing data and machine learning techniques. More specifically, using cloud computing technologies as a platform for satellite image resolution enhancement with deep learning.

Cloud computing platforms were reviewed with detailed descriptions of remote sensing data processing applications. In order to understand the market needs and the trends in remote sensing data processing on the cloud, a survey was conducted to measure these aspects so that we could guide our research direction based on real needs. Based on the obtained results from this survey, an elastic conceptual cloud-based remote sensing data processing model was designed to fit with its 5Vs characteristics.

The model was implemented in two applications during this study. The first application was a pilot test for a land-cover supervised classification service. The service was built as a SAAS model based on the AWS cloud vendor. The second application utilised the conceptual model to generate a data processing pipeline to automate the creation of training datasets for satellite image resolution enhancement tasks.

Satellite image spatial resolution enhancement can be achieved using several methodologies. Different methodologies were reviewed with particular focus on learning-based methods. Super-resolution using deep learning was adopted to enhance satellite images. The SRCNN architecture was introduced as the state-of-the-art in the field of conventional photo super-resolution. Hence, the SRCNN architecture was studied in detail and the architecture was modified to fit with the nature of satellite data accordingly.

Medium resolution datasets such as Sentinel-2 and Landsat-8 were used as input to SRCNN. The results were qualitatively and quantitatively compared to highlight the feasibility of satellite image super resolution applications. In addition, we aimed at enhancing the super resolution accuracy using data

augmentation techniques. Standard data augmentation techniques were applied to measure the gains compared to non-augmented datasets. A customised fusion-based data augmentation methodology was presented to boost the accuracy of satellite image super resolution.

Experiments with the proposed augmentation methodology scored the highest accuracy using the SRCNN model. In order to evaluate satellite image super resolution more pragmatically, the evaluation was extended to a land-cover classification task. The classification task targeted Landsat-8 and Sentinel-2 data to derive more frequent global monitoring of land-cover change. Crowd-sourced data were used to form 200 ground-truth points over the study area (250 km^2). Results revealed a potential application for satellite image super resolution given the achieved classification accuracy.

7.3 Contributions

The main achievements of this thesis can be outlined as follows:

- We study the up-and-running cloud computing platforms to be able to decide which one is competent enough to host satellite image processing services.
- A new integrated cloud-based framework for remote sensing big data processing is developed to validate the suitability of cloud computing services as a convenient platform.
- An extension of deep learning based super-resolution algorithm SRCNN is developed and optimised using data augmentation techniques.

7.4 Future work

The obtained results from this study suggested a considerable potential for extending cloud computing with deep learning technologies to process earth

observation big data. Although we managed to secure 10,000$ of cloud credit from Amazon Web Services, the grant expired by the end of the second year of this study which prevented us from publishing the services for public users. Therefore, allowing public users to access such services might open new fields of geo-processing applications and use-cases.

In this study the super resolution evaluation methodologies covered both quantitative and qualitative measurements, and can be extended to include super-resolution effects on object detection tasks such as ship detection or oil spill detection.

Although we trained the model to super-resolve Landsat-8 and Sentinel-2 scenes, other problems such as haze removal might be solved if appropriate datasets are created. The similarity between hazy images and blurring effects might be an interesting aspect which can be solved using the same model.

Moreover, although the proposed approach was applied on Sentinel-2 and Landsat-8 data, more investigations on very high resolution VHR datasets might lead to interesting findings and more complicated object-based classification functions.

One more room for improvement could be utilising tensor processing units TPUs instead of graphical processing units GPUs in training super resolution deep learning models.

Training/running deep learning models is computationally demanding. TPUs are designed to run cutting-edge machine learning models with AI services on Google Cloud and using Google's Tensorflow framework. However, only Google allows running/using TPUs on their cloud computing platform and till now it is not available from any other cloud vendors, e.g., Amazon Web Services.

Bibliography

[AWS, 2018] (2018). Amazon Web Services (AWS) - Cloud Computing Services. https://aws.amazon.com/.

[EIJ, 2018] (2018). Managing big data - earth imaging journal. "http://eijournal.com/print/articles/managing-big-data.".

[Ahn et al., 2015] Ahn, B., Cho, N. I., and Member, S. (2015). Self-Commmittee Approach for Image Restoration Problems using Convolutional Neural Network. *unpublished*, 14(8):1–5.

[Almeer, 2012] Almeer, M. H. (2012). Cloud Hadoop Map Reduce For Remote Sensing Image Analysis. *Journal of Emerging Trends in Computing and Information Sciences*, 3(4):637–644.

[Almeida et al., 2014] Almeida, N., Catarino, N., Gutierrez, A., Martinho, F., Rosado, H., Andrade, J., Caumont, P. H., Goncalves, P., Brito, F., and Terradue (2014). Sensyf: Processing Framework For Sentinel Data N. *Proc. of the 2014 conference on Big Data from Space (BiDS'14)*, (November):12–14.

[ALOS, 2018] ALOS (2018). Eo-1 hyperion. https://www.restec.or.jp/en/solution/product-alos.

[Aly and Dubois, 2005] Aly, H. A. and Dubois, E. (2005). Image up-sampling using total-variation regularization with a new observation model. *IEEE Transactions on Image Processing*, 14(10):1647–1659.

[Apache Foundation, 2017a] Apache Foundation (2017a). Apache Airflow. https://airflow.apache.org. Accessed: 2017-01-05.

[Apache Foundation, 2017b] Apache Foundation (2017b). Apache Solr. http://lucene.apache.org/solr/. Accessed: 2017-10-09.

[AWS, 2017a] AWS (2017a). Landsat on aws. https://aws.amazon.com/public-datasets/landsat/. Accessed: 2017-11-20.

[AWS, 2017b] AWS (2017b). Sentinel-2 on AWS. https://aws.amazon.com/public-datasets/sentinel-2/. Accessed: 2017-11-20.

[Azzari and Lobell, 2017] Azzari, G. and Lobell, D. (2017). Landsat-based classification in the cloud: An opportunity for a paradigm shift in land cover monitoring. *Remote Sensing of Environment*, 202:64–74.

[Ball et al., 2017] Ball, J. E., Anderson, D. T., and Chan, C. S. (2017). A Comprehensive Survey of Deep Learning in Remote Sensing: Theories, Tools and Challenges for the Community. 11(4).

[Bastian et al., 2010] Bastian, S., Bastian, B., and Theodor, F. (2010). Towards Spatial Data Infrastructures in the Clouds. *Geo-Information Science*, pages 1–20.

[Benecki et al., 2018] Benecki, P., Kawulok, M., Kostrzewa, D., and Skonieczny, L. (2018). Evaluating super-resolution reconstruction of satellite images. *Acta Astronautica*, 153(February):15–25.

[Bevilacqua, 2014] Bevilacqua, M. (2014). *Algorithms for super-resolution of images and videos based on learning methods*. Theses, Université Rennes 1.

[Bevilacqua et al., 2012a] Bevilacqua, M., Roumy, A., Guillemot, C., and Alberi Morel, M.-L. (2012a). Low-Complexity Single-Image Super-Resolution based on Nonnegative Neighbor Embedding. In *British Machine Vision Conference (BMVC)*, pages 1–10.

[Bevilacqua et al., 2012b] Bevilacqua, M., Roumy, A., Guillemot, C., and Alberi Morel, M.-L. (2012b). Low-Complexity Single-Image Super-Resolution based on Nonnegative Neighbor Embedding. In *British Machine Vision Conference (BMVC)*, pages 1–10.

[Blanc et al., 1998] Blanc, P., Wald, L., and Ranchin, T. (1998). Importance and effect of co-registration quality in an example of " pixel to pixel " fusion process. In *2nd International Conference " Fusion of Earth Data : merging point measurements, raster maps and remotely sensed images "*, pages 67–74, Sophia Antipolis, France. SEE/URISCA, Nice, France.

[Borman and Stevenson, 1998] Borman, S. and Stevenson, R. L. (1998). Super-resolution from image sequences-a review. In *1998 Midwest Symposium on Circuits and Systems (Cat. No. 98CB36268)*, pages 374–378.

[Castelluccio et al., 2015] Castelluccio, M., Poggi, G., Sansone, C., and Verdoliva, L. (2015). Land use classification in remote sensing images by convolutional neural networks. *CoRR*, abs/1508.00092.

[Cavallaro et al., 2015] Cavallaro, G., Riedel, M., Richerzhagen, M., Benediktsson, J. A., and Plaza, A. (2015). On Understanding Big Data Impacts in Remotely Sensed Image Classification Using Support Vector Machine Methods. *IEEE Journal of Selected Topics in Applied Earth Observations and Remote Sensing*, PP(99):1–13.

[Celery-Project, 2018] Celery-Project, C. (2018). Celery: Distributed Task Queue. http://www.celeryproject.org. Accessed: 2018-03-09.

[Celik, 2018] Celik, N. (2018). Change detection of urban areas in ankara through google earth engine. In *2018 41st International Conference on Telecommunications and Signal Processing (TSP)*, pages 1–5.

[CERN, 2018] CERN (2018). Helix Nebula — Big Science Teams Up With Big Business. http://www.helix-nebula.eu/.

[Chapelle et al., 2006] Chapelle, O., Schölkopf, B., and Zien, A. (2006). Semi-Supervised Learning edited by. Technical report.

[Chavarr et al., 2012] Chavarr, D., Huang, Z., Member, S., Chen, Y., and Member, S. (2012). High-Performance Computing (HPC): Application & Use in the Power Grid. *Power and Energy Society General Meeting, 2012 IEEE*, pages 1–7.

[Chen et al., 2017] Chen, F., Zhang, M., Tian, B., and Li, Z. (2017). Extraction of glacial lake outlines in tibet plateau using landsat 8 imagery and google earth engine. *IEEE Journal of Selected Topics in Applied Earth Observations and Remote Sensing*, 10(9):4002–4009.

[Chen et al., 2012a] Chen, Z., Chen, N., Yang, C., and Di, L. (2012a). Cloud computing enabled web processing service for earth observation data processing. *IEEE Journal of Selected Topics in Applied Earth Observations and Remote Sensing*, 5(6):1637–1649.

[Chen et al., 2012b] Chen, Z., Chen, N., Yang, C., Di, L., and Member, S. (2012b). Cloud Computing Enabled Web Processing Service for Earth Observation Data Processing. 5(6):1637–1649.

[Cirean et al., 2012] Cirean, D., Meier, U., and Schmidhuber, J. (2012). Multi-column Deep Neural Networks for Image Classification. *International Conference of Pattern Recognition*, (February):3642–3649.

[Computing, 2018] Computing, A. C. (2018). Cloud readiness index 2016. http://www.asiacloudcomputing.org/images/documents/cri2016_acca.pdf.

[Contributors, 2018] Contributors, G. (2018). Gdal/ogr geospatial data abstraction software library. http://gdal.org.

[Corp, 2016] Corp, S. I. (2016). Ikonos satellite sensor (0.82m). https://www.satimagingcorp.com/satellite-sensors/ikonos/.

[Corp, 2018] Corp, S. I. (2018). Image Processing Services, Satellite Map — Satellite Imaging Corp. https://www.satimagingcorp.com/services/image-processing/.

[Cortes and Vapnik, 1995] Cortes, C. and Vapnik, V. (1995). Support-Vector Networks. *Machine Learning*, 20(3):273–297.

[Cui et al., 2014] Cui, Z., Chang, H., Shan, S., Zhong, B., and Chen, X. (2014). *Deep Network Cascade for Image Super-resolution*, pages 49–64. Springer International Publishing, Cham.

[Demirel and Anbarjafari, 2010] Demirel, H. and Anbarjafari, G. (2010). Satellite image resolution enhancement using complex wavelet transform. *IEEE Geoscience and Remote Sensing Letters*, 7(1):123–126.

[Development Seeds, 2017] Development Seeds (2017). Landsat-util is a command line utility that makes it easy to search, download, and process landsat imagery. https://github.com/developmentseed/landsat-util/blob/master/README.rst.

[Digital Globe, 2017] Digital Globe (2017). Worldview4. http://worldview4.digitalglobe.com. Accessed: 2017-11-20.

[Ding et al., 2016] Ding, J., Chen, B., Liu, H., and Huang, M. (2016). Convolutional neural network with data augmentation for sar target recognition. *IEEE Geoscience and Remote Sensing Letters*, 13(3):364–368.

[Dong et al., 2016] Dong, C., Loy, C. C., He, K., and Tang, X. (2016). Image super-resolution using deep convolutional networks. *IEEE Transactions on Pattern Analysis and Machine Intelligence*, 38(2):295–307.

[Elastic Co, 2018] Elastic Co (2018). ElasticSearch. https://www.elastic.co/products/elasticsearch. Accessed: 2016-04-01.

[EPU Malaysia, 2018] EPU Malaysia (2018). Economic planning unit malaysia: Eleventh malaysia plan 2016-2020 anchoring growth on people. http://www.epu.gov.my/sites/default/files/RMKe-11\%20Book.pdf.

[Ernest, 1979] Ernest, H. (1979). Computer image processing and recognition.

[ESA, 2016] ESA (2016). Copernicus Open Access Hub. https://scihub.copernicus.eu. Accessed: 2018-01-10.

[ESA, 2018a] ESA (2018a). Sentinel-2 - the payload data ground segment. https://sentinel.esa.int/web/sentinel/missions/sentinel-2/ground-segment/core-ground-segment/pdgs. Accessed: 2018-09-15.

[ESA, 2018b] ESA (2018b). Sentinel online faq. https://sentinel.esa.int/web/sentinel/faq.

[Febrier and Montmory, 2014] Febrier, B. and Montmory, A. (2014). Thales CIC Vision On Space Big-Data Projects. *Proc. of the 2014 conference on Big Data from Space (BiDS'14)*, (November):12–14.

[Ferrn et al., 2013] Ferrn, A., Bernab, S., Rodrguez, P. G., and Plaza, A. (2013). A web-based system for classification of remote sensing data. *IEEE Journal of Selected Topics in Applied Earth Observations and Remote Sensing*, 6(4):1934–1948.

[Foundation, 2018] Foundation, A. (2018). Apache Hadoop. http://hadoop.apache.org/. Accessed: 2018-08-27.

[Freeman et al., 2002] Freeman, W. T., Jones, T. R., and Pasztor, E. C. (2002). Example-based super-resolution. *IEEE Computer Graphics and Applications*, 22(2):56–65.

[Fritz et al., 2012] Fritz, S., McCallum, I., Schill, C., Perger, C., See, L., Schepaschenko, D., van der Velde, M., Kraxner, F., and Obersteiner, M. (2012).

Geo-Wiki: An online platform for improving global land cover. *Environmental Modelling & Software*, 31:110–123.

[Fu et al., 2015] Fu, X., Wang, J., Zeng, D., Huang, Y., and Ding, X. (2015). Remote sensing image enhancement using regularized-histogram equalization and dct. *IEEE Geoscience and Remote Sensing Letters*, 12(11):2301–2305.

[Gançarski, 2014] Gançarski, P. (2014). Big data and Earth observation New challenges in remote sensing images interpretation. Technical report.

[Gardner Daniel, 2017] Gardner Daniel, N. (2017). Multi-label classification of satellite images with deep learning. *CoRR*.

[Gartner, 2018] Gartner (2018). Deep learnings permanent peak on gartners hype cycle. https://medium.com/machine-learning-in-practice/deep-learnings-permanent-peak-on-gartner-s-hype/-cycle-96157a1736e. Accessed: 2018-12-01.

[Ghaffar and Vu, 2015] Ghaffar, M. A. A. and Vu, T. T. (2015). Cloud computing providers for satellite image processing service: A comparative study. In *2015 International Conference on Space Science and Communication (IconSpace)*, pages 61–64. IEEE.

[Ghaffar et al., 2016] Ghaffar, M. A. A., Vu, T. T., and Maul, T. (2016). An integrated cloud-based framework for remote sensing data processing. *International Journal of Geoinformatics*, 12(2):41–47.

[Golpayegani and Halem, 2009] Golpayegani, N. and Halem, M. (2009). Cloud computing for satellite data processing on high end compute clusters. In *2009 IEEE International Conference on Cloud Computing*, pages 88–92.

[Google, 2018] Google (2018). Google earth engine api. https://developers.google.com/earth-engine/. Accessed: 2018-08-12.

[GoogleEarth, 2018] GoogleEarth (2018). Eo-1 hyperion. https://www.google.com/earth/.

[Goor, 2014] Goor, E. (2014). An Improved Infrastructure For The Exploitation Of Eo- Data Sources At Vito. *Proc. of the 2014 conference on Big Data from Space (BiDS'14)*, (November):12–14.

[Gorelick et al., 2017a] Gorelick, N., Hancher, M., Dixon, M., Ilyushchenko, S., Thau, D., and Moore, R. (2017a). Google earth engine: Planetary-scale geospatial analysis for everyone. *Remote Sensing of Environment*.

[Gorelick et al., 2017b] Gorelick, N., Hancher, M., Dixon, M., Ilyushchenko, S., Thau, D., and Moore, R. (2017b). Google earth engine: Planetary-scale geospatial analysis for everyone. *Remote Sensing of Environment*.

[Grizonnet et al., 2017] Grizonnet, M., Michel, J., Poughon, V., Inglada, J., Savinaud, M., and Cresson, R. (2017). Orfeo ToolBox: open source processing of remote sensing images. *Open Geospatial Data, Software and Standards*, 2(1):15.

[Haut et al., 2018] Haut, J. M., Fernandez-Beltran, R., Paoletti, M. E., Plaza, J., Plaza, A., and Pla, F. (2018). A new deep generative network for unsupervised remote sensing single-image super-resolution. *IEEE Transactions on Geoscience and Remote Sensing*, 56(11):6792–6810.

[He and Siu, 2011] He, H. and Siu, W. (2011). Single image super-resolution using gaussian process regression. In *CVPR 2011*, pages 449–456.

[Ho, 1995] Ho, T. K. (1995). Random decision forests. *Proceedings of 3rd International Conference on Document Analysis and Recognition*, 1:278–282.

[Huang et al., 2017a] Huang, N., Yang, Y., Liu, J., Gu, X., and Cai, H. (2017a). Single-Image Super-Resolution for Remote Sensing Data Using Deep Residual-Learning Neural Network. In Liu, D., Xie, S., Li, Y., Zhao, D.,

and El-Alfy, E.-S. M., editors, *Neural Information Processing*, pages 622–630, Cham. Springer International Publishing.

[Huang et al., 2017b] Huang, N., Yang, Y., Liu, J., Gu, X., and Cai, H. (2017b). Single-Image Super-Resolution for Remote Sensing Data Using Deep Residual-Learning Neural Network. In Liu, D., Xie, S., Li, Y., Zhao, D., and El-Alfy, E.-S. M., editors, *Neural Information Processing*, pages 622–630, Cham. Springer International Publishing.

[Huang et al., 2013] Huang, Q., Yang, C., Benedict, K., Chen, S., Rezgui, A., and Xie, J. (2013). Utilize cloud computing to support dust storm forecasting. *International Journal of Digital Earth*, 6(4):338–355.

[Huang et al., 2010] Huang, Q., Yang, C., Nebert, D., Liu, K., and Wu, H. (2010). Cloud computing for geosciences: Deployment of geoss clearinghouse on amazon's ec2. In *Proceedings of the ACM SIGSPATIAL International Workshop on High Performance and Distributed Geographic Information Systems*, HPDGIS '10, pages 35–38, New York, NY, USA. ACM.

[Huang et al., 2015] Huang, W., Xiao, L., Wei, Z., Liu, H., and Tang, S. (2015). A New Pan-Sharpening Method With Deep Neural Networks. *IEEE Geoscience and Remote Sensing Letters*, 12(5):1037–1041.

[Hui et al., 2018] Hui, Z., Wang, X., and Gao, X. (2018). Fast and Accurate Single Image Super-Resolution via Information Distillation Network.

[Hyperion, 2018] Hyperion (2018). Eo-1 hyperion. https://www.europeandataportal.eu/data/dataset/usgs_edc_eo1_hyperion.

[Ian, 2018] Ian, S. (2018). Powering Landsat Power Tools. https://developmentseed.org/blog/2015/03/19/aws-landsat-archive/. Accessed: 2018-08-19.

[Joshi et al., 2016] Joshi, K., Yadav, R., and Allwadhi, S. (2016). Psnr and mse based investigation of lsb. In *2016 International Conference on Computational*

Techniques in Information and Communication Technologies (ICCTICT), pages 280–285.

[Katiyar and Arun, 2014] Katiyar, S. K. and Arun, P. V. (2014). Comparative analysis of common edge detection techniques in context of object extraction. *IEEE TGRS*, 50(11b):68–79.

[Kawulok Michałand Benecki et al., 2018] Kawulok Michałand Benecki, P. N. J., Kostrzewa, D., and Skonieczny, Ł. (2018). Towards Robust Evaluation of Super-Resolution Satellite Image Reconstruction. In Nguyen, N. T., Hoang, D. H., Hong, T.-P., Pham, H., and Trawiński, B., editors, *Intelligent Information and Database Systems*, pages 476–486, Cham. Springer International Publishing.

[Khizar, 2017] Khizar, H. (2017). Super-Resolution via Deep Learning. http://arxiv.org/abs/1706.09077.

[Kiemle et al., 2016] Kiemle, S., Molch, K., Schropp, S., Weiland, N., and Mikusch, E. (2016). Big data management in earth observation: The german satellite data archive at the german aerospace center. *IEEE Geoscience and Remote Sensing Magazine*, 4(3):51–58.

[Kristof et al., 2014] Kristof, D., Giachettab, R., Olasza, A., and Thai, B. N. (2014). Big Geospatial Data Processing And Analysis Developments In The Iqmulus Project. *Proc. of the 2014 conference on Big Data from Space (BiDS'14)*, (November):12–14.

[Kussul et al., 2017] Kussul, N., Lavreniuk, M., Skakun, S., and Shelestov, A. (2017). Deep Learning Classification of Land Cover and Crop Types Using Remote Sensing Data. *IEEE Geoscience and Remote Sensing Letters*, 14(5):778–782.

[Lanaras et al., 2018] Lanaras, C., Bioucas-Dias, J., Galliani, S., Baltsavias, E., and Schindler, K. (2018). Super-resolution of Sentinel-2 images: Learning a

globally applicable deep neural network. *ISPRS Journal of Photogrammetry and Remote Sensing*, 146:305–319.

[LeCun et al., 2015] LeCun, Y., Bengio, Y., and Hinton, G. (2015). Deep learning. *Nature*, 521(7553):436–444.

[LeCun et al., 1990] LeCun, Y., Boser, B. E., Denker, J. S., Henderson, D., Howard, R. E., Hubbard, W. E., and Jackel, L. D. (1990). Handwritten Digit Recognition with a Back-Propagation Network. In Touretzky, D. S., editor, *Advances in Neural Information Processing Systems 2*, pages 396–404. Morgan-Kaufmann.

[Li and Orchard, 2001] Li, X. and Orchard, M. T. (2001). New edge-directed interpolation. *IEEE Transactions on Image Processing*, 10(10):1521–1527.

[Liebel and Körner, 2016] Liebel, L. and Körner, M. (2016). Single-image Super Resolution for Multispectral Remote Sensing Data using Convolutional Neural Networks. In *The International Archives of the Photogrammetry, Remote Sensing and Spatial Information Sciences*, pages 883–890.

[Liu et al., 2017] Liu, P., Zhang, H., and Eom, K. B. (2017). Active Deep Learning for Classification of Hyperspectral Images. *IEEE Journal of Selected Topics in Applied Earth Observations and Remote Sensing*, 10(2):712–724.

[Long et al., 2018] Long, T., Zhang, Z., He, G., Jiao, W., Tang, C., Wu, B., Zhang, X., Wang, G., and Yin, R. (2018). 30m resolution Global Annual Burned Area Mapping based on Landsat images and Google Earth Engine. Technical report.

[Luo et al., 2017] Luo, W., Li, Y., Urtasun, R., and Zemel, R. S. (2017). Understanding the effective receptive field in deep convolutional neural networks. *CoRR*, abs/1701.04128.

[Ma et al., 2015] Ma, Y., Wu, H., Wang, L., Huang, B., Ranjan, R., Zomaya, A., and Jie, W. (2015). Remote sensing big data computing: Challenges and opportunities. *Future Generation Computer Systems*, 51:47–60.

[Maheshwari and Pati, 2014] Maheshwari, S. and Pati, U. C. (2014). Mosaicing of images using unsharp masking algorithm for interest point detection. In *2014 IEEE International Conference on Advanced Communications, Control and Computing Technologies*, pages 1431–1434. IEEE.

[Malaysia, 2018] Malaysia, T. S. (2018). Cloud adoption expands by 100%. https://www.thestar.com.my/metro/smebiz/news/2016/06/15/.

[Mandal et al., 2018] Mandal, D., Kumar, V., Bhattacharya, A., Rao, Y. S., Siqueira, P., and Bera, S. (2018). Sen4rice: A processing chain for differentiating early and late transplanted rice using time-series sentinel-1 sar data with google earth engine. *IEEE Geoscience and Remote Sensing Letters*, pages 1–5.

[Marc Ferrer1, 2014] Marc Ferrer1, M. S. (2014). Helix Nebula - Towards An Earth Observation Data Paas For Oil & Gas Market. *Proc. of the 2014 conference on Big Data from Space (BiDS'14)*, (November):12–14.

[Mark Brinda, 2018] Mark Brinda, M. H. (2018). The changing faces of the cloud. http://www.bain.com/Images/BAIN_BRIEF_The_Changing_Faces_of_the_Cloud.pdf.

[Mascolo et al., 2014] Mascolo, L., Quartulli, M., Guccione, P., Nico, G., and Olaizola, I. G. (2014). Scalable analysis and retrieval of polarimetric sar data on elastic computing clouds. pages 150–153.

[Mateo-Garca et al., 2017] Mateo-Garca, G., Muoz-Mar, J., and Gmez-Chova, L. (2017). Cloud detection on the google earth engine platform. In *2017 IEEE International Geoscience and Remote Sensing Symposium (IGARSS)*, pages 1942–1945.

[Mei et al., 2017] Mei, S., Yuan, X., Ji, J., Zhang, Y., Wan, S., and Du, Q. (2017). Hyperspectral Image Spatial Super-Resolution via 3D Full Convolutional Neural Network. *Remote Sensing*, 9(11).

[Nair and Hinton, 2010] Nair, V. and Hinton, G. E. (2010). Rectified Linear Units Improve Restricted Boltzmann Machines. *Proceedings of the 27th International Conference on Machine Learning*, (3):807–814.

[NASA, 2016] NASA (2016). NASA Earth Exchange (NEX). https://nex.nasa.gov/nex/. Accessed: 2016-09-02.

[NASA, 2018a] NASA (2018a). Landsat 8 science. https://landsat.gsfc.nasa.gov/landsat-data-continuity-mission/. Accessed: 2018-08-23.

[NASA, 2018b] NASA (2018b). Landsat 9 has been fast-tracked for a december 2020 launch.

[NASA, 2018c] NASA (2018c). Moderate resolution imaging spectroradiometer. https://modis.gsfc.nasa.gov/data/.

[Nguyen et al., 2018] Nguyen, N., Hoang, D., Hong, T., Pham, H., and Trawiński, B. (2018). *Towards Robust Evaluation of SuperResolution Satellite Image Reconstruction, March 19-21, 2018, Proceedings*. Number pt. 1 in Lecture Notes in Computer Science. Springer International Publishing.

[Niggemann et al., 2014] Niggemann, F., Appel, F., de la Mar, H. B. J., and Schirpke, B. (2014). The Use Of Cloud Computing Resources For Processing Of Big Data From Space For Operational Land Surface Monitoring In Germany. *Proc. of the 2014 conference on Big Data from Space (BiDS'14)*, (November):12–14.

[NIST, 2018] NIST (2018). The NIST Definition of Cloud Computing. https://nvlpubs.nist.gov/nistpubs/legacy/sp/nistspecialpublication800-145.pdf.

[OGC-Consortium, 2018] OGC-Consortium (2018). Open Geospatial Consortium (OGC). http://www.opengeospatial.org. Accessed: 2016-10-10.

[Packyanathan et al., 2015] Packyanathan, G., Veeraraghavalu, R., B.S, S., Kalist, V., and K. Khamar Basha, S. (2015). Satellite image segmentation based on ycbcr color space. *Indian Journal of Science and Technology*, 8:35.

[Padarian et al., 2015] Padarian, J., Minasny, B., and Mcbratney, a. B. (2015). Computers & Geosciences Using Google ' s cloud-based platform for digital soil mapping. *Computers and Geosciences*, 83:80–88.

[Pan and Zhang, 2013] Pan, X. and Zhang, S. (2013). A remote sensing image cloud processing system based on Hadoop. *Proceedings - 2012 IEEE 2nd International Conference on Cloud Computing and Intelligence Systems, IEEE CCIS 2012*, 1:492–494.

[Park et al., 2003] Park, S. C., Park, M. K., and Kang, M. G. (2003). Super-resolution image reconstruction: a technical overview. *IEEE Signal Processing Magazine*, 20(3):21–36.

[Patel et al., 2015] Patel, N. N., Angiuli, E., Gamba, P., Gaughan, A., Lisini, G., Stevens, F. R., Tatem, A. J., and Trianni, G. (2015). Multitemporal settlement and population mapping from Landsat using Google Earth Engine. *International Journal of Applied Earth Observation and Geoinformation*, 35:199–208.

[Pivotal, 2018] Pivotal (2018). RabbitMQ. https://www.rabbitmq.com. Accessed: 2018-01-05.

[Plaza et al., 2011] Plaza, A., Du, Q., Chang, Y.-L., and King, R. L. (2011). High Performance Computing for Hyperspectral Remote Sensing. *IEEE Journal of Selected Topics in Applied Earth Observations and Remote Sensing*, 4(3):528–544.

[Pouliot et al., 2018] Pouliot, D., Latifovic, R., Pasher, J., and Duffe, J. (2018). Landsat Super-Resolution Enhancement Using Convolution Neural Networks and Sentinel-2 for Training. *Remote Sensing*, 10(3).

[Project, 2018] Project, I. (2018). IQmulus — A High-volume Fusion and Analysis Platform for Geospatial Point Clouds, Coverages and Volumetric Data Sets.

[Qin et al., 2018] Qin, M., Xie, F., Li, W., Shi, Z., and Zhang, H. (2018). Dehazing for multispectral remote sensing images based on a convolutional neural network with the residual architecture. *IEEE Journal of Selected Topics in Applied Earth Observations and Remote Sensing*, 11(5):1645–1655.

[Robila, 2006] Robila, S. A. (2006). Use of Remote Sensing Applications and its Implications to the Society. In *2006 IEEE International Symposium on Technology and Society*, pages 1–6. IEEE.

[Romero et al., 2016] Romero, A., Gatta, C., and Camps-Valls, G. (2016). Unsupervised Deep Feature Extraction for Remote Sensing Image Classification. *IEEE Transactions on Geoscience and Remote Sensing*, 54(3):1349 – 1362.

[Saranya and Muralidharan, 2017] Saranya, K. and Muralidharan, K. B. (2017). Real time surveillance of paddy field using landsat images. In *2017 International Conference on Intelligent Computing, Instrumentation and Control Technologies (ICICICT)*, pages 695–698.

[Satellite Imaging Corp, 2018] Satellite Imaging Corp (2018). Worldview-2 satellite sensor - satellite imaging corp. https://www.satimagingcorp.com/satellite-sensors/worldview-2/.

[Scaling, 2018] Scaling, C. (2018). Grid, cloud, hpc what's the difference? http://cloudscaling.com/blog/cloud-computing/grid-cloud-hpc-whats-the-diff/.

[Schepaschenko et al., 2015] Schepaschenko, D., See, L., Lesiv, M., McCallum, I., Fritz, S., Salk, C., Moltchanova, E., Perger, C., Shchepashchenko, M., Shvidenko, A., Kovalevskyi, S., Gilitukha, D., Albrecht, F., Kraxner, F., Bun, A., Maksyutov, S., Sokolov, A., Dürauer, M., Obersteiner, M., Karminov, V., and Ontikov, P. (2015). Development of a global hybrid forest mask through the synergy of remote sensing, crowdsourcing and FAO statistics. *Remote Sensing of Environment*, 162:208–220.

[Schmitt and Zhu, 2016] Schmitt, M. and Zhu, X. (2016). Data fusion and remote sensing an ever-growing relationship. *IEEE Geoscience and Remote Sensing Magazine*, 4:6–23.

[SenSyF Project, 2018] SenSyF Project (2018). The SenSyF Project. http://www.sensyf.eu/framework.html. Accessed: 2018-08-27.

[Shelestov et al., 2017] Shelestov, A., Lavreniuk, M., Kussul, N., Novikov, A., and Skakun, S. (2017). Large scale crop classification using google earth engine platform. In *2017 IEEE International Geoscience and Remote Sensing Symposium (IGARSS)*, pages 3696–3699.

[Sinergise Ltd, 2018] Sinergise Ltd (2018). Sentinel Hub. https://sentinel-hub.com/. Accessed: 2018-07-06.

[Tappen et al., 2003] Tappen, M. F., Russell, B. C., and Freeman, W. T. (2003). Exploiting the sparse derivative prior for super-resolution and image demosaicing. In *In IEEE Workshop on Statistical and Computational Theories of Vision*.

[Tatem et al., 2008] Tatem, A. J., Goetz, S. J., and Hay, S. I. (2008). Fifty Years of Earth Observation Satellites: Views from above have lead to countless advances on the ground in both scientific knowledge and daily life. *American scientist*, 96(5):390–398.

[Tatem et al., 2001] Tatem, A. J., Lewis, H. G., Atkinson, P. M., and Nixon, M. S. (2001). Super-resolution mapping of urban scenes from ikonos imagery using a hopfield neural network. In *IGARSS 2001. Scanning the Present and Resolving the Future. Proceedings. IEEE 2001 International Geoscience and Remote Sensing Symposium (Cat. No.01CH37217)*, volume 7, pages 3203–3205 vol.7.

[Thomas et al., 2008] Thomas, C., Ranchin, T., Wald, L., and Chanussot, J. (2008). Synthesis of multispectral images to high spatial resolution: A critical review of fusion methods based on remote sensing physics. *IEEE Transactions on Geoscience and Remote Sensing*, 46(5):1301–1312.

[Titus et al., 2013] Titus, J., Cse, M. T. S., and Geroge, S. (2013). A Comparison Study On Different Interpolation Methods Based On Satellite Images. 2(6):82–85.

[Tsai and Huang, 1984] Tsai, R. Y. and Huang, T. S. (1984). Multiframe image restoration and registration, Advances in Computer Vision and Image Processing, vol. *Multiframe Image Restoration and Registration*, pages 317–339.

[Tuia et al., 2015] Tuia, D., Go, B. L., Moser, G., and Camps-valls, G. (2015). Multimodal Classification of Remote Sensing Images : A Review and Future Directions. *Proceedings of the IEEE*, 103(9).

[UNOOSA, 2018] UNOOSA (2018). Online index of objects launched into outer space. http://www.unoosa.org/oosa/osoindex/.

[USGS, 2017] USGS (2017). Landsatlook. https://landsatlook.usgs.gov/viewer.html. Accessed: 2017-06-14.

[USGS, 2018a] USGS (2018a). Landsat Processing Details — Landsat Missions. https://landsat.usgs.gov/landsat-processing-details. Accessed: 2018-09-15.

[USGS, 2018b] USGS (2018b). MOD09A1 V006 LP DAAC : NASA Land Data Products and Services. https://lpdaac.usgs.gov/dataset_discovery/modis/modis_products_table/mod09a1_v006.

[Vivone et al., 2015] Vivone, G., Alparone, L., Chanussot, J., Mura, M. D., Garzelli, A., Licciardi, G. A., Restaino, R., and Wald, L. (2015). A critical comparison among pansharpening algorithms. *IEEE Transactions on Geoscience and Remote Sensing*, 53(5):2565–2586.

[Wang, 2011] Wang (2011). Towards building a cloud for scientific applications. *Advances in Engineering Software*, 42(9):714–722.

[Wang and Perez, 2017] Wang, J. and Perez, L. (2017). The Effectiveness of Data Augmentation in Image Classification using Deep Learning. *unpublished*.

[Wang et al., 2013] Wang, P., Wang, J., Chen, Y., and Ni, G. (2013). Rapid processing of remote sensing images based on cloud computing. *Future Generation Computer Systems*, 29(8):1963–1968.

[Wang et al., 2018a] Wang, P., Zhang, G., and Leung, H. (2018a). Utilizing parallel networks to produce sub-pixel shifted images with multiscale spatio-spectral information for soft-then-hard sub-pixel mapping. *IEEE Access*, 6:57485–57496.

[Wang et al., 2015] Wang, Q., Shi, W., Atkinson, P. M., and Zhao, Y. (2015). Downscaling MODIS images with area-to-point regression kriging. *Remote Sensing of Environment*, 166:191–204.

[Wang et al., 2016] Wang, Q., Shi, W., Li, Z., and Atkinson, P. M. (2016). Fusion of Sentinel-2 images. *Remote Sensing of Environment*, 187(December):241–252.

[Wang et al., 2018b] Wang, T., Sun, W., Qi, H., and Ren, P. (2018b). Aerial Image Super Resolution via Wavelet Multiscale Convolutional Neural Networks. *IEEE Geoscience and Remote Sensing Letters*, PP(99):1–5.

[Wu et al., 2012] Wu, B., Li, C., and Zhan, X. (2012). Integrating spatial structure in super-resolution mapping of hyper-spectral image. *Procedia Engineering*, 29:1957–1962.

[Xiaoqiang and Yuejin, 2010] Xiaoqiang, Y. and Yuejin, D. (2010). Exploration of cloud computing technologies for geographic information services. *2010 18th International Conference on Geoinformatics*, pages 1–5.

[Xing et al., 2014] Xing, J., Sieber, R., and Kalacska, M. (2014). The challenges of image segmentation in big remotely sensed imagery data. *Annals of GIS*, 20(4):233–244.

[Xu and Bai, 2015] Xu, H. and Bai, Y. (2015). Evaluation of urban lake evolution using google earth engine - a case study of wuhan, china. In *2015 Fourth International Conference on Agro-Geoinformatics (Agro-geoinformatics)*, pages 322–325.

[Yang, 2011] Yang, C. (2011). Thinking and computing spatiotemporally to enable cloud computing nd science discoveries. *Proceedings - 2011 19th International Conference on Geoinformatics, 2011*.

[Yang et al., 2016a] Yang, C., Huang, Q., Li, Z., Liu, K., and Hu, F. (2016a). Big Data and cloud computing: innovation opportunities and challenges. *International Journal of Digital Earth*, 10(1):13–53.

[Yang et al., 2016b] Yang, N., Tang, H., Sun, H., and Yang, X. (2016b). Dropband: a convolutional neural network with data augmentation for scene classification of vhr satellite images.

[Ye et al., 2013] Ye, F., Wang, Z.-J., Zhou, F.-C., Wang, Y.-P., and Zhou, Y.-C. (2013). Cloud-Based Big Data Mining & Analyzing Services Platform Integrating R. *2013 International Conference on Advanced Cloud and Big Data*, pages 147–151.

[Young et al., 2017] Young, N. E., Anderson, R. S., Chignell, S. M., Vorster, A. G., Lawrence, R., and Evangelista, P. H. (2017). A survival guide to Landsat preprocessing. *Ecology*, 98(4):920–932.

[Yu et al., 2016] Yu, W., Xie, J., and Li, G. (2016). Cloud computing for environmental monitoring using multi-source earth observation data. In *2016 Fifth International Conference on Agro-Geoinformatics (Agro-Geoinformatics)*, pages 1–4.

[Yue et al., 2016] Yue, L., Shen, H., Li, J., Yuan, Q., Zhang, H., and Zhang, L. (2016). Image super-resolution: The techniques, applications, and future. *Signal Processing*, 128:389–408.

[Zhang, 2010] Zhang, J. (2010). Towards Personal High-Performance Geospatial Computing (HPC-G): Perspectives and a Case Study 2 . 3 Spatial Database : parallel DB or. *ACM HPDGIS'10*, pages 3–10.

[Zhang et al., 2012] Zhang, K., Gao, X., Tao, D., and Li, X. (2012). Single image super-resolution with non-local means and steering kernel regression. *IEEE Transactions on Image Processing*, 21(11):4544–4556.

[Zhang and Wang, 2015] Zhang, T. and Wang, Q. (2015). Deep Learning Based Feature Selection for Remote Sensing Scene Classification. *IEEE Geoscience and Remote Sensing Letters*, 12(11):2321–2325.

[Zhong et al., 2012] Zhong, Y., Han, J., Zhang, T., and Fang, J. (2012). A distributed geospatial data storage and processing framework for large-scale webgis. In *2012 20th International Conference on Geoinformatics*, pages 1–7.